UAH Research Report No. 248

NUMERICAL SIMULATION OF ADVECTION FOG FORMATION ON MULTI-DISPERSE AEROSOLS DUE TO COMBUSTION-RELATED POLLUTANTS

by

R. J. Hung and G. S. Liaw

Final Technical Report

This research work was supported by
the National Aeronautics and Space Administration
George C. Marshall Space Flight Center
Contract NAS8-31729

The University of Alabama in Huntsville
School of Science and Engineering
Huntsville, Alabama 35899

July 1980

UAH Research Report No. 248

NUMERICAL SIMULATION OF ADVECTION FOG FORMATION ON MULTI-DISPERSE AEROSOLS DUE TO COMBUSTION-RELATED POLLUTANTS

by

R. J. Hung and G. S. Liaw

Final Technical Report

This research work was supported by
the National Aeronautics and Space Administration
George C. Marshall Space Flight Center
Contract NAS8-31729

The University of Alabama in Huntsville
School of Science and Engineering
Huntsville, Alabama 35899

July 1980

ACKNOWLEDGMENT

This work was supported by the National Aeronautics and Space Administration, George C. Marshall Space Flight Center, under Contract NAS8-31729, with the technical coordination of Mr. O. H. Vaughan, Jr., of the Atmospheric Science Division, Space Sciences Laboratory. His encouragement and consultation during the course of this study was greatly appreciated.

The authors also express their gratitude to the Aviation Safety Technology Branch, Office of Advanced Research and Technology (OAST), NASA Headquarters, for the support of this research.

The manuscript was typed by Ms. Carol Holliday. Her patient and skillful typing were essential in bringing this report to the present form.

SUMMARY

The most noticeable effect of air pollution on the properties of the atmosphere is the reduction in visibility. By considering dynamical and microphysical processes, the present study investigates the formation of advection fog associated with aerosols, due to combustion-related pollutants, as condensation nuclei. We are particularly interested in the study of the effects of multi-disperse distribution of the aerosol population, and also single component and multi-component aerosol species on the condensation/nucleation processes which affect the reduction in visibility.

The results show that the aerosol population with a high particle concentration provides more favorable conditions for the formation of a denser fog than the aerosol population with a greater particle size distribution if the value of the mass concentration of the aerosols is kept constant.

The results of the present study can be used as numerical prediction of fog formation. Two-dimensional observations in horizontal and vertical coordinates, together with time-dependent measurements are needed as initial values for the following physical parameters: (1) wind profiles; (2) temperature profiles; (3) humidity profiles; (4) mass concentration of aerosol particles; (5) particle size distribution of aerosols; and (6) chemical composition of aerosols. Formation and dissipation of advection fog, thus, can be forecasted numerically by introducing initial values obtained from the observations.

The present research supported G. S. Liaw, a former graduate student, who obtained his degree of Doctor of Philosophy from The University of Alabama in Huntsville.

The present research also produced the following publications:

(1) Hung, R. J., and O. H. Vaughan, Numerical Simulation of Life Cycles of Advection Warm Fog, AIAA Paper No. 77-130, p. 1-9, 1977.

(2) Hung, R. J., G. S. Liaw, and O. H. Vaughan, Numerical Simulation of Warm Fog and Its Application to Warm Fog Prediction and Modification, Proc. Atmospheric Environment of Aerospace Systems and Applied Meteorology, American Meteorological Society, Boston, Mass., pp. 169-173, 1978.

(3) Hung, R. J., and G. S. Liaw, Hygroscopic Chemicals and the Formation of Advection Warm Fog - A Numerical Simulation, NASA Contractor Report 3085, Scientific and Technical Information Office, pp. 58, December 1978.

(4) Hung, R. J., G. S. Liaw, and O. H. Vaughan, Aerosol Particles and the Formation of Advection Fog, J. Rech. Atmos., 13, 37-61, 1979.

(5) Hung, R. J., and G. S. Liaw, Fluid Mechanics Simulation of Fog Formation Associated with Polluted Atmosphere Produced by Energy Related Fuel Combustion, Developments in Theoretical and Applied Mechanics, 10, pp. 355-372, 1980.

(6) Hung, R. J., G. S. Liaw and O. H. Vaughan, Advection Fog Formation and Aerosols Produced by Combustion-Originated Air Pollution, Proc. on Application of Air Pollution Meteorology, American Meteorological Society, Boston, Mass, 1980 (in press).

(7) Hung, R. J., and G. S. Liaw, Advection Fog Formation Associated with Atmospheric Aerosols Due to Combustion-Related Pollutants - Monodisperse, Multi-Component Model, Water, Air and Soil Pollution, 13, 1980 (in press).

(8) Hung, R. J., G. S. Liaw and R. E. Smith, Mathematical Simulation of the Advection Fog Formation on Multi-Disperse, Single-Component Aerosols Due to Combustion-Related Pollutants, J. Rech. Atmos., 14, 1980 (submitted for publication).

(9) Hung, R. J., and G. S. Liaw, Numerical Simulation of Fog Formation and Liquid Water Content on Multi-Disperse, Multi-Component Aerosols Due to Combustion-Related Pollutants, Atmospheric Environment, 1980 (submitted for publication).

TABLE OF CONTENTS

LIST OF FIGURES

List of Symbols

a	Parameter defined in Equation (2-15)
b	The slope of a linearized $e_{sat}(T)$ and T curve
c	Parameter defined in Equation (2-16)
C_p	Constant pressure specific heat
C_{va}	Water vapor-air mixing ratio
C_{wa}	Liquid water-air mixing ratio
D	Diffusivity of water vapor in the air
D_{eff}	Effective diffusion coefficient, also defined in Equation (2-11)
f	Coriolis parameter
F_{cv}	Source function for condensation and evaporation for water vapor
F_{cw}	Source function for condensation and evaporation for liquid water
g	Gravitational acceleration
i	Factor of Van't Hoff
K	Thermal conductivity of the mixture
K_d	Turbulent exchange coefficient for turbulent transfer of water vapor diffusion
K_h	Turbulent exchange coefficient for turbulent transfer of heat flux
K_m	Turbulent exchange coefficient for vertical turbulent transfer of momentum
λ	Parameter defined in Equation (2-12)
λ_α	Parameter defined in Equation (2-13)
λ_β	Parameter defined in Equation (2-14)
L	Latent heat of evaporation for water
m_s	Mass of hygroscopic material dissolved

M_a	Molecular weight of air
M_b	Gram molecular weight of hygroscopic nucleus
M_v	Molecular weight of vapor
M_w	Molecular weight of water
N	Number density of water droplet which is a function of droplet size
p	Pressure of the mixture
r	Radius of the droplet
r_o	Radius of nucleus
R_f	Net upward flux of infrared radiation
S	Saturation ratio of water vapor in air
T	Temperature
U_t	Mean terminal velocity of fog drops
U_x	Wind velocity in horizontal x-direction
U_y	Wind velocity in horizontal y-direction
U_z	Wind velocity in vertical z-direction
U_{gx}	x-component of the velocity of geostrophic wind
U_{gy}	y-component of the velocity of geostrophic wind
V_a	Diffusion volume of air
V_v	Diffusion volume of vapor
α	Accommodation coefficient
β	Sticking coefficient
θ	Potential temperature
θ_0	Potential temperature of dry adiabatic value
ρ	Density of dry air

ρ Density of dry air

ρ_h Density of hygroscopic nucleus

ρ_v Water vapor density

ρ_w Liquid water density

$\rho_{sat}(\infty)$ Saturation vapor density at infinity

σ Surface tension of water

I. INTRODUCTION

The basic ingredients of a fog or cloud droplet are liquid water (or ice) and condensation nuclei (or ice nuclei in the case of an ice fog or ice cloud). These nuclei are aerosol particles, generally with diameters equal to or greater than 0.1 μm, and are nearly always at least partially hygroscopic.

During the absence of aerosol particles in the atmosphere, condensation of water vapor will occur only if the supersaturation reaches several hundred percent. However, in the atmosphere, there are abundant foreign particles to serve as ready-prepared nuclei, both naturally produced and produced by energy-related combustion, for condensation and to present the large supersaturations from being achieved.

The atmospheric aerosols cover a wide range of particle size, from about 10^{-3} μm radius for the small ions consisting of a few neutral air molecules clustered around a charged molecule to more than 10 μm for the largest salt and dust particles. Their concentration also covers an enormous range, from less than 1000 per cm^3 over the ocean, to perhaps 10^6 per cm^3 in the highly polluted air of large industrial cities (Mason, 1971). A recent study of New York City aerosol particles indicated that the average number of particles is (4 to 9) x 10^4 particles cm^{-3} for the lowest point at 5 AM, and for the highest point at 9 AM local time, with a sampling ranging in size from 0.1 to 1.3 μm diameter (Leaderer et al., 1978).

As to the chemical composition of atmospheric aerosols, the large quantities of $SO_4^=$, NO_3^-, NH_4^+ and a strong acid such as H_2SO_4 have been detected in highly industrialized areas (Leaderer et al., 1978). A

substantial portion of this aerosol production is the result of energy-related fuel combustion. Sulfur, an impurity found both in coal and petroleum, reacts with O_2 at high temperatures producing oxides of S, SO_x. Furthermore, since air (79% N_2) is the O_2 source for combustion, the formation and subsequent emission of NO_x, especially an elevated combustion temperatures, are common occurrences. The internal combustion engine is the dominant source of the production of NO_x. This production of SO_x and NO_x due to energy-related fuel combustion is, in turn, transformed into aerosol particles through photochemical reaction (Council on Environmental Quality, 1973).

Based on the estimation made by the Council on Environmental Quality, energy conversion processes account for 84% of the SO_x, 97% of the NO_x, and 78% of the CO emissions (Council on Environmental Quality, 1973). However, the figures are quite different based on anthropogenic source points of view. For example, volcanic emissions account for more than 50% of SO_2, thunderstorms for more than 75% of NO_x, etc. Since the dispersal of air pollution is unaffected by national boundaries, the emission of pollutants often results in global problems and concerns.

Some of the atmospheric aerosols, in particular the salt aerosols with hygroscopic properties, are known to exhibit the property of deliquescence when exposed to a humid environment. The critical humidity at which a given salt particle abruptly transforms from the crystalline state to a saline droplet is related to the water vapor pressure in equilibrium with the saturated salt solution at the ambient temperature. Recently, Tang et al. (1977, 1978) and Tang and Munkelwitz (1977), conducted a series of experiments to investigate the onset of growth which took place at a specific deliquescence humidity determined by the water activity at the eutonic composition for some mixed salt

aerosols NaCl-KCl, and $(NH_4)_2SO_4$-H_2SO_4. The result showed that the onset of growth occurs at 73.8 ± 0.5% relative humidity for mixed NaCl-KCl aerosols, and at 69.0 ± 0.5% relative humidity for sulfate aerosols containing 0.75 to 0.95 mole fraction $(NH_4)_2SO_4$.

In general, for a nucleus, or an aerosol particle to grow into a droplet, the air must have attained a certain degree of supersaturation (Fletcher, 1966; Weinstein and Silverman, 1973). At low supersaturation, only the nuclei large and hygroscopic enough will go across the hump of the so-called Köhler curve (Mason, 1971). Once over the hump (i.e., the so-called critical size or critical supersaturation), these nuclei formally become cloud droplets and can, in theory, grow to any size, provided a small amount of supersaturation is maintained. The figure for the presence of supersaturation to be a necessary condition to produce cloud droplets can be changed for condensation occurring in the polluted atmosphere (Hung and Liaw, 1979).

The correlation of the fog formation with a high concentration of air pollutants associated with fuel combustion has been observed experimentally. With high concentrations of SO_x due to fuel combustion, the formation of sulfuric acid by oxidation of SO_2 on the surface of particles in a humid environment leads to the formation of small droplets of fog which would not otherwise have formed. For example, in determining the correlation between SO_x concentrations and fog formation in the German cities of Gelsenkirchen and Hamburg, Georgii (1969) found that 80 percent of all cases of high SO_x concentrations occurred with visibilities below 5 km. In addition to fog formation, increased precipitation has been linked to areas with high aerosol concentrations (Changnon, 1968).

The average mass concentration of aerosol particles from the National Air Sampling Network in the United States ranges from about 20 $\mu g/m^3$ in clean air in remote areas, to values of 100 to 280 $\mu g/m^3$ in urban areas (Hidy and Brock, 1971). In the heavily polluted atmosphere of the highly industrialized areas, mass concentration with values as high as 2000 $\mu g/m^3$, have been reported. As for particle number concentration, it varies from 10^2 particles/cm^3 for very clean air to 10^5 particles/cm^3 in polluted air. The radius of condensation nucleus with combustion as a source ranges from 0.01 to 1 μm (Seinfeld, 1975). Thus, combustion is listed as a source of particles for sizes up to 1 μm diameter (Seinfeld, 1975).

The percentage distribution of mass concentration for SO_x is about 18%, and for NO_x it is about 6% (Hidy and Brock, 1971). This means that the mass concentration for SO_x is roughly less than 10 $\mu g/m^3$ in clean air, and ranges from about 20 to 50 $\mu g/m^3$ in polluted air. The range of mass concentration for NO_x is roughly one-third of the amount of the SO_x range.

Results obtained from Hung and Liaw (1980) show that the major contribution of combustion-related pollutants as condensation nuclei in the formation of fog comes from aerosols with species of SO_x. However, NO_x as condensation nuclei also gives a considerable contribution to the formation of fog, but the weight is much less than that due to SO_x. In this study, our major attention is focused on the effect of fog formation due to SO_x as condensation nuclei with the consideration of the influences made by the variety of particle size distribution.

To elucidate the fog optical properties, Low et al. (1978) examined the effects of different spectral shapes and widths on gamma and lognormal distributions with the same liquid water content, and concluded that the drop size distribution greatly affects the result of visibility even-though the liquid water content is the same. Observations show that

particle size distribution for combustion related aerosols are widely spread. In the present paper, we are interested in studying the effect of particle size distribution of aerosols as condensation nuclei for fog formation with keeping mass concentration fixed. To simplify the calculation, and also to make the results easy to compare, a combination of three step functions are chosen to modify the particle size distribution of aerosols.

Acid rain is a major environmental problem on both sides of the Atlantic Ocean. Originally noticed and studied in the Scandinavian countries and in Canada, acid rain has been documented in this country; first in the Northeast and now throughout much of the United States. Increasing levels of acidity have already caused measurable damage to the environment. Many lakes are now totally devoid of fish population; monuments and other man-made structures are being degraded; and yields of agricultural crops and forests may be decreasing.

Acid rain, based on the definition of the terminology given by the Environmental Protection Agency, includes the wet removal processes such as rain and snow; the dry deposition component such as particulate sedimentation and/or gaseous aborption and adsorption; and special events such as fog, frost and dew which also contribute to the overall acidic deposition in amounts that need to be quantified.

In the production of NO_x, strong evidence indicates that the major producer comes from the automobile. There is no doubt that stationary source fuel combustions also contribute a heavy fraction of the total NO_x emitted to the atmosphere. Fuel-bound nitrogen compounds are ammonia, pyridine, and many other amines (Glassman, 1977). Similar to NO_x production by combustion, S as an inherent impurity in both coal and petroleum, SO_x

is also produced through fuel combustion. This production of SO_x and NO_x due to energy-related fuel combustion is, in turn, transformed into aerosol particles through photochemical reaction (Council on Environmental Quality, 1973).

Energy conversion processes account for 84% of the SO_x, 97% of the NO_x, and 78% of the CO emissions based on the estimation made by the Council on Environmental Quality (1973). However, the figures are quite different for data chosen from anthropogenic source points of view. For example, volcanic eruption, such as ash coughed up by Mount St. Helens, Washington, on May 18, 1980, could account for more than 50% of SO_2, thunderstorms for more than 75% of NO_x, etc. Since the dispersal of air pollution is unaffected by national boundaries, the emission of pollutants often results in global problems and concerns.

The production of SO_x and NO_x became the major sources of acid rain through the transformation of gas molecules to aerosol particles via photochemical reaction, and condensation processes in which the aerosol particles serve as condensation nuclei. The present study, in particular, deals with the mathematical simulation of the formation of advection fog and the accumulation of liquid water content in the atmosphere through the condensation processes in which the effects of the multi-disperse distribution of the initial aerosol population and multi-component species of aerosol particles as condensation nuclei are taken into consideration.

II. MATHEMATICAL MODEL

A theoretical model is employed which describes the evolution of potential temperature, water vapor content, liquid water content, and horizontal and vertical winds as determined by the processes of vertical turbulent transfer and horizontal advection of momentum, energy and moisture, as well as radiation cooling, growth of water droplets based on microphysical processes, and drop sedimentation.

The mathematical model is time-dependent two-dimensional in the X-Z plane, and the boundary layer model is assumed. All the quantities are uniform in the Y direction. The fundamental equations governing the macrophysical processes of the evolution of wind components, water vapor content, liquid water content and potential temperature under the influences of vertical turbulent diffusion transfer, turbulent momentum transfer and turbulent energy transfer can be expressed in the following three sets of conservation equations:

(a) Mass conservation equation of the air and diffusion equations for water vapor and liquid water contents

$$\frac{\partial U_x}{\partial x} + \frac{\partial U_z}{\partial z} = 0 \qquad (2\text{-}1)$$

$$\frac{\partial C_{va}}{\partial t} = - U_x \frac{\partial C_{va}}{\partial x} - U_z \frac{\partial C_{va}}{\partial z} + \frac{\partial}{\partial z}\left(K_d \frac{\partial C_{va}}{\partial z}\right) + F_{cv} \qquad (2\text{-}2)$$

$$\frac{\partial C_{wa}}{\partial t} = - U_x \frac{\partial C_{wa}}{\partial x} - U_z \frac{\partial C_{wa}}{\partial z} + \frac{\partial}{\partial z}\left(K_d \frac{\partial C_{wa}}{\partial z}\right)$$

$$+ \frac{\partial}{\partial z}\left(U_t C_{wa}\right) + F_{cw} . \qquad (2\text{-}3)$$

(b) Momentum conservation equations

$$\frac{\partial u_x}{\partial t} = - U_x \frac{\partial u_x}{\partial x} - U_z \frac{\partial u_x}{\partial z} - \frac{1}{\rho} \frac{\partial p}{\partial x} + \frac{\partial}{\partial z} \left(K_m \frac{\partial u_x}{\partial z} \right) + F(U_{gx} - U_x) \quad (2\text{-}4)$$

$$\frac{\partial u_y}{\partial t} = - U_x \frac{\partial u_y}{\partial x} - U_z \frac{\partial u_y}{\partial z} + \frac{\partial}{\partial z} \left(K_m \frac{\partial u_y}{\partial z} \right) + F(U_{gy} - U_y) \quad (2\text{-}5)$$

$$\frac{\partial U_z}{\partial t} = - U_x \frac{\partial U_z}{\partial x} - U_z \frac{\partial U_z}{\partial z} + \frac{\partial}{\partial z} \left(K_m \frac{\partial U_z}{\partial z} \right) + g \left(\frac{\theta - \theta_0}{\theta_0} \right) . \quad (2\text{-}6)$$

(c) Energy conservation equation

$$\frac{\partial \theta}{\partial t} = - U_x \frac{\partial \theta}{\partial x} - U_z \frac{\partial \theta}{\partial z} + \frac{\partial}{\partial z} \left(K_h \frac{\partial \theta}{\partial z} \right)$$

$$+ \frac{1}{\rho C_p} \left(\frac{1000}{P} \right)^{2/7} \left(L F_{ev} \rho - \frac{\partial R_f}{\partial z} \right) \quad (2\text{-}7)$$

where

$$C_{va} = \frac{\rho_v}{\rho} \quad (2\text{-}8)$$

$$C_{wa} = \frac{4\pi}{\rho} \left[\rho_w \sum_i \int_0^\infty N_i(r) r^2 dr - \frac{1}{3} \sum_i \rho_{hi} N_i r_{oi}^3 \right] . \quad (2\text{-}9)$$

Equation (2-1) is the expression of incompressible fluid for the continuity equation of dry air. This expression is true only when the wind velocity is much less than the speed of sound. In this case, the wind velocity up to 100 m altitude is in general less than 10 m s^{-1} which is less than 3% of the speed of sound.

The change of the water droplet radius, in Equation (2-9), due to condensation/evaporation is governed by microphysical processes, and is given by (Carstens et al., 1974)

$$\frac{dr}{dt} = \frac{\rho_{sat}(\infty)\,\rho_{eff}}{\rho_w (r+\ell)} \left(3 - 1 - \frac{a}{r} + \frac{c}{r^3}\right) \qquad (2\text{-}10)$$

where

$$D_{eff}^{-1} = D^{-1} + \left(\frac{bL}{K}\right) \qquad (2\text{-}11)$$

$$\ell = \left(\frac{\ell_\beta}{D} + \frac{\ell_\alpha bL}{K}\right) D_{eff}^{-1} \qquad (2\text{-}12)$$

$$\ell_\alpha = \left(1 - \frac{\alpha}{2}\right) \frac{K}{\alpha p} \frac{\gamma - 1}{\gamma + 1} \left(\frac{8\pi T}{R}\right)^{\frac{1}{2}} \qquad (2\text{-}13)$$

$$\ell_\beta = \left(1 - \frac{\beta}{2}\right) \frac{D}{\beta} \left(\frac{2\pi}{R_v T}\right)^{\frac{1}{2}} \qquad (2\text{-}14)$$

$$a = \frac{2\sigma}{R_v T \rho_w} \qquad (2\text{-}15)$$

$$c = \frac{3iM_w m_s}{4\pi M_s} \quad . \qquad (2\text{-}16)$$

The nucleation process as considered in this paper, more specifically the constants of Equations (2-13) and (2-14), is valid only for pure hygroscopic salts. The overwhelming fraction or urban particulates is hydrocarbon coated or mixed and therefore much less active as a nucleating agent. Therefore, the proper modification is necessary for the model to be applied to the simulation of particular problems associated with urban pollutants as condensation nuclei for fog formation.

In the present study, the diffusivity of water vapor in the air follows the model presented by Fuller et al. (1966)

$$D = \frac{0.001\,(M_a^{-1} + M_v^{-1})^{\frac{1}{2}}\,T^{1.75}}{p\,(V_a^{1/3} + V_v^{1/3})^2} = \frac{11.43\,T^{1.75}}{p} \quad . \qquad (2\text{-}17)$$

The other constants, employed in Equations (2-10) to (2-16) which are temperature dependent can be simplified as follows (Paluch, 1971):

$$K = 0.1675 \times 10^{-6} \ (T - 273.16) + 0.5725 \times 10^{-4} \ (\text{cal/cm-}^{0}\text{K-sec}) \qquad (2\text{-}18)$$

$$L = 737.44 - 0.52 \ T(\text{cal/g}) \qquad (2\text{-}19)$$

$$\sigma = 75.7 - 0.148 \ (T - 273.16) \ (\text{dynes cm}^{-1}). \qquad (2\text{-}20)$$

The semi-empirical expression is used for $\rho_{sat}(\infty)$ and b, i.e.,

$$\rho_{sat}(\infty) = 4.847 \times 10^{-6} \left(\frac{273.16}{T}\right)^{5.7373} \cdot \exp\left[\ 6718. \ \left(\frac{1}{273.16} - \frac{1}{T}\right)\right] \qquad (2\text{-}21)$$

$$b = \rho_{sat}(\infty) \left(\frac{6718}{T} - 5.7373\right) \frac{1}{T} \ . \qquad (2\text{-}22)$$

Equation (2-20) shows how surface tension of thepure water depends on the temperature. A recent study of water droplets exposed to polluted air indicates that the evaporation is greatly different over a surface with pure water than over a surface covered with a monolayer (Hoffer and Mallen, 1970). A Skylab experiment involving water droplets indicated that the surface tension of the water droplet decreased drastically from 72.7 dyne cm^{-1} to less than 50 dyne cm^{-1} at 20°C for droplets contaminated with grape drink and strawberry drink (Hung et al., 1976). Therefore, the decrease in the surface tension of the water droplet exposed to a polluted atmosphere is taken into account. However, the order estimation of two terms in Equation (2-10) between a/r and c/r^3 for the condition of a polluted atmosphere indicates that a/r is at least an order, or more, smaller than c/r^3. This means that the variation of the surface tension is not significant in the fog formation under polluted

atmospheric conditions. Nevertheless, the exposure of the water droplets in a polluted atmosphere makes a surface covered with a monolayer, which drastically decreases the effective diffusion coefficient, $\mathcal{D}$ in equation (2-11), of the water droplet and makes the evaporation rate slow down.

III. STUDY OF THE NUMERICAL SIMULATION

The analysis of the chemical composition of atmospheric aerosols, the large quantities of $SO_4^{=}$, NO_4^{-}, NH_4^{+} and a strong acid such as H_2SO_4 have been detected in highly industrialized areas (Leaderer et al., 1978). Strong evidence exists that the major producer of NO_x has been the automobile. There is no doubt that stationary source fuel combustions also contribute a heavy fraction of the total NO_x emitted to the atmosphere. Fuel-bound nitrogen compounds are ammonia, pyridine, and many other amines (Glassman, 1977). Similar to NO_x production by combustion, sulfer as an inherent impurity in both coal and petroleum, SO_x is also produced through fuel combustion.

There are some very basic differences between the S problem and that posed by the formation of NO_x. The two possible sources of N in any combustion process are either atmospheric or organically bound. S can be present in elemental form, organically bound, or as a species in various inorganic compounds. Once it enters the combustion process it is very reactive with oxidizing species, and similar to fuel N, its conversion to the SO_x is fast compared to the other energy releasing reactions (Glassman, 1977). The great quantity of atmospheric aerosols is thus formed from the pollutants of NO_x and SO_x through the gas-phase photooxidation reaction.

The average mass concentration of aerosol particles from the National Air Sampling Network in the United States ranges from about 20 $\mu g\ m^{-3}$ in clean air in remote areas, to values of 60 to 200 $\mu g\ m^{-3}$ in urban areas (Hidy and Brock, 1971). In the heavily polluted atmosphere of the highly industrialized areas, mass concentration with values as high as 2000 $\mu g\ m^{-3}$, have been reported (Seinfeld, 1975). As for particle number

concentration, it varies from 10^2 particles cm^{-3} in very clean air to 10^5 particles cm^{-3} in polluted air. The radius of condensation nuclei with combustion as a source ranges from 0.01 to 1 μm (Twomey and Warner, 1967).

The average particulates percentage distribution of mass concentration for SO_x is about 18%, and for NO_x it is about 6% (Hidy and Brock, 1971). This means that mass concentration for SO_x is roughly less than 10 $\mu g\ m^{-3}$ in clean air, and ranges from about 20 to 90 $\mu g\ m^{-3}$ in polluted air. The range of mass concentration for NO_x is roughly one-third of the amount of SO_x.

In studying fog droplet formation based on aerosol population, four steps are considered. It can be shown as follows:

Step I. Monodisperse, Single-Component Aerosol Model;

Step II. Monodisperse, Multi-Component Aerosol Model;

Step III. Non-Monodisperse, Single-Component Aerosol Model;

Step IV. Non-Monodisperse, Multi-Component Aerosol Model.

Step I was adopted by Hung et al. (1979) and Hung and Liaw (1979). Step II was considered by Hung and Liaw (1980). In the present study, Step III will be described by Chapter IV, and Step IV will be discussed in Chapter V of this report.

The numerical techniques of the application of macroscopic Equations (2-1) to (2-9), with the inclusion of the evaluation of turbulent diffusion parameters and other related physical parameters for the study of the dynamical behavior of warm fog, are given in Hung and Vaughan (1977). As for the scheme of numerical computation, the method of implicit integration of the finite difference equation was used to solve the governing partial differential equations. In other words, the numerical technique employed is essentially similar to that of Richtmyer (1957). The utilization of microscopic Equations (2-10)-(2-22) in solving the initial stage of the nucleation

and the growth of the water droplets associated with aerosol particles is discussed in Hung and Huckle (1977); while the growth and decay of water droplets in terms of seeding of hygroscopic chemicals and aerosol particles are discussed in Hung et al. (1978).

Recently, Hung et al. (1979) showed that the aerosol particles with the higher number density, larger size nuclei, the heavier mass of the nuclei, and the higher ratio of the Van't Hoff factor to the molecular weight favor the formation of the lower visibility advection fogs with stronger vertical energy transfer during thenucleation andcondensation time period.

The turbulent exchange coefficients employed in this study are based on empirical flux gradient relations. The detailed descriptions are listed in Appendix A.

In this computation, the method of implicit integration of the finite difference equations has been used to solve the governing partial differential equations. The initial values of the wind profile, temperature profile, and the relative humidity use the results of field measurements taken along the California coast by Mack et al. (1973, 1974, 1975). The similar initial values of field measurements had also been used in fog formation studies with detailed descriptions given by Hung et al. (1979).

In the horizontal geometrical X-coordinate, the initial temperature at the ground was 14°C everywhere, and decreased to 12.5°C within one and a half hours linearly at the location of the temperature sink 3 km $\leq x \leq$ 6 km. The source terms of Equations (2-2) and (2-3) were assumed to be zero at time, t = 0; and $F_{cv} = F_{cw}$ at time, $t > 0$. Here, $F_{cw} = \sum F_{cw_i}$, where the subscript i denotes the species of hygroscopic aerosols serving as the condensation nucleus. F_{cw} is computed from the time rate of change of C_{wa} defined in Equation (2-9) with the substitution of the growth of a water droplet radius obtained from microphysical processes based on various

species of hygroscopic aerosols given in Equation (2-10). Thus, the microphysics equation can be coupled with the macrophysical dynamic equations through source and sink terms, F_{cv} and F_{cw}. Reasonably large time steps have been used to obtain a computationally stable solution.

The visibility is computed by using the relation

$$\text{visibility} = \frac{3.912}{\beta} \text{ (m)} \tag{3-1}$$

where β is related to the drop size distribution, N(r), and to Mie scattering efficiency, S_M, which is important for droplets larger than 1 μm, according to

$$\beta = 4\pi \int_0^\infty S_M N(r) r dr. \tag{3-2}$$

S_M is very close to the value unity if the drop size distribution is of the same size. It takes a higher value, exceeding, perhaps 2, with a broad spectrum of the drop size distribution (Mason, 1971). To elucidate the fog optical properties, Low et al. (1978) examined the effects of different spectral shapes and widths on gamma and lognormal distributions with the same liquid water content, and concluded that the drop size distribution greatly affects the result of visibility even though the liquid water content is the same.

Fog is define in terms of visibility. When the distribution of aerosol particles causes the visibility to go below the 1 km range the onset of fog has been determined (Silverman and Weinstein, 1974). In this study, the formation of fog implies that the visibility is below 1000m range.

In this study, the radius of condensation nucleus, r, depends on the relative humidity S, mass of nucleus m_s, and chemical composition in terms of Van't Hoff factor and molecular weight i/M_s, which may be

written (Mason, 1971)

$$\frac{S}{100} = e^{a/r}\left(1 - \frac{c}{r^3}\right) \qquad (3\text{-}3)$$

where a and c are expressed in Equations (2-15) and (2-16), respectively.

In this study, computer program documentation, and Fortran listing of the computer program are described and listed in Appendices B, and C, respectively.

IV. ADVECTION FOG IN A POLLUTED ATMOSPHERE BASED ON MULTI-DISPERSE, SINGLE-COMPONENT MODEL

In the present chapterwe consider multi-disperse particle size distribution as aerosol population in contrast to monodisperse aerosol distribution considered by Hung and Liaw (1980).

Three types of particle size distribution are considered with keeping the total mass concentration as a fixed value. To simplify the calculation, and also to make the comparison of results easier, the combination of three step functions for each distribution is chosen. These three types of particle size distribution are expressed in Figure 1. These distributions can be shown as follows:

(1) Type A Distribution:

$N = 8100$ particles/cm^3, for $r = 0.075$ μm;

$N = 4000$ particles/cm^3, for $r = 0.100$ μm;

$N = 1700$ particles/cm^3, for $r = 0.125$ μm;

(2) Type B Distribution:

$N = 3225$ particles/cm^3, for $r = 0.075$ μm;

$N = 4500$ particles/cm^3, for $r = 0.100$ μm;

$N = 2500$ particles/cm^3, for $r = 0.125$ μm;

(3) Type C Distribution:

$N = 2150$ particles/cm^3, for $r = 0.075$ μm;

$N = 3000$ particles/cm^3, for $r = 0.100$ μm;

$N = 3500$ particles/cm^3, for $r = 0.125$ μm;

where N stands for the number density, and r implies radius of nucleus. The total initial value mass concentration of the aerosol particles as condensation nuclei for Types A, B and C distribution are constant and with a value of 54.9 $\mu g/m^3$. With keeping the mass concentration fixed, the total number of densities of Type A, B and C are 13,800, 10,225,

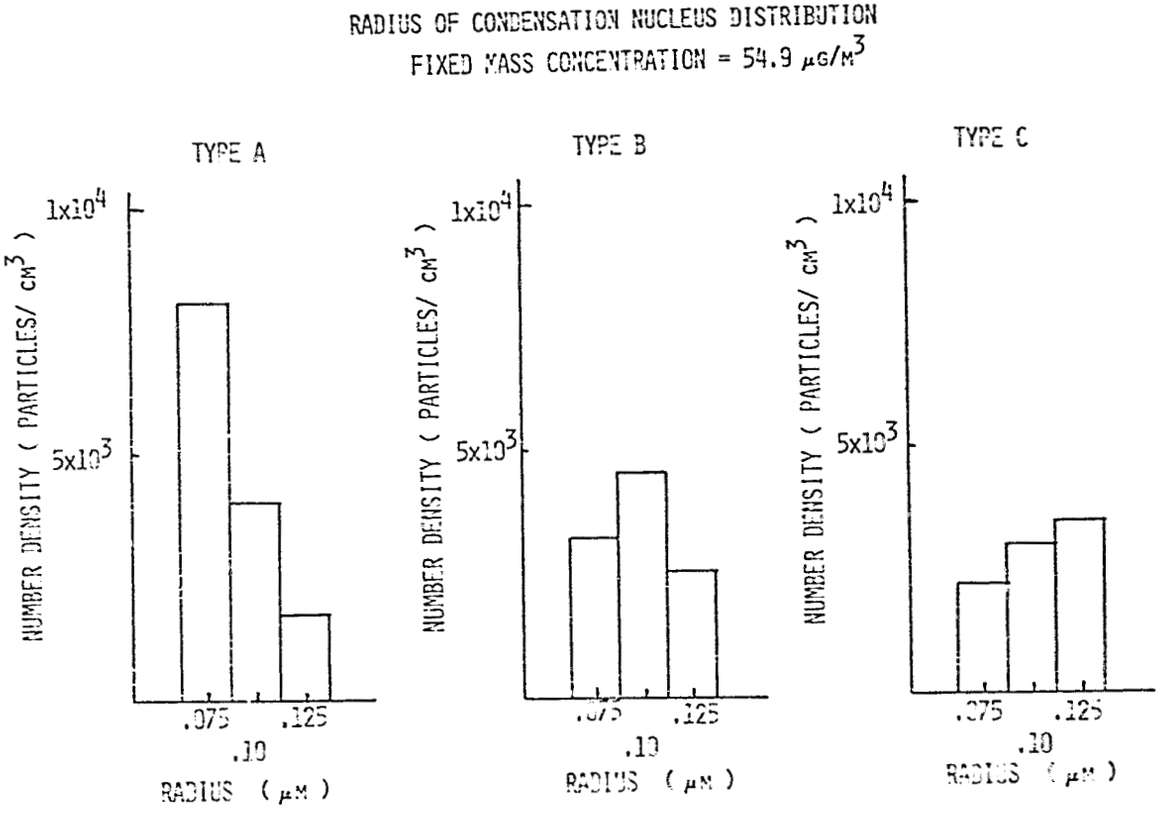

Figure 1. Three types of aerosol population distributions. Each distribution is a combination of three step functions in which the total mass concentration is conserved and equal to 54.9 $\mu g/m^3$.

and 8,650 particles/cm^3, respectively.

Since the pollutant, SO_x, dominates the combustion-related air pollution as indicated by Hidy and Brock (1971). The present study considers the contribution of SO_x as a major condensation nucleus for fog formation, considering the effect of various non-monodisperse distribution aerosol population.

In the present study, the initial values of the wind profile, temperature profile, and the relative humidity use the results of field measurements taken along the California coast by Mack et al. (1973, 1974 and 1975). The similar initial values of field measurements have also been used in fog formation studies, with detailed descriptions, given by Hung et al. (1979).

In this study, the computation was carried out with one hour time coordinate after the fundamental equations were solved simultaneously in conjunction with the initial values adopted from field measurements provided by Mack et al. (1973, 1974 and 1975). The computation of a one hour time coordinate was conducted for the purpose of making all the physical parameters involved in the model self-consistant. In the horizontal geometrical x-coordinate, the initial temperature at the ground was 14^oC everywhere. After a one hour time coordinate computation, the ground temperature decreased one degree linearly in one hour at the location of the horizontal x-coordinate 3 km $\leq x \leq$ 6 km. The result of the time coordinate indicated in this paper, began at the time the ground temperature started to decrease linearly.

Comparison of the degree of fog formation in terms of visibility is made for the variety of aerosol particle size distribution with total mass concentration of aerosols produced by energy-related combustion kept at a constant value. Ammonia sulfate is chosen in this paper as an example of the species of air pollutant SO_x which dominates the combustion-related air pollution as indicated by Hidy and Brock (1971).

Figure 2 illustrates relative humidity and visibility profiles at two horizontal locations, x = 3 and 6 km, and both at vertical location, z = 1 m, of the formation of advection fog associated with type A distribution, shown in Figure 1, of the aerosol as condensation nuclei. Figure 3 shows the similar relative humidity and visibility profiles of the formation of advection fog associated with type A distribution aerosols for different vertical location at z = 4 m, with the same conditions as Figure 2. These two figures show that advection fog with visibility below 1000 m was formed at time t = 52 min. and relative humidity s = 98.6% for altitude z = 1 m; and at time t = 86 min and relative humidity s = 97.8% for altitude z = 4 m associated with type A aerosol particle size distribution.

Similar computations are also accomplished for advection fog formation associated with aerosol particles, $(NH_4)_2SO_4$ as condensation nuclei with size distributions types B and C, as shown in Figure 1. Figures 4 and 5 illustrate similar relative humidity and visibility profiles at two different

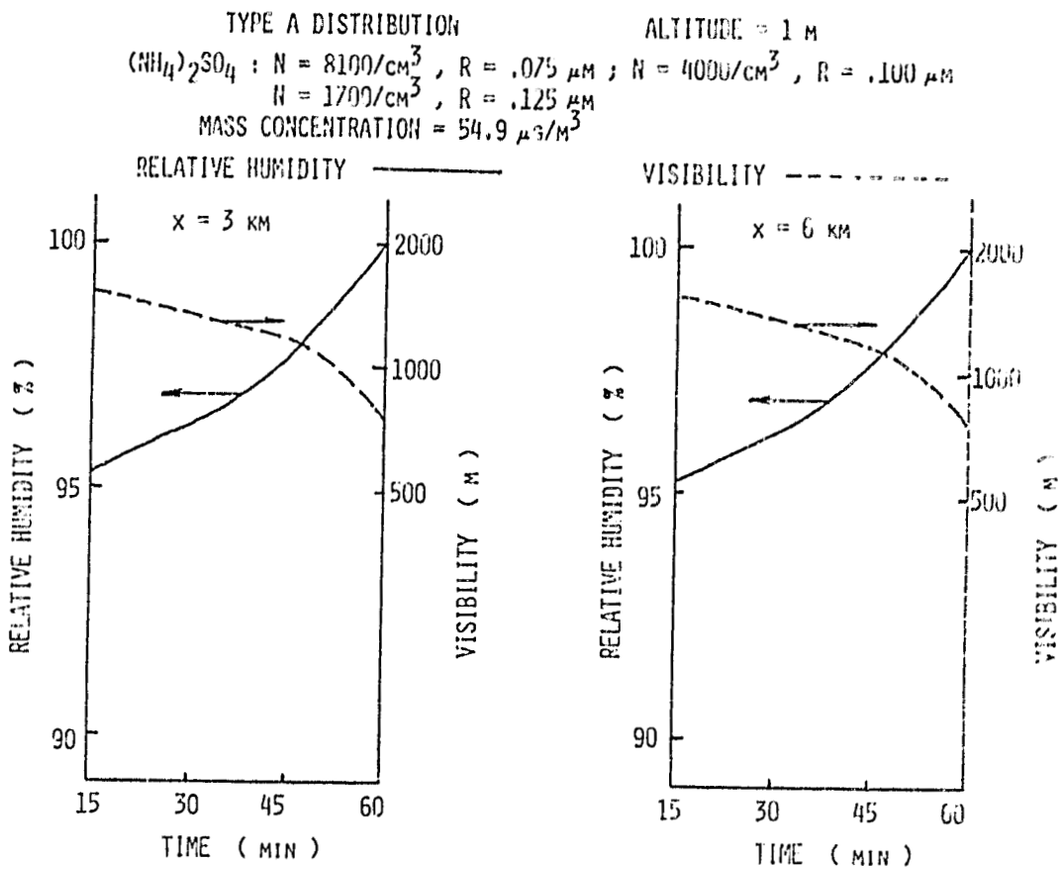

Figure 2. Visibility and relative humidity profiles of fog formation due to condensation nuclei, $(NH_4)_2SO_4$, with type A aerosol population distribution, as shown in Figure 1, at two horizontal locations, x = 3 and 6 km, and both at vertical location, z = 1m.

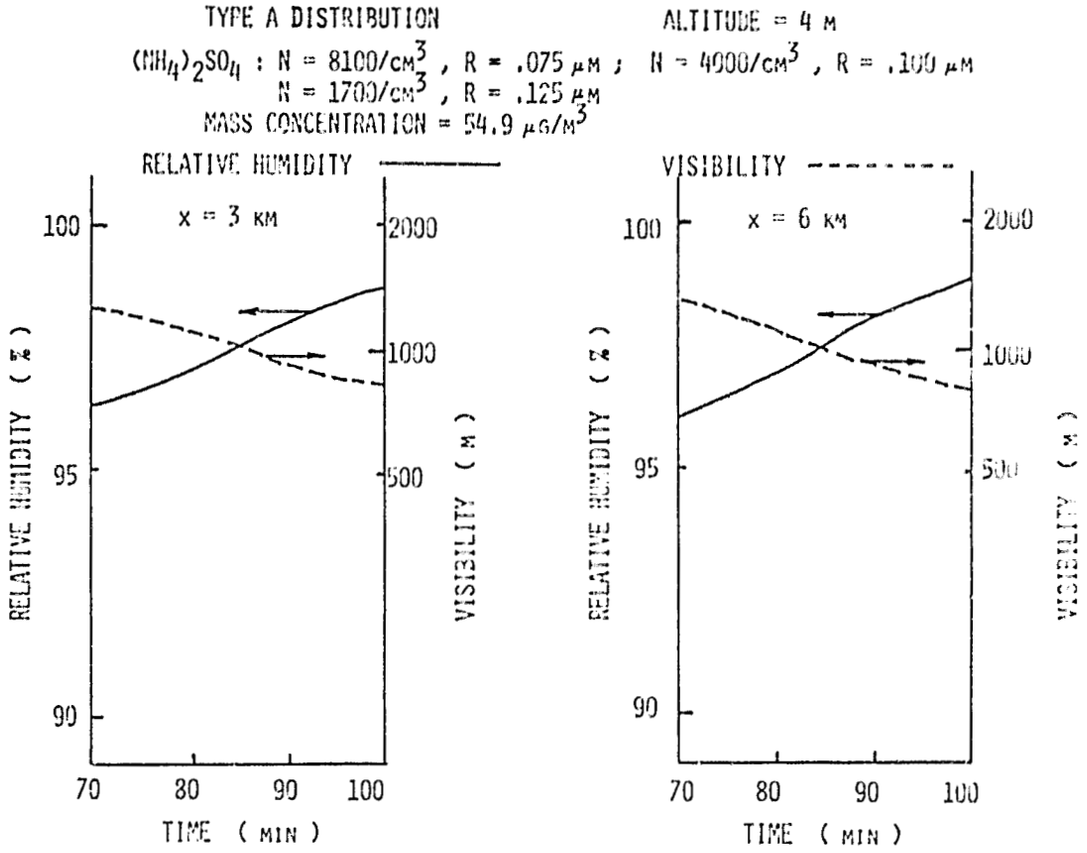

Figure 3. Visibility and relative humidity profiles of fog formation due to condensation nuclei, $(NH_4)_2SO_4$, with type A aerosol population distribution, as shown in Figure 1, at two horizontal locations, x = 3 and 6 km, and both at vertical location, z = 4 m.

altitudes z = 1 and 4 m, respectively, with type B aerosol size distribution, and the rest of the other conditions the same as that of Figure 2 for the formation of advection fog with ammonia sulfate as condensation nuclei. These two figures show that advection fog with visibility below 1000 m was formed at time t = 53 min and relative humidity s = 99.0% for altitude z = 1 m; and at time t = 92 min and relative humidity s = 98.1% for altitude z = 4 m associated with type B aerosol particle size distribution. Comparison between Figures 2 and 4, and Figures 3 and 5 indicate that condensation nuclei with type A distribution initiates the formation of advection fog at least more than 1 min at altitude z = 1 m, and 6 min at altitude z = 4 m earlier than the condensation nuclei with type B distribution in this particular case. Furthermore, relative humidity at which fog starts to form is lower for aerosols as condensation nuclei with type A distribution than type B distribution. By re-examining Figures 1 to 5, it can be concluded that the effect of particle size distribution of aerosols as condensation nuclei is significant enough to affect the degree of fog formation, and also that the distribution with higher particle number and small particle size is more favorable in dense fog formation than the distribution with lower particle number and larger particle size aerosols when the value of mass concentration is kept constant.

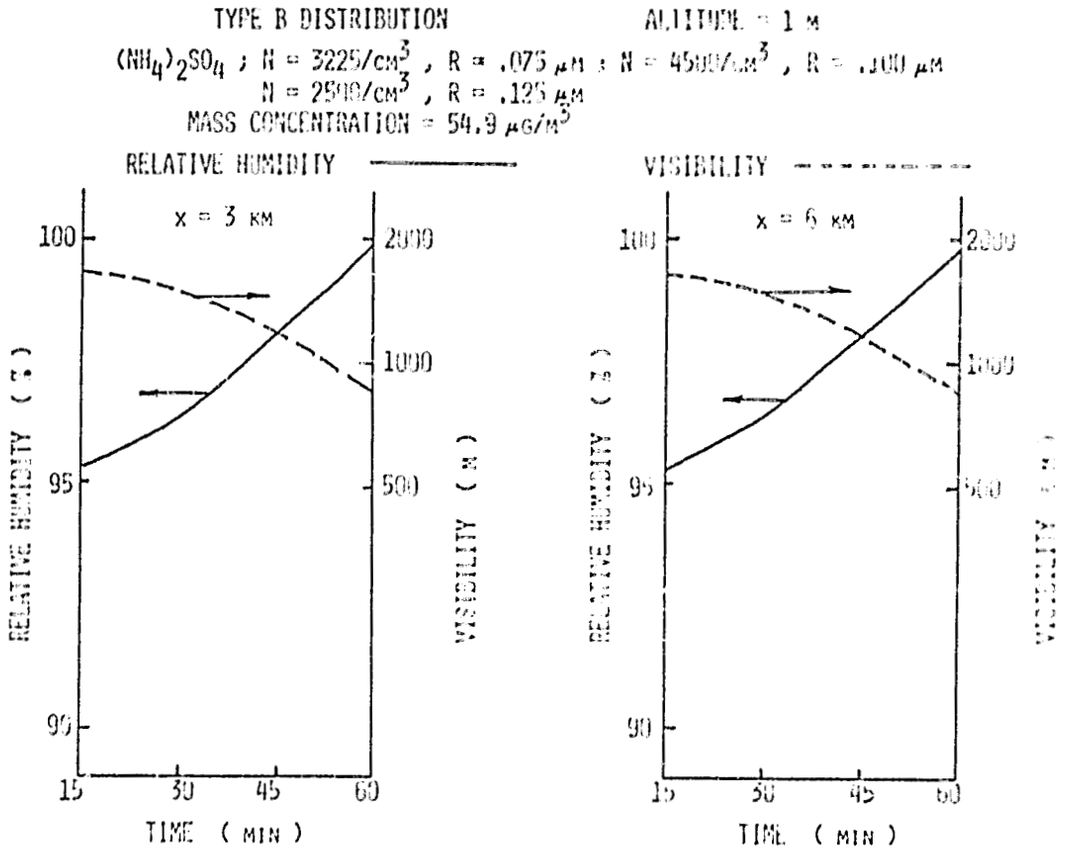

Figure 4. Visibility and relative humidity profiles of fog formation due to condensation nuclei, $(NH_4)_2SO_4$, with type B aerosol population distribution, as shown in Figure 1, at two horizontal locations, x = 3 and 6 km, and both at vertical location, z = 1 m.

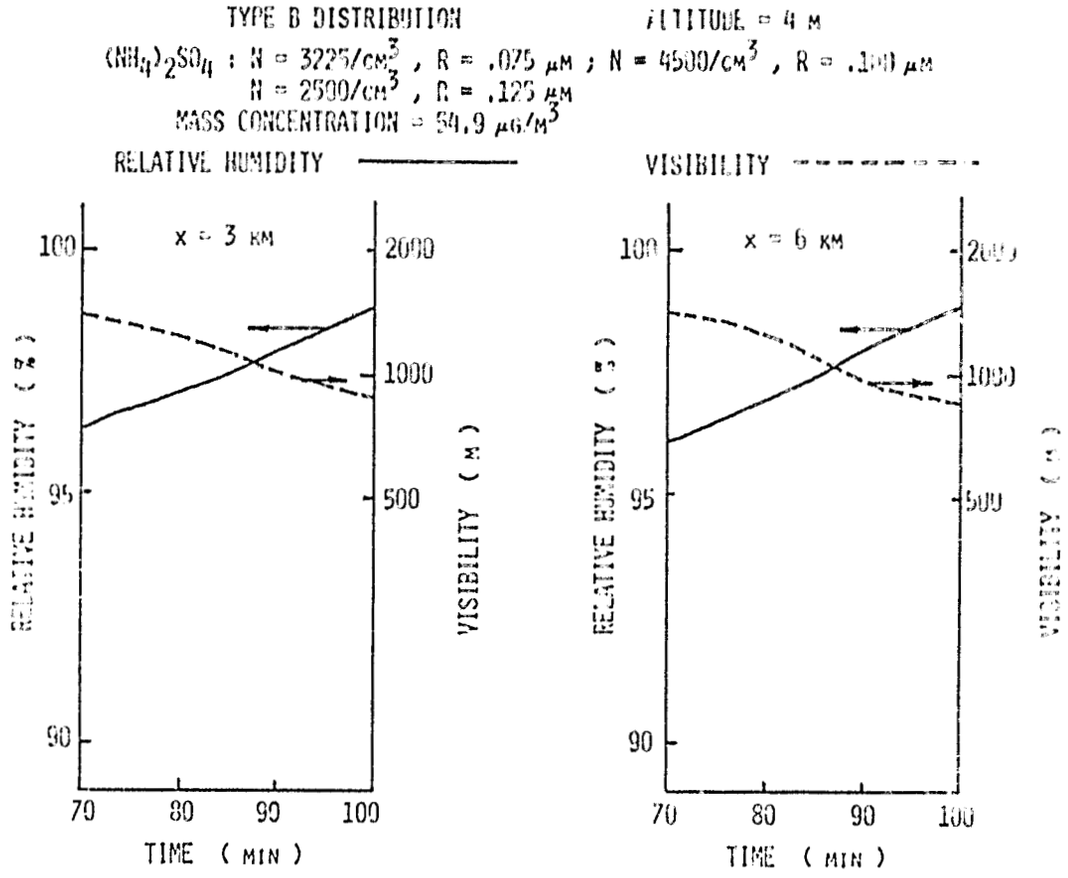

Figure 5. Visibility and relative humidity profiles of fog formation due to condensation nuclei, $(NH_4)_2SO_4$, with type B aerosol population distribution, as shown in Figure 1, at two horizontal locations, x = 3 and 6 km, and both at vertical location, z = 4 m.

As to advection fog formation associated with type C distribution of aerosols as condensation nuclei, Figures 6 and 7 show similar relative humidity and visibility profiles for two different vertical locations, z = 1 and 4 m, respectively, with the same conditions as Figures 2 and 4, except the different particle size distribution as indicated. These two figures again show that advection fog with visibility below 1000 m was formed at t = 55.5 min and relative humidity s = 99.5% for altitude at z = 1 m; and at time t = 94 min and relative humidity s = 96.5% for altitude at z = 4 m. In comparison with Figures 2, 4 and 6, the results show that condensation nuclei with type A distribution initiates the formation of advection fog at least more than 3.5 min; and type B distribution, at least more than 2.5 min earlier than the condensation nuclei with type C distribution at altitude z = 1 m in this particular case. For the altitude z = 4 m in comparison with Figures 3, 5 and 7, the results show that condensation nuclei with type A distribution initiates the formation of advection fog at least more than 8 min; and type B distribution, at least more than 2 min earlier than the condensation nuclei with type C distribution in this particular case. Furthermore, relative humidity at which fog starts to form is lower for aerosols as condensation nuclei with type A distribution than type B distribution, which are in turn lower than type C distribution.

Among the effects of air pollution on atmospheric properties, the most noticeable effect is perhaps the reduction in visibility, with and without the occurrence of condensation. The series of the present study is particularly interested in how aerosols, produced by energy-related combustion, as condensation nuclei affect the formation of advection

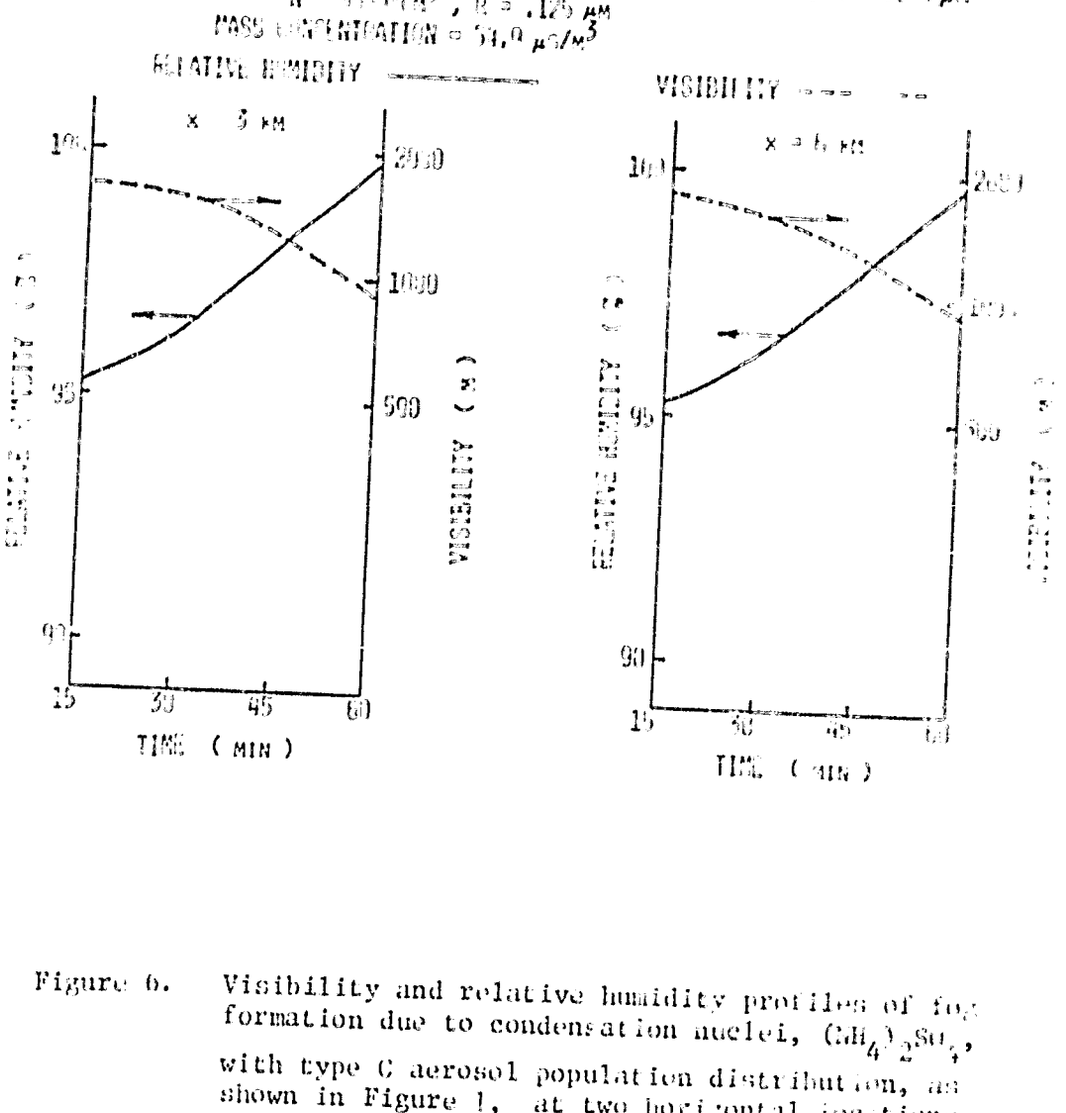

Figure 6. Visibility and relative humidity profiles of fog formation due to condensation nuclei, $(NH_4)_2SO_4$, with type C aerosol population distribution, as shown in Figure 1, at two horizontal locations, x = 3 and 6 km, and both at vertical location, z = 1 m.

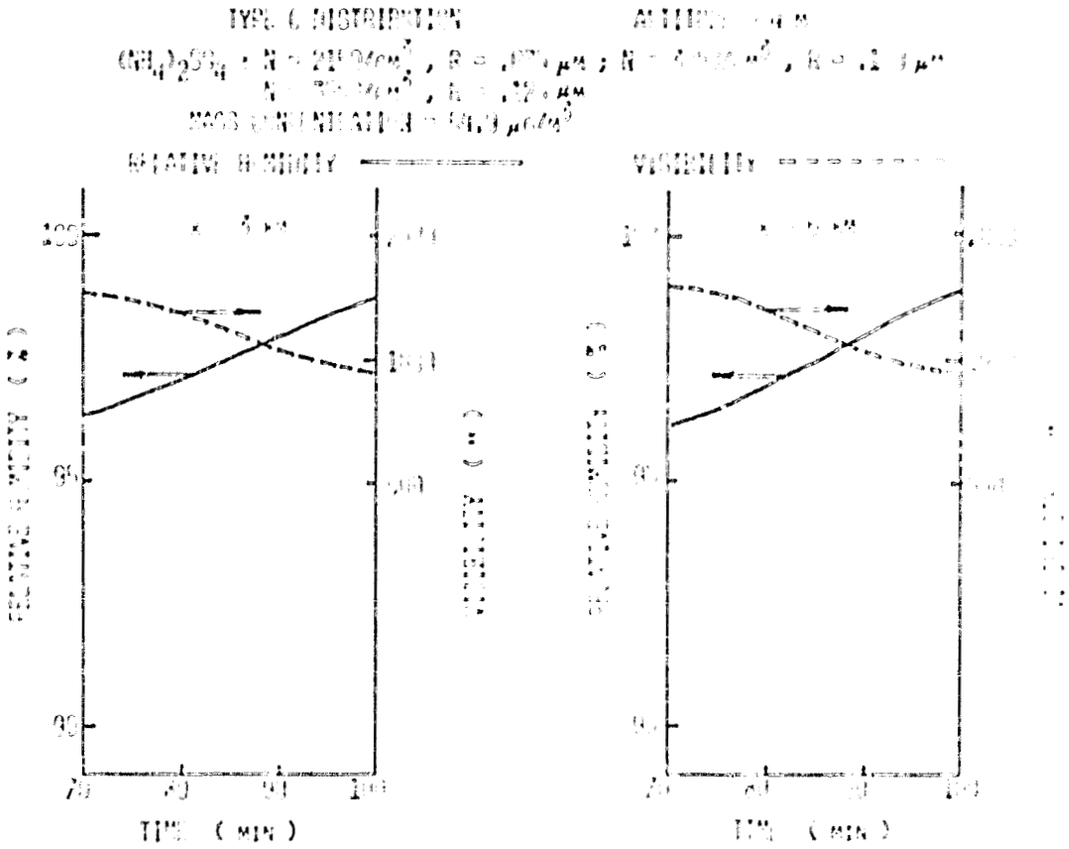

Figure 7. Visibility and relative humidity profiles of fog formation due to condensation nuclei, $(NH_4)_2SO_4$, with type C aerosol population distribution, as shown in Figure 1, at two horizontal locations, x = 3 and 6 km, and both at vertical location, z = 4 m.

fog. Hung and Liaw (1980) showed that the greater the mass concentration, the particle concentration, and the size of the radius of condensation nuclei, the denser the fog is that is formed. However, by using the monodipserse distribution model, Hung and Liaw (1980) indicates that the particle concentration, rather than the size of the radius of nuclei provides greater contribution to the formation of fog, if the value of mass concentration is kept constant.

Observation shows that particle size distribution for combustion related aerosols are widely spread rather than monodisperse distribution. The results given in this study are based on multi-disperse distribution which is the combination of the three step functions for each distribution, and a single component aerosol model. The following conclusions resulted from the present study:

(1) Aerosol distribution with higher particle concentration, rather than the size of aerosol nuclei, support a greater contribution to the formation of fog, if the value of mass concentration is kept constant.

(2) Relative humidity, at which advection fog with visibility below 000 m is formed, is lower for aerosols of distribution with the higher particle concentration, which is in turn the smaller size of aerosol nuclei, than lower particle concentration, which is in turn the larger size aerosol nuclei, if the value of mass concentration is kept constant.

(3) Aerosol population with high particle concentration-shifted distribution [see Figure 8(a)] provides more favorable conditions for the formation of dense fog than the aerosol population with low particle concentration-shifted distribution [see Figure 8(b) for description].

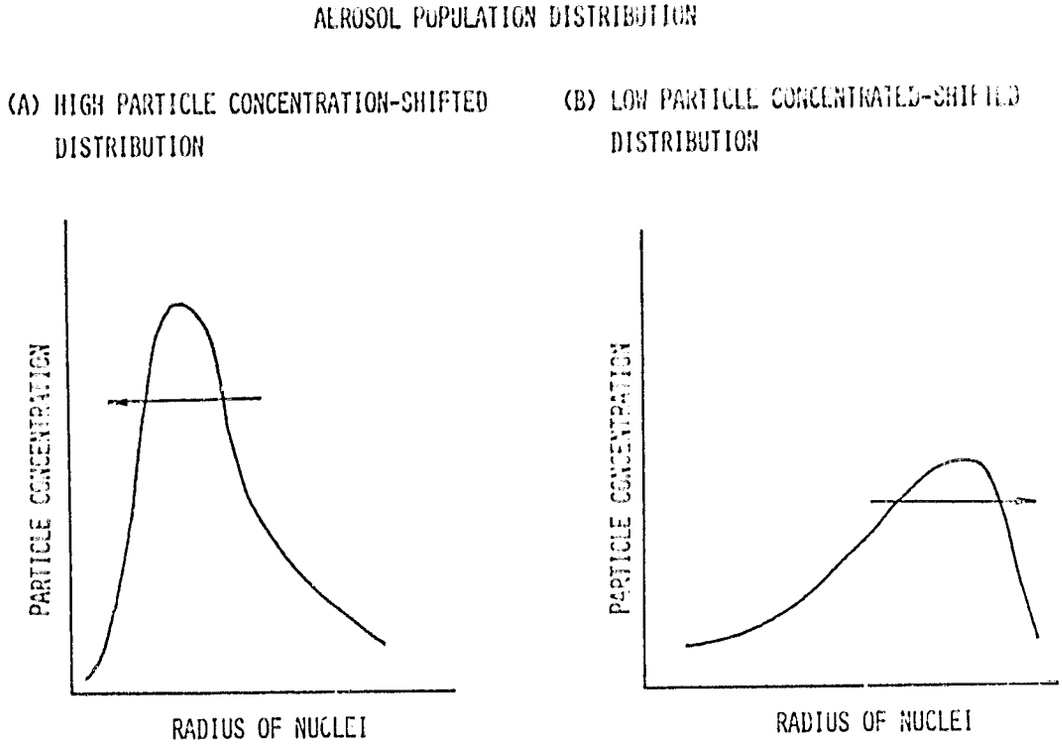

Figure 8. Aerosol population distribution with a fixed value of mass concentration: (a) High particle concentration - shifted distribution; (b) Low particle concentration - shifted distribution.

V. ADVECTION FOG IN A POLLUTED ATMOSPHERE BASED ON A MULTI-DISPERSE, MULTI-COMPONENT MODEL

In contrast to monodisperse aerosol distribution considered by Hung and Liaw (1980), the present chapter adopts multi-disperse particle size distribution as the aerosol population and the multi-component aerosol model to investigate the behavior of fog formation.

For each different species, three types of particle size distributions are considered with keeping the total mass concentration of the aerosol particles as a constant value. To simplify the calculation, and also to make the comparison of the results easier, a combination of the three step functions for each distribution is chosen. Two components of pollutants, $(NH_4)_2SO_4$ and $Ca(NO_3)_2$, each component with three types of particle size distribution, are expressed in Figure 9. The total mass concentration for each component of pollutants is fixed. They are 54.9 and 18.3 $\mu g/m^3$ for $(NH_4)_2SO_4$ and $Ca(NO_3)_2$, respectively. The range of mass concentration for $Ca(NO_3)_2$ is roughly one-third of the amount of $(NH_4)_2SO_4$. These distributions can be shown as follows:

(1) Type A Distribution

$(NH_4)_2SO_4$ N = 8100 particles/cm^3, for r = 0.075 μm

N = 4000 particles/cm^3, for r = 0.100 μm

N = 1700 particles/cm^3, for r = 0.125 μm

$Ca(NO_3)_2$ N = 1800 particles/cm^3, for r = 0.075 μm

N = 1250 particles/cm^3, for r = 0.100 μm

N = 600 particles/cm^3, for r = 0.125 μm

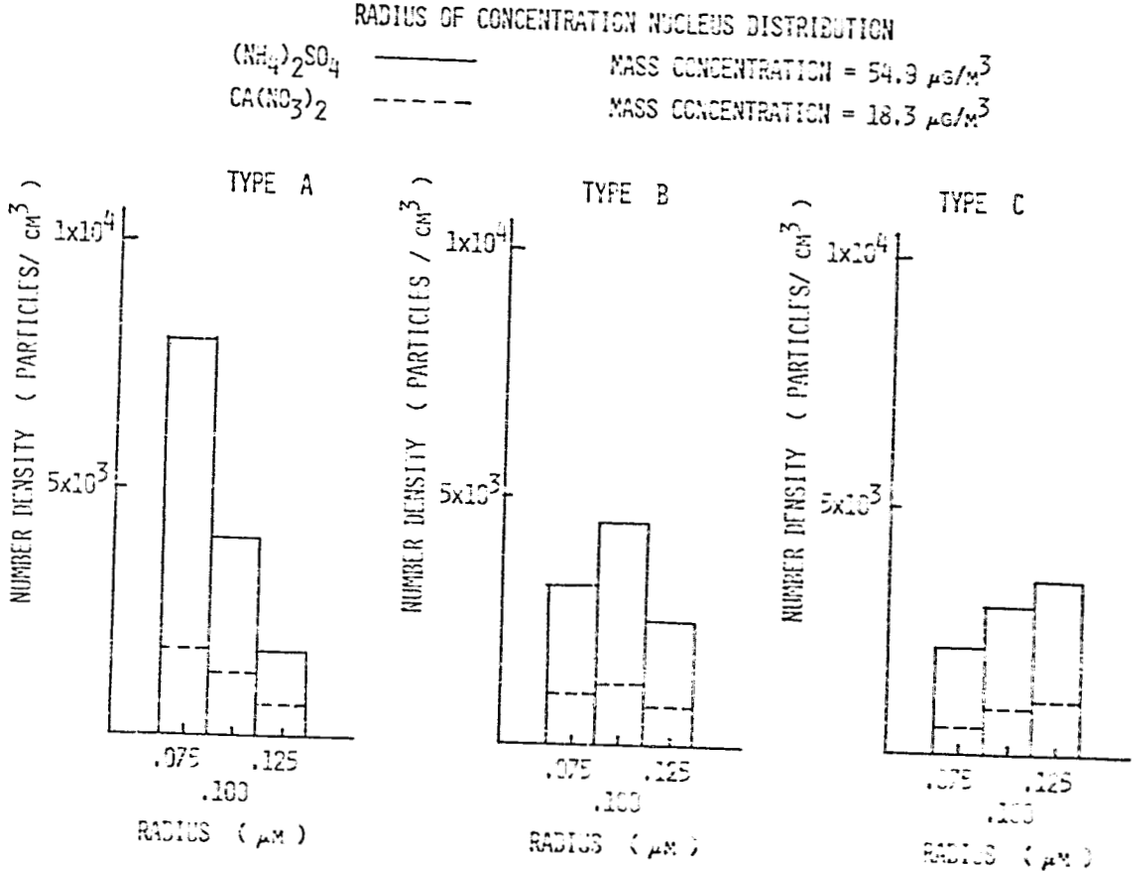

Figure 9. Three types of aerosol population distribution. Each distribution is a combination of three step functions in which the total mass concentration are conserved and equal to 54.9 $\mu g/m^3$, for $(NH_4)_2SO_4$, and 18.3 $\mu g/m^3$ for $Ca(NO_3)_2$. The solid line denotes the distribution for $(NH_4)_2SO_4$, and the broken line implies the distribution for $Ca(NO_3)_2$.

(2) Type B Distribution

$(NH_4)_2SO_4$ N = 3225 particles/cm^3, for r = 0.075 μm

N = 4500 particles/cm^3, for r = 0.100 μm

N = 2500 particles/cm^3, for r = 0.125 μm

$Ca(NO_3)_2$ N = 1000 particles/cm^3, for r = 0.075 μm

N = 1200 particles/cm^3, for r = 0.100 μm

N = 800 particles/cm^3, for r = 0.125 μm

(3) Type C Distribution

$(NH_4)_2SO_4$ N = 2150 particles/cm^3, for r = 0.075 μm

N = 3000 particles/cm^3, for r = 0.100 μm

N = 3500 particles/cm^3, for r = 0.125 μm

$Ca(NO_3)_2$ N = 550 particles/cm^3, for r = 0.075 μm

N = 900 particles/cm^3, for r = 0.100 μm

N = 1050 particles/cm^3, for r = 0.125 μm

where N stands for the number density, and r implies radius of nucleus. In Figure 9, the solid lines express the particle size distribution for $(NH_4)_2SO_4$; and the broken lines show the particle size distribution for $CA(NO_3)_2$. With keeping mass concentration fixed, the total number densities of $(NH_4)_2SO_4$ for Types A, B, and C are 13,800, 10,225 and 8,650 particles/cm^3, respectively; and the number densities of $Ca(NO_3)_2$ for Types A, B, and C are 3,650, 3,000, and 2,500 particles/cm^3, respectively.

In the present study, the initial values of the wind profile, temperature profile, and the relative humidity use the results of field measurements taken along the California coast by Mack et al. (1973, 1974 and 1975). Similar initial values of field measurements have also been used in fog formation studies, with detailed descriptions, given by Hung et al. (1979).

The numerical study of the application of macroscopic equations, as shown in Equations (2-1)-(2-9), with the inclusion of the evaluation of turbulent diffusion parameters and other related physical parameters for the study of the dynamical behavior of warm fog, is given by Hung and Vaughan (1977). As for the scheme of numerical computation, the method of implicit integration of the finite difference equation was used to solve the governing partial differential equations. In other words, the numerical technique employed is essentially similar to that of Richtmyer (1967). The utilization of microscopic equations in solving the initial stage of the nucleation and the growth of the water droplets associated with aerosol particles is discussed in Hung and Huckle (1977); while the growth and decay of water droplets in terms of seeding of hygroscopic chemicals and aerosol particles is discussed in Hung et al. (1978). Mathematical expressions of the computation of the visibility of fog from the drop size distribution of the water drop spectrum, are given in Hung et al. (1979).

For the purpose of making all the physical parameters involved in this model self-consistant, the computation of a one hour time coordinate was conducted after the fundamental equations were solved simultaneously in conjunction with the initial value adopted from field measurements provided by Mack et al. (1973, 1974 and 1975). In the horizontal geometrical x-coordinate, the initial temperature at the ground was 14°C everywhere. After a one hour time coordinate computation, the ground temperature decreased one degree linearly in one hour at the location of the horizontal x-coordinate 3 km $\leq$ x $\leq$ 6 km. The results of the time coordinate indicated in this paper, again, began at the time the ground temperature started to decrease linearly.

Comparison of the degree of fog formation in terms of visibility is made for a variety of aerosol particle size distribution for multi-component species with the total mass concentration for each species of aerosols produced by energy-related combustion kept at a constant value. Both ammonia sulfate and calcium nitrate are chosen as the example of the species of air pollutants SO_x and NO_x which dominate the combustion-related air pollution as indicated by Hidy and Brock (1971).

Figure 10 illustrates relative humidity and visibility profiles at two horizontal locations, x = 3 and 6 km, and both at the vertical location z = 1 m, of the formation of advection fog associated with type A distribution, as shown in Figure 9 of the aerosol as condensation nuclei. Figure 11 shows a similar relative humidity and visibility profiles of the formation of advection fog associated with type A distribution aerosols for different vertical locations at z = 4 m, with the same conditions as Figure 10. These two figures show that advection fog with visibility below 1000 m was formed at time t = 26 min and relative humidity S = 96.1% for altitude z = 1 m; and at time t = 51 min and relative humidity S = 95.6% for altitude z = 4 m associated with type A aerosol particle size distribution.

Similar computations are also accomplished for advection for formation associated with two-component aerosols, $(NH_4)_2SO_4$ and $Ca(NO_3)_2$, as condensation nuclei with size distributions of types B and C, as shown in Figure 9. Figures 12 and 13 illustrate similar relative humidity and visibility profiles at two different altitudes z = 1 and 4 m, respectively, with type B aerosol size distribution, and the rest of the other conditions the same as that of Figure 10 for the formation of advection fog with both ammonia sulfate and calcium nitrate as condensation nuclei. These two

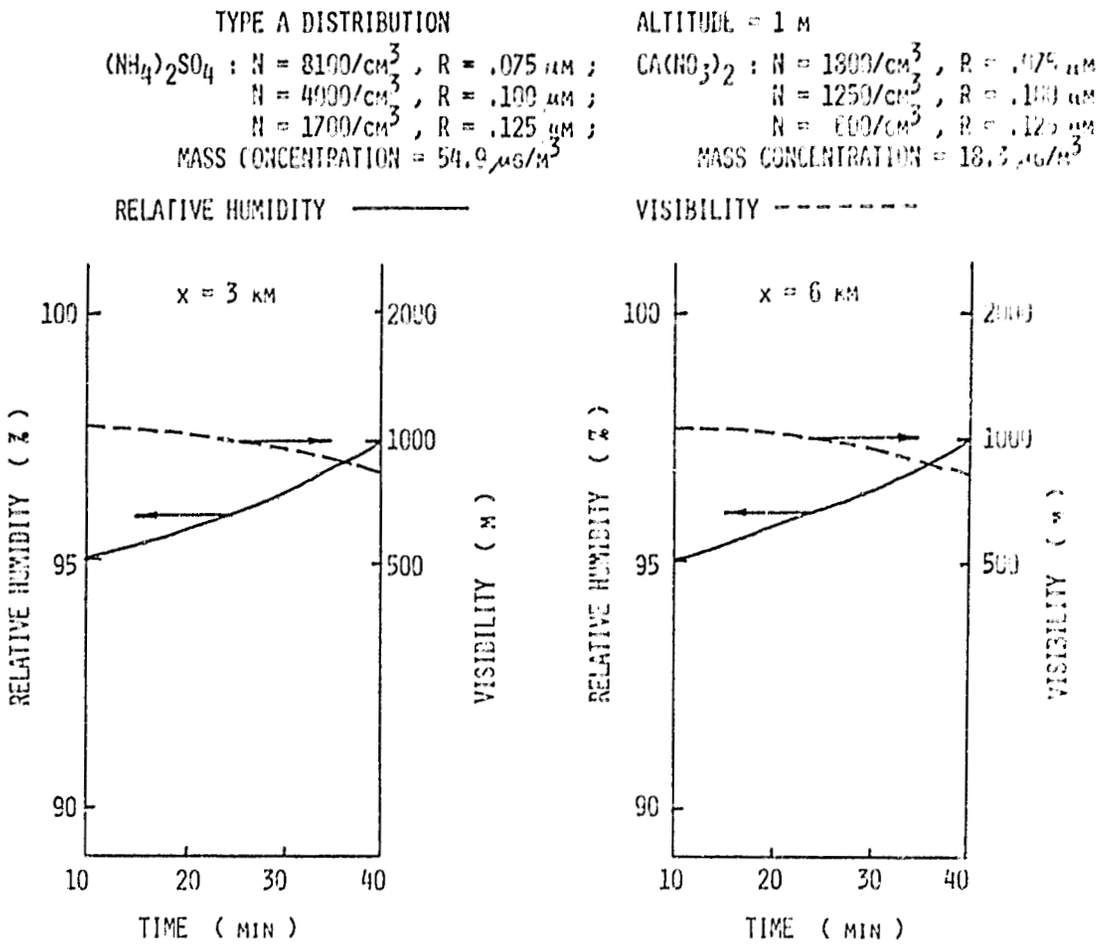

Figure 10. Visibility and relative humidity profiles of fog formation due to condensation nuclei, $(NH_4)_2SO_4$ and $Ca(NO_3)_2$, with type A aerosol population distribution, as shown in Figure 9, at two horizontal locations, x = 3 and 6 km, and both at vertical location, z = 1m.

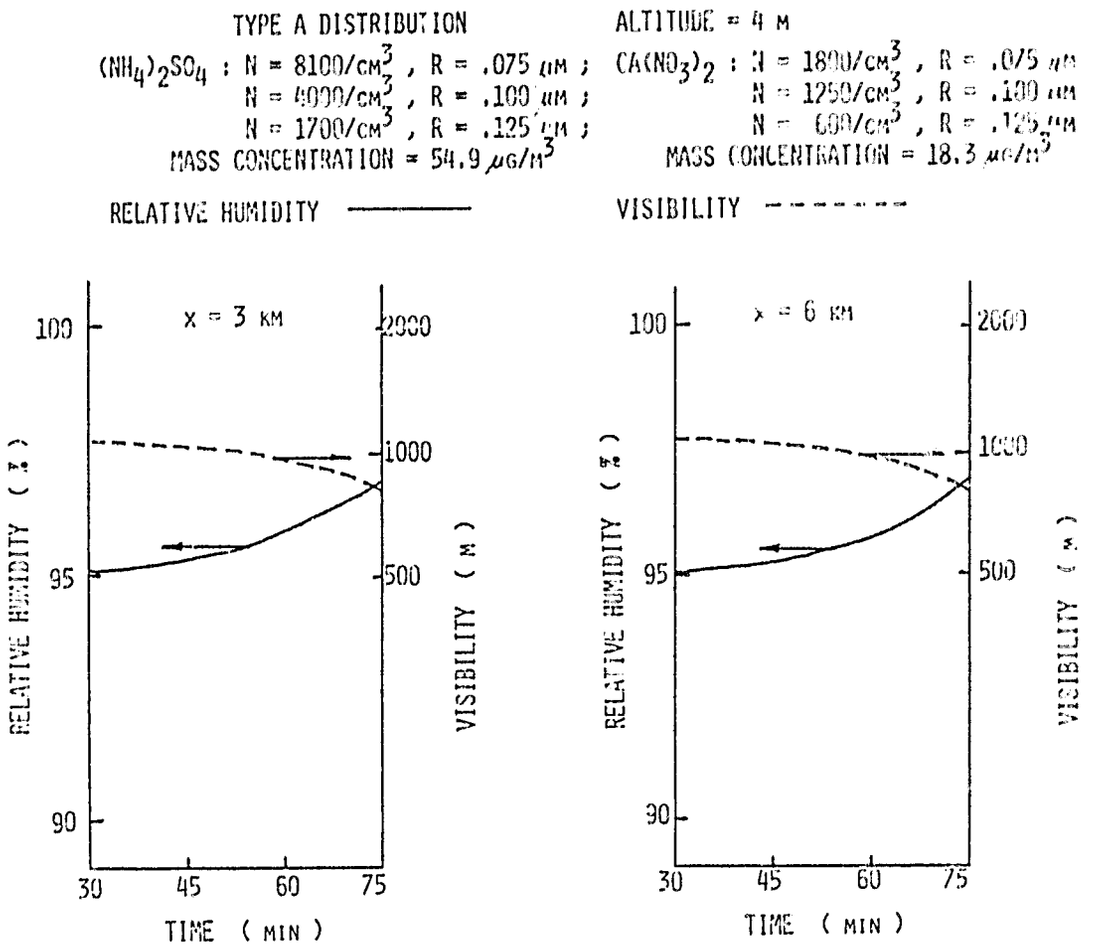

Figure 11. Visibility and relative humidity profiles of fog formation due to condensation nuclei, $(NH_4)_2SO_4$ and $Ca(NO_3)_2$, with type A aerosol population distribution, as shown in Figure 9, at two horizontal locations, x = 3 and 6 km, and both at vertical location, z = 4m.

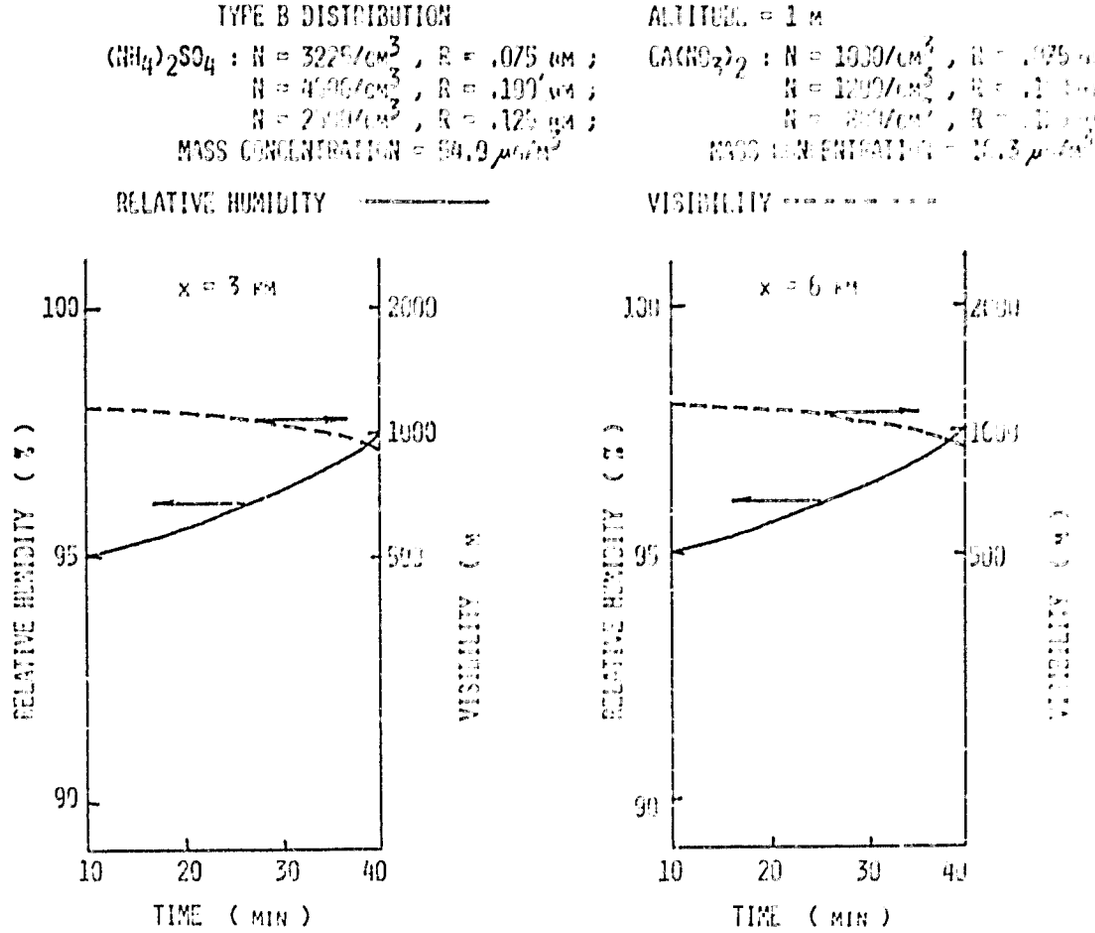

Figure 12. Visibility and relative humidicy profiles of fog formation due to condensation nuclei, $(NH_4)_2SO_4$ and $Ca(NO_3)_2$, with type B aerosol population distribution, as shown in Figure 9, at two horizontal locations, x = 3 and 6 km, and both at vertical location, z = 1m.

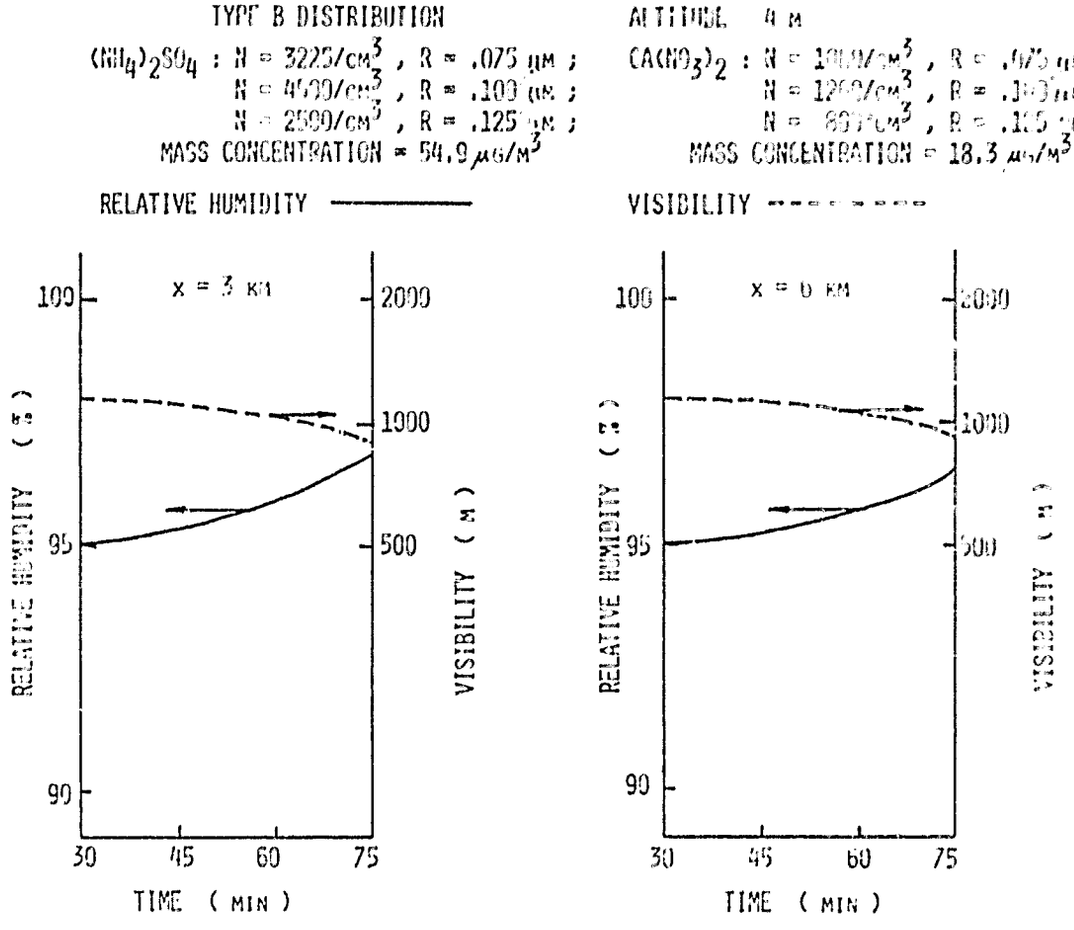

Figure 13. Visibility and relative humidity profiles of fog formation due to condensation nuclei, $(NH_4)_2SO_4$ and $Ca(NO_3)_2$, with type B aerosol population distribution, as shown in Figure 9, at two horizontal locations, x = 3 and 6 km, and both at vertical location, z = 4m.

figures show that advection fog with visibility below 1000 m was formed at time t = 96.0 min and relative humidity S = 97.0 for altitude z = 1 m; and at time t = 67 min and relative humidity S = 96.2 for altitude z = 4 m, associated with type B aerosol particle size distribution. Comparisons between Figures 10 and 12 and Figures 11 and 13 indicate that condensation nuclei with type A distribution imitates the formation of advection fog at least more than 10 min at altitude z = 1 m, and 16 min at altitude z = 4 m earlier than the condensation nuclei with type B distribution in this particular case. Furthermore, relative humidity at which fog starts to form is lower for aerosols as condensation nuclei with type A distribution than type B distribution. By re-examining Figures 1-5, it can be concluded that the effect of the particle size distribution of the aerosols as condensation nuclei is significant enough to affect the degree of fog formation and also that the distribution with a higher particle number and a smaller particle size is more favorable in dense fog formation than distribution with a lower particle number and larger particle size aerosols when the value of mass concentration is kept constant. This result further confirms the computation obtained for the various aerosol size distributions with the single-component model. Comparisons between single-component and multi-component models show that the multi-component model definitely enhances the dense fog formation more than the single-component model.

As to advection fog formation associated with type C distribution of aerosols as condensation nuclei, Figures 14 and 15 show similar relative humidity and visibility profiles for two different vertical locations, z = 1 and 4 m, respectively, with the same conditions as Figures 10 and 11

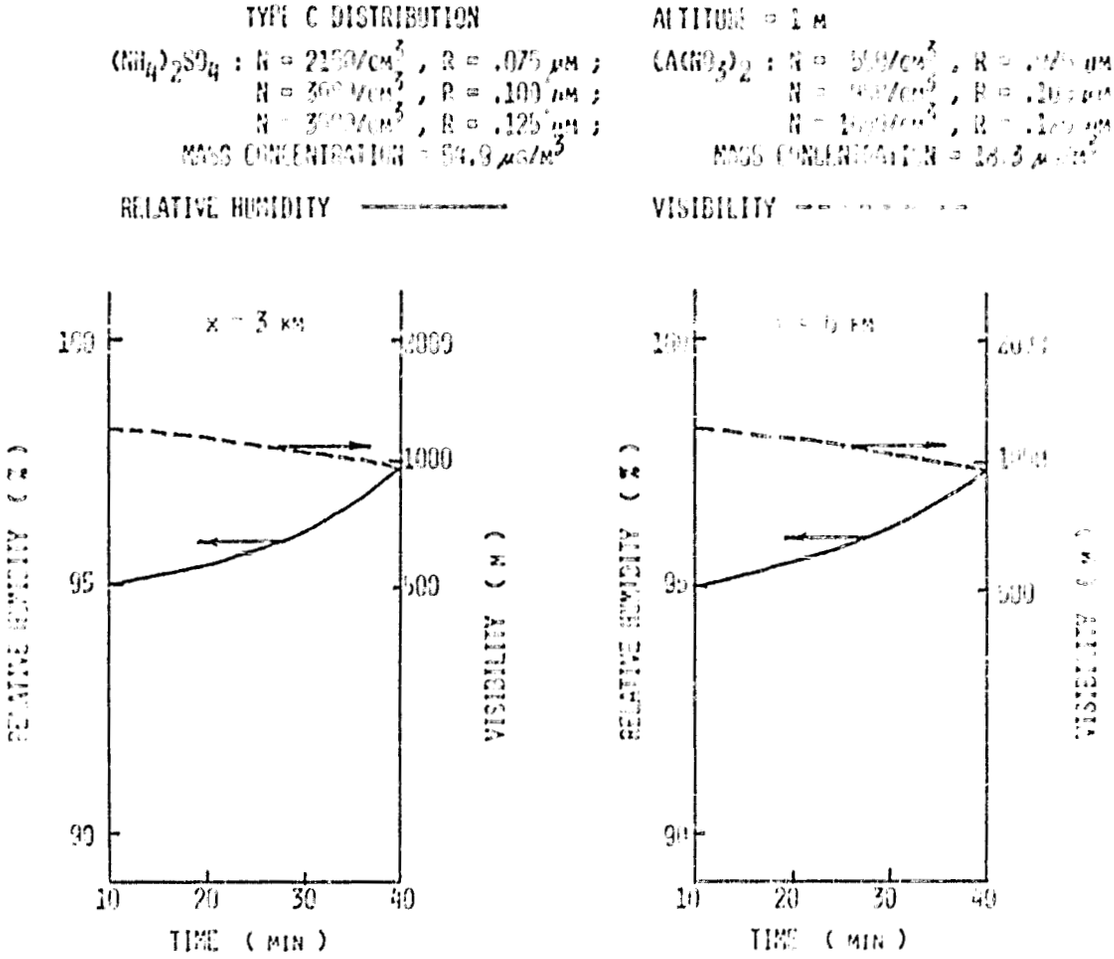

Figure 14. Visibility and relative humidity profiles of fog formation due to condensation nuclei, $(NH_4)_2SO_4$ and $Ca(NO_3)_2$, with type C aerosol population distribution, as shown in Figure 9, at two horizontal locations, x = 3 and 6 km, and both at vertical location, z = 1m.

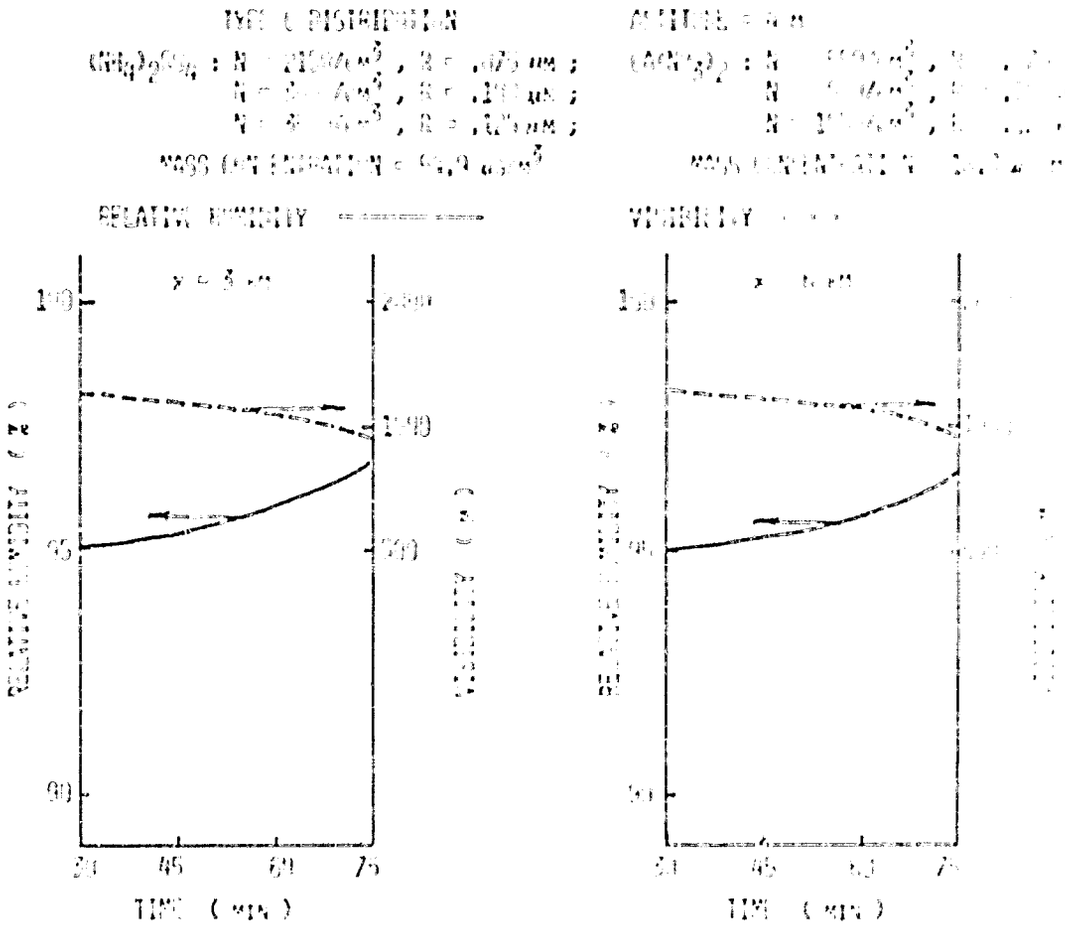

Figure 15. Visibility and relative humidity profiles of fog formation due to condensation nuclei, $(NH_4)_2SO_4$ and $Ca(NO_3)_2$, with type C aerosol population distribution, as shown in Figure 9, at two horizontal locations, x = 4 and 6 km, and both at vertical location, z = 4m.

with the exception of the different particle size distribution as indicated. These two figures again show that advection fog with visibility below 1000 m was formed at t = 38 min and relative humidity S = 97.2% for altitude at z = 1 m; and at time t = 71 min and relative humidity S = 96.4% for altitude at z = 4 m. In comparison with Figures 10, 12 and 14, the results show that condensation nuclei with type A distribution initiates the formation of advection fog at least more than 12 min; and type B distribution, at least more than 2 min earlier than the condensation nuclei with type C distribution at altitude z = 1 m, in this particular case. For the altitude z = 4 m, in comparison with Figures 11, 13 and 15, the results show that condensation nuclei with type A distribution initiates the formation of advection fog at least more than 20 min, and type B distribution, at least more than 4 min earlier than the condensation nuclei with type C distribution in this particular case. Furthermore, the relative humidity at which fog starts to form is lower for aerosols as condensation nuclei with type A distribution, than type B distribution, which in turn, is lower than type C distribution.

The results given in this chapter are obtained from multi-disperse distribution, which is the combination of three step functions for each distribution, and a multi-component aerosol model. The following conclusions resulted:

(1) Aerosol distribution with a higher number density, rather than the greater size of aerosol nuclei, produce a more favorable contribution to the formation of lower visibility of fog, if the value of mass concentration of aerosols is kept constant.

(2) Relative humidity, at which advection fog with visibility below

1000 m is formed, is lower for aerosols of distribution with a higher particle concentration if the value of mass concentration of aerosols is kept constant.

(3) In addition to the contribution made by SO_x which dominates the air pollution produced by energy-related combustion, NO_x, which is roughly one-third of the amount of SO_x, provides a considerable contribution to fog formation, and is important enough to be included in the fog formation prediction.

VI. LIQUID WATER CONTENT RESULTING FROM CONDENSATION EFFECTS

The mathematical simulation of the formation of advection fog based on the multi-disperse distribution of the aerosol population shows that the aerosol distribution with a higher number density, rather than greater size of aerosol nuclei, produce more favorable conditions for the formation of denser fog, if the value of mass concentration of the aerosol particles is kept constant. It is of considerable interest to study the liquid water content resulting from the effects of the condensation processes in which the aerosol particles with a variety of distribution functions are taken into consideration. The results of liquid water content are very important in the study of the acid rain problem.

A growing body of evidence suggests that acid rain may have substantial adverse effects on the environment. Such effects include acidification of lakes, rivers, and groundwaters, with resultant damage to fish and other components of the aquatic ecosystem; acidification and demineralization of soils; reduction of forest productivity; damage to crops; and deterioration of man-made materials. These effects may be cumulative or may result from peak acidity episodes. The study of liquid water content due to condensation processes associated with SO_x and NO_x as condensation nuclei of multi-disperse distribution may be beneficial to the study of potentially impacted ecosystems due to acid rain.

With the same initial and boundary conditions we considered in the previous section, the time dependent liquid water contents were calculated with types A, B and C particle size distributions, as shown in Figure 9 for $(NH_4)_2SO_4$ and $Ca(NO_3)_2$ as two major components of the aerosol particles as condensation nuclei. Figure 16 illustrates the time change of the

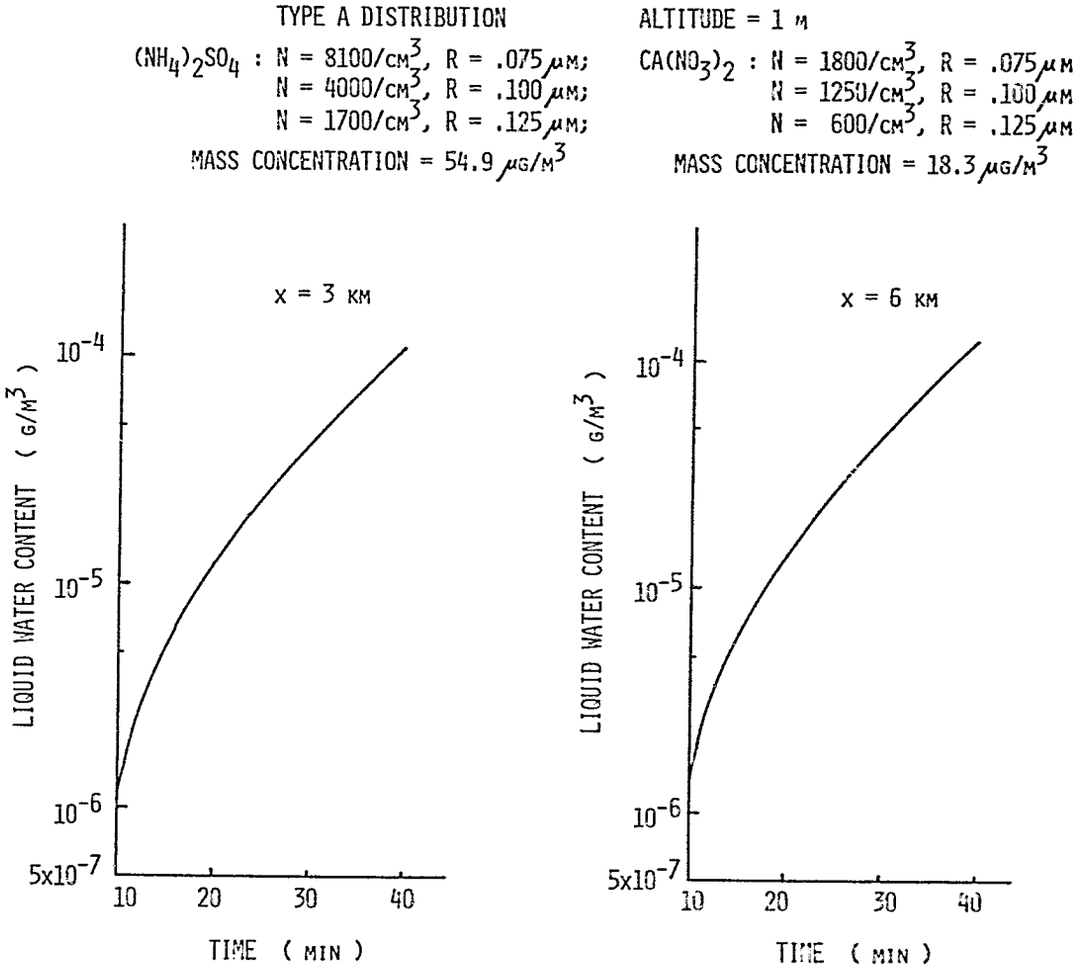

Figure 16. Time rate of change of the amount of liquid water content associated with condensation nuclei, $(NH_4)_2SO_4$ and $Ca(NO_3)_2$, with type A aerosol population distribution, as shown in Figure 9, at two horizontal locations, x = 3 and 6 km, and both at vertical location, z = 1 m.

increase of the liquid water contents at two horizontal locations, x = 3 and 6 km, and both at the vertical location z = 1 m, of the formation of atmospheric acid deposition of wet removal processes associated with type A distribution of aerosol as condensation nuclei. Figure 17 shows a similar time change of the increase of the liquid water content of the formation of acidic deposition of wet removal processes associated with type A distribution aerosols for different vertical locations at z = 4 m, with the same condition as Figure 16. These two figures show that acidic deposition of the liquid water content becomes 102 $\mu g/m^3$ at time t = 40 min for altitude z = 1 m; and 130 $\mu g/m^3$ at time t = 75 min for altitude z = 4 m associated with type A aerosol particle size distribution.

As to the type B aerosol size distribution, Figures 18 and 19 illustrate a similar time change of increase of acidic deposition of liquid water contents at two different altitude z = 1 and 4 m, respectively, with the remaining conditions the same as that of Figure 16. A comparison between Figures 16 and 18, and Figures 17 and 19 indicate that the formation of atmospheric acid deposition of wet removal makes no difference for condensation nuclei with types A and B distributions.

As to the time change of increase of liquid water content associated with type C distribution, Figures 20 and 21 show similar profiles at two different altitudes, z = 1 and 4 m, respectively. Comparison with Figures 16, 18 and 20, and Figures 17, 19 and 21 show that the atmospheric acid deposition for wet removal processes make no difference for the aerosol population with any distributions so long as the mass concentration of the aerosol particles is the same value.

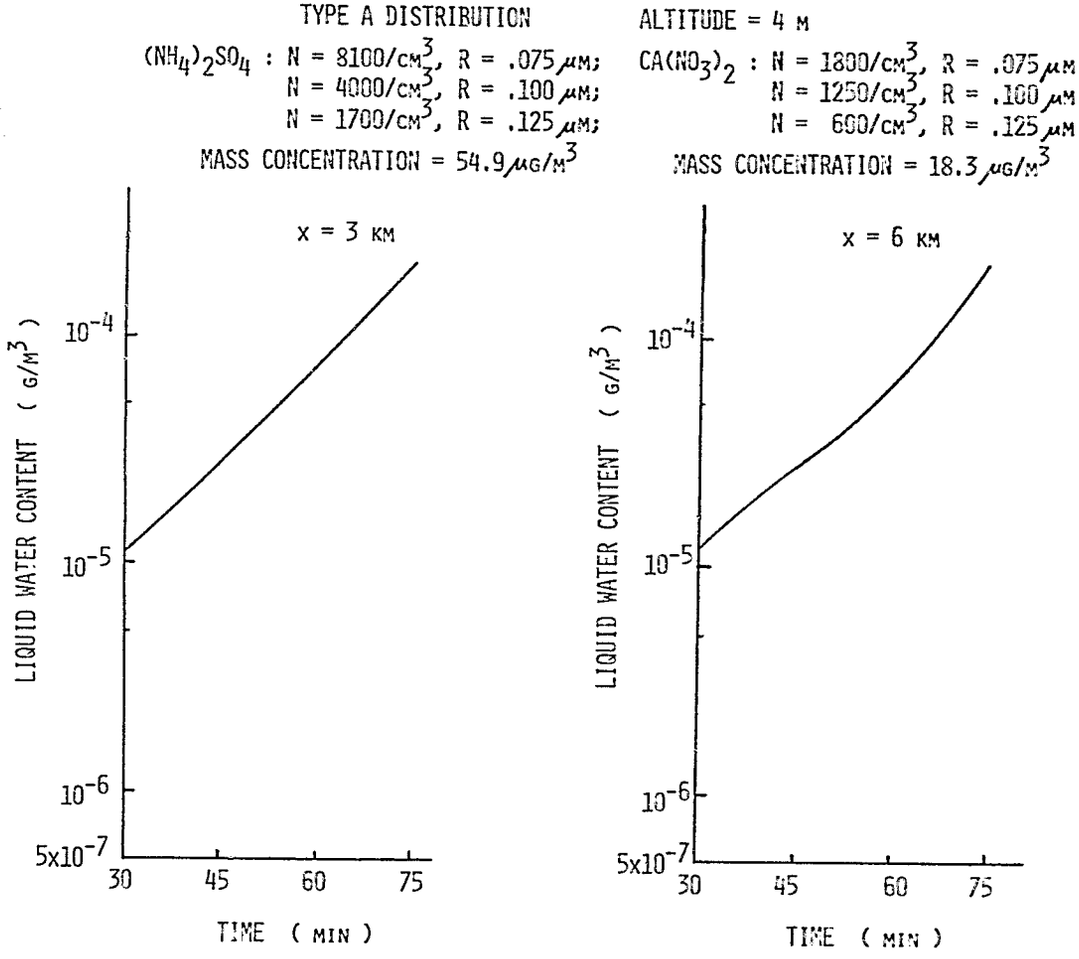

Figure 17. Time rate of change of the amount of liquid water content associated with condensation nuclei, $(NH_4)_2SO_4$ and $Ca(NO_3)_2$, with type A aerosol population distribution, as shown in Figure 9, at two horizontal locations, x = 3 and 6 km, and both at vertical location, z = 1 m.

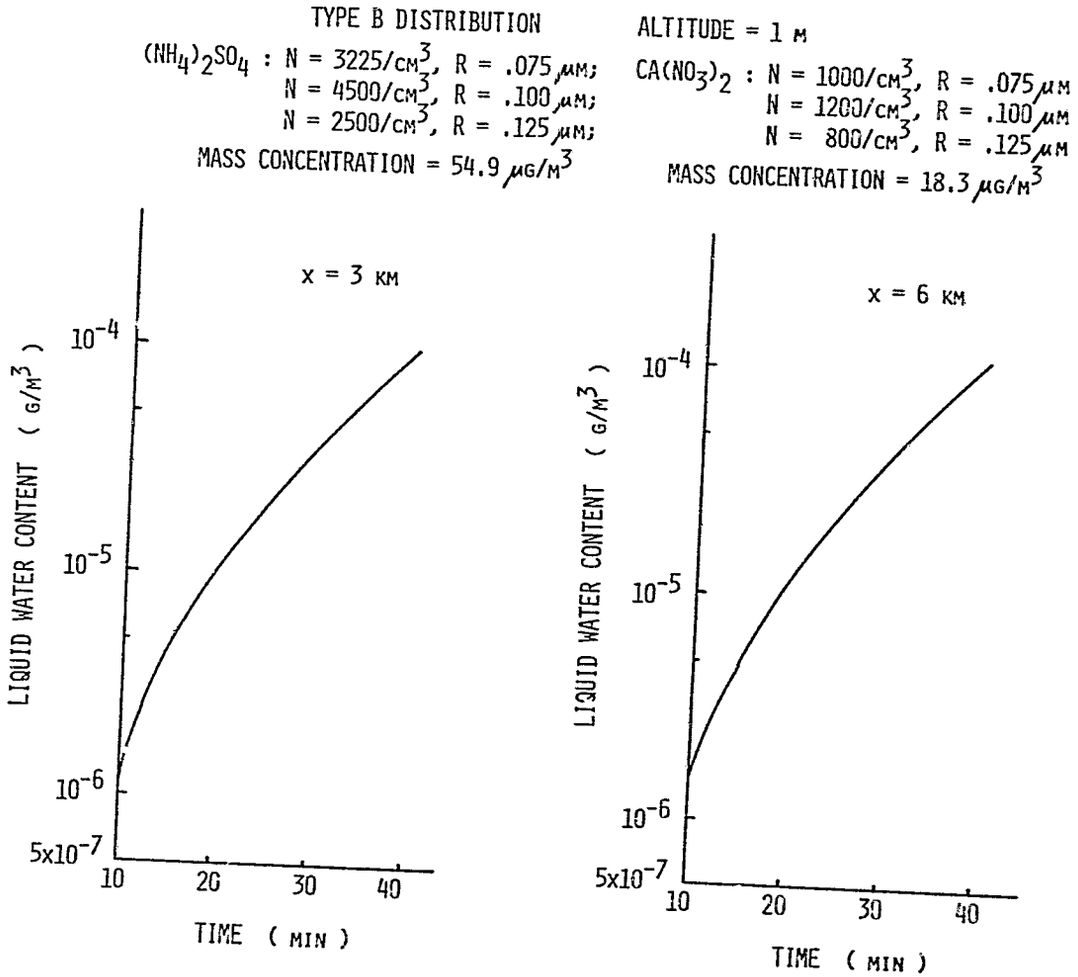

Figure 18. Time rate of change of the amount of liquid water content associated with condensation nuclei, $(NH_4)_2SO_4$ and $Ca(NO_3)_2$, with type B aerosol population distribution, as shown in Figure 9, at two horizontal locations, x = 3 and 6 km, and both at vertical location, z = 1 m.

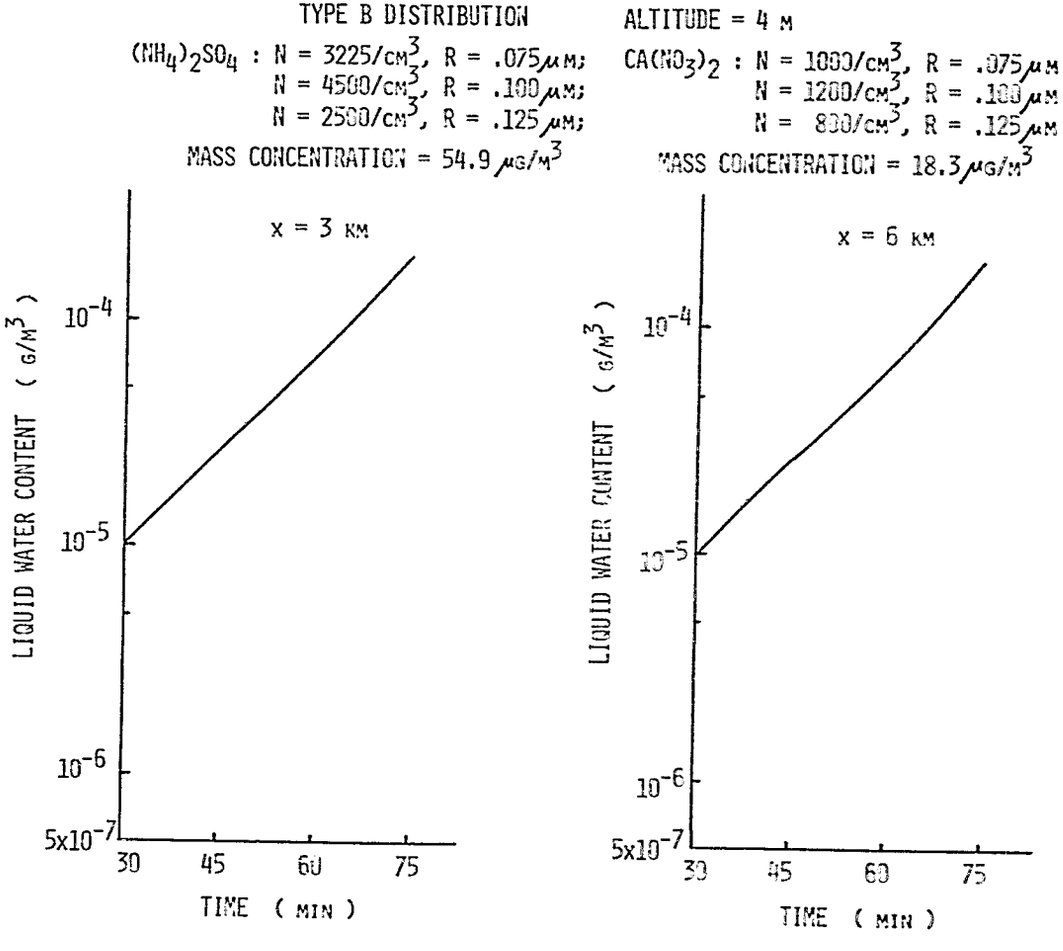

Figure 19. Time rate of change of the amount of liquid water content associated with condensation nuclei, $(NH_4)_2SO_4$ and $Ca(NO_3)_2$, with type B aerosol population distribution, as shown in Figure 9, at two horizontal locations, x = 3 and 6 km, and both at vertical location, z = 4 m.

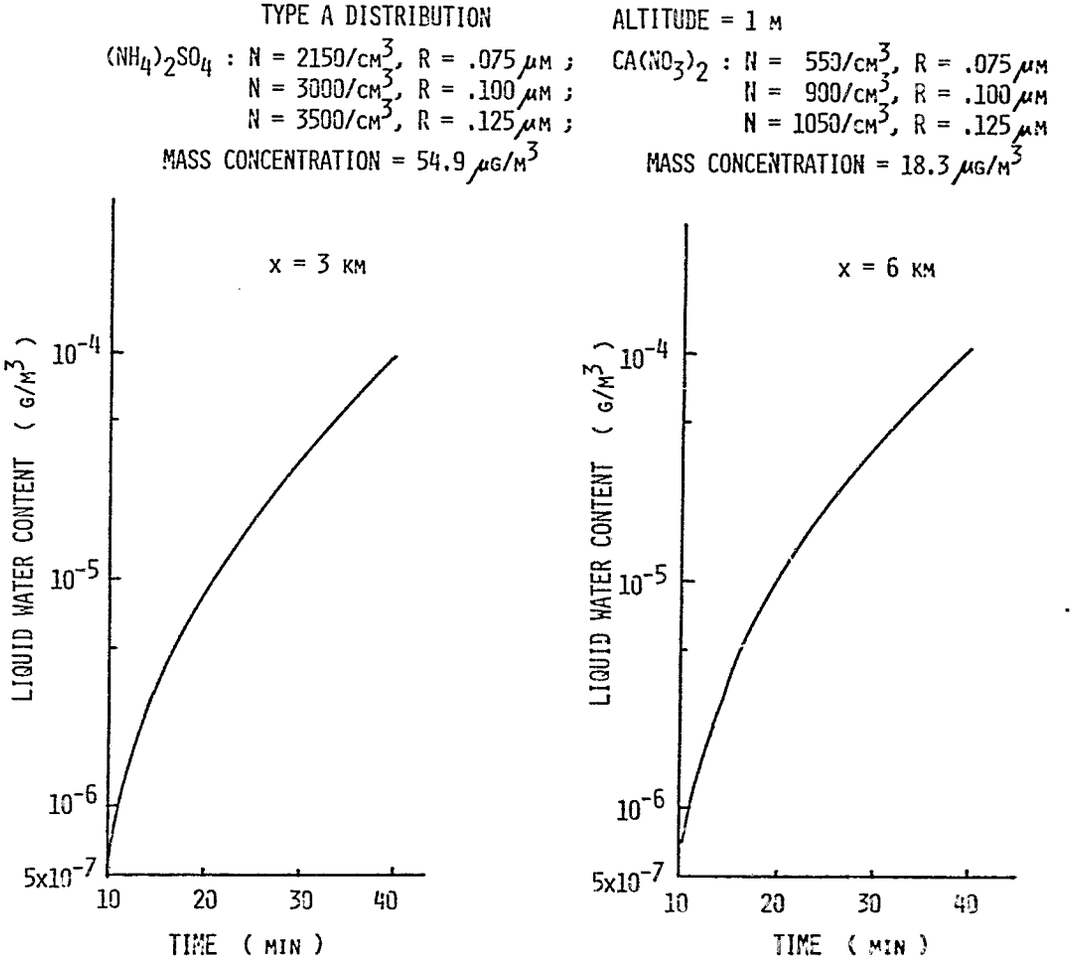

Figure 20. Time rate of change of the amount of liquid water content associated with condensation nuclei, $(NH_4)_2SO_4$ and $Ca(NO_3)_2$, with Type C aerosol population distribution, as shown in Figure 9, at two horizontal locations, x = 3 and 6 km, and both at vertical location z = 1 m.

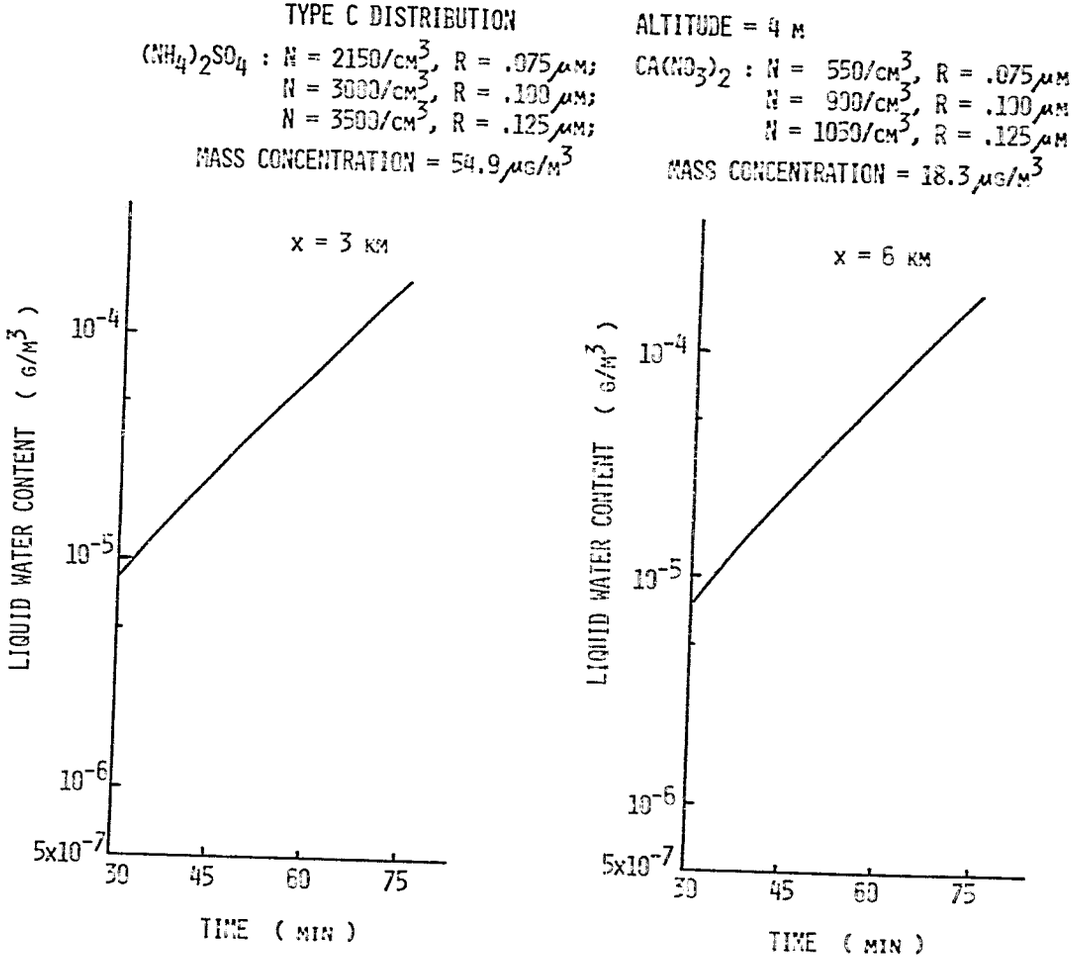

Figure 21. Time rate of change of the amount of liquid water content associated with condensation nuclei, $(NH_4)_2SO_4$ and $Ca(NO_3)_2$, with type C aerosol population distribution, as shown in Figure 9, at two horizontal locations, x = 3 and 6 km, and both at vertical location, z = 4 m.

VII. CONCLUSIONS AND DISCUSSION

The analysis of the chemical composition of atmospheric aerosols, the large quantities of $SO_4^=$, NO_3^-, NH_4^+ and a strong acid such as H_2SO_4 have been detected in highly industrialized areas (Leaderer et al., 1978). Strong evidence exists that the major producer of NO_x has been the automobile. There is no doubt that stationary source fuel combustions also contribute a heavy fraction of the total NO_x emitted to the atmosphere. Fuel-bound nitrogen compounds are ammonia, pyridine, and many other amines (Glassman, 1977). Similar to NO_x production by combustion, sulfur as an inherent impurity in both coal and petroleum, SO_x is also produced through fuel combustion.

There are some very basic difference between the sulfur problem and that posed by the formation of the nitrogen oxides. The two possible sources of nitrogen in any combustion process are either atmospheric or organically bound. Sulfur can be present in elemental form, organically bound, or as a species in various inorganic compounds. Once it enters the combustion process it is very reactive with oxidizing species, and similar to fuel nitrogen, its conversion to the sulfurous oxides is fast compared to the other energy releasing reaction reactions (Glassman, 1977). The great quantity of atmospheric aerosols is thus formed from the pollutants of NO_x and SO_x through the gas-phase photooxidation reaction.

Among the effects of air pollution on atmospheric properties, the most noticeable effect is perhaps the reduction in visibility, with and without the occurrence of condensation. The series of present study, which we have accomplished here, have been particularly interested in how aerosols, produced by energy-related combustion, as condensation nuclei affect the formation of advection fog. These aerosols provide the major source of condensation nuclei for the formation of fog in the areas of busy highways, airports, seaports, etc. How these pollutants affect our living environment, in particular the formation of advection fog, is also our major concern in the present study.

The conclusions obtained from the present series of studies can be summarized as follows:

(1) Hygroscopic chemicals with higher ratio of the Van't Hoff factor to molecular weight produce more favorable conditions for denser advection fog than chemicals with lower values of the ratio.

(2) A higher number density of aerosol nuclei produces advection fog with lower visibility during the nucleation and condensation processes than a lower nuclei number density.

(3) Heavier mass nuclei aerosol particles favor the formation of advection fog with a lower visibility than do lighter mass nuclei during the nucleation processes.

(4) Condensation nuclei with larger radii cause a denser advection fog than condensation nuclei with smaller radii.

(5) For a condensation nucleus to grow into a droplet, the air

must have attained a certain degree of supersaturation. This condition is not necessarily true for a condensation nucleus associated with a polluted atmosphere which can be easily grown into a droplet and produce a dense fog without having the air attaining supersaturation.

(6) In the analysis of air pollutants, the range of mass concentration for NO_x is roughly one-third of the amount of SO_x. The major contribution of combustion-related pollutants as condensation nuclei in the formation of fog comes from aerosols with species of SO_x. However, NO_x as condensation nuclei also gives a considerable great contribution to the formation of fog.

(7) Aerosol distribution with higher particle concentration, rather than the size of aerosol nuclei, support a greater contribution to the formation of fog, if the mass concentration is kept constant.

(8) Relative humidity, at which advection fog with visibility below 1000 m is formed, is lower for aerosols of distribution with the higher particle concentration, which is in turn the smaller size aerosol nuclei, if the value of mass concentration is kept constant.

(9) Aerosol population with high particle concentration-shifted distribution provides more favorable conditions for the formation of dense fog than the aerosol population with low particle particle concentration-shifted distribution.

The results of the present study are in reasonably good agreement

with field observations from the California coast made by Mack et al. (1973, 1974 and 1975), and others, although a detailed comparison is not possible at this time because of the limit number of time dependent measurements of dynamic conditions and aerosol data in the horizontal and vertical coordinates.

The present study can be developed as a numerical prediction of the formation of advection fog with the values of following parameters as initial input: (1) wind profile; (2) temperature profile; (3) humidity profile; (4) mass concentration of aerosol particles; (5) particle size distribution of aerosols; and (6) chemical composition of aerosols.

REFERENCES

Carstens, J. C., J. Podzimek, and A. N. Saad, J. Amos. Sci., 31, 592, 1974.

Changnon, S. A., Jr., Bull Am. Meteorol. Soc., 49, 4, 1968.

Council on Environmental Quality, Environmental Quality, p. 756, U. S. Gov't. Printing Office, Washington, D. C., 1973.

Fletcher, E. N., The Physics of Rain Clouds, p. 380, Cambridge Univ. Press, Cambridge, England, 1976.

Fuller, E. N., P. D. Schettler, and J. C. Giddings, Ind. Eng. Chem., 58, 19, 1966.

Georgii, H. W., Bull. World Health Organ., 40, 624, 1969.

Glassman, I., Combustion, p. 275, Academic Press, New York, 1977.

Hidy, G. M., and J. R. Brock, An assessment of the global sources of tropospheric aerosols, in Proc. Second International Clean Air Congress, ed. by H. M. Englund and W. T. Beery, Academic Press, New York, 1971.

Hoffer, T. E., and S. C. Mallen, J. Atmos. Sci., 27, 914, 1970.

Hung, R. J., and J. R. Huckle, J. Rech. Atmos., 11, 165, 1977.

Hung, R. J., and G. S. Liaw, will appear in J. Aerosol Sci., 10, 1979.

Hung, R. J., and G. S. Liaw, Water, Air and Soil Pollution, 13, 1980 (in press).

Hung, R. J., and O. H. Vaughan, AIAA Paper, No. 77-130, 1977.

Hung, R. J., G. S. Liaw and O. H. Vaughan, Numerical simulation of warm fog prediction and modification, in Proc. Atmospheric Environment of Aerospace Systems and Applied Meteorology, Amer. Meteor. Soc., Boston, Mass., p. 169, 1978.

Hung, R. J., G. S. Liaw and O. H. Vaughan, J. Rech. Atmos., 13, 37, 1979.

Hung, R. J., O. H. Vaughan, and R. E. Smith, Progr. in Astronaut. and Aeronaut., 48, 515, 1976.

Leaderer, B. P., D. M. Bernstein, J. M. Daisey, M. T. Kleinman, T. J. Kneip, E. O. Knutson, M. Lippmann, P. J. Lioy, K. A. Rahn, D. Sinclair, R. L. Tanner, and G. T. Wolff, J. Air. Poll. Control Assoc., 28, 321, 1978.

Low, R. D. H., L. D. Duncan, and R. B. Gomez, The microphysical basis of fog optical characterization, p. 24, ASL-TR-0011, Atmos. Sci. Lab., White Sands Missile Range, New Mexico, 1978.

Mack, E. J., R. J. Pilie, and W. C. Kockmond, An investigation of the microphysical and micrometeorological properties of sea fog, p. 33, Calspan Corp., New York, 1973.

Mack, E. J., U. Katz, C. W. Rogers, and R. J. Pilie, The microstructure of California coastal stratus and fog at sea, p. 67, Calspan Corp., New York, 1974.

Mack, E. J., R. J. Pilie, and U. Katz, Marine fog studies off the California coast, p. 69, Calspan Corp., New York, 1975.

Mason, B. J., The physics of clouds, 2nd edition, p. 671, Clarendon Press, Oxford.

Paluch, I. R., J. Atmos. Sci., 28, 629, 1971.

Richtmyer, R. D., Difference methods for initial-value problems, p. 2??, Interscience Publ., New York, 1957.

Seinfeld, J. H., Air pollution-physical and chemical fundamentals, McGraw-Hill New York, p. 523, 1975.

Silverman, B. A., and A. I. Weinstein, Fog, in Weather and climate modification, p. 355, ed. by N. Hess, John Wiley, New York, 1974.

Tang, I. N., and H. R. Munkelwitz, J. Aerosol. Sci., 8, 321, 1977.

Tang, I. N., H. R. Munkelwitz, and J. G. Davis, J. Aerosol Sci., 8, 149, 1977.

Tang, I. N., H. R. Munkelwitz, and J. G. Davis, J. Aerosol Sci., 9, 505, 1978.

Weinstein, A. I., and B. A. Wilverman, J. Appl. Meteor., 12, 771, 1973.

APPENDICES

APPENDIX A

EVALUATION OF KEY PARAMETERS IN THE MATHEMATICAL MODEL

The turbulent exchange coefficients proposed in this model are based on empirical flux gradient relations which have been measured in studies of turbulent transfer in the lowest 50 m or so of the atmosphere (Businger et al., 1971; Panofsky, 1974; Pasquill, 1974; Huang, 1975).

(i) Parameterized Fluxes of Momentum, Heat and Moisture

The parameterized fluxes through the surface boundary layer serve as the boundary conditions for the turbulent exchange processes in the transition layer. The "bulk aerodynamic" method (Roll, 1965) was used to parameterize the surface boundary layer fluxes of momentum, heat and moisture.

$$u^{*2} = K_m \frac{\partial U_y}{\partial z} \qquad \text{(A-1)}$$

$$\frac{-H}{\rho C_p} = K_h \frac{\partial \theta}{\partial z} \qquad \text{(A-2)}$$

$$-\frac{E}{\rho} = K_d \frac{\partial C_{vn}}{\partial z} \qquad \text{(A-3)}$$

Here $u^* = (\tau/\rho)^{1/2}$ is the friction velocity; H, the vertical heat flux through the surface boundary layer; E, the flux of vapor through the surface boundary layer; and τ, the surface stress tensor. Within

the constant flux layer, it can be shown that the non-dimensional wind shear, temperature gradient and vapor flux gradient can be expressed in the form

$$\frac{kz}{u^*} \frac{\partial U_y}{\partial z} = \phi_m\left(\frac{z}{L_s}\right) \qquad \text{(A-4)}$$

$$\frac{z}{T^*} \frac{\partial \theta}{\partial z} = \phi_h \left(\frac{z}{L_s}\right) \qquad \text{(A-5)}$$

$$\frac{z}{C^*_{va}} \frac{\partial C_{va}}{\partial z} = \phi_d\left(\frac{z}{L_s}\right) \qquad \text{(A-6)}$$

where

$$L_s = - \frac{u^* C_p \rho T}{k g H} = \text{Monin-Obokhov scaling length}$$

$k = 0.4$ = Von Karman constant

$$T^* = - \left(\frac{1}{ku^*}\right) \left(\frac{H}{\rho C_p}\right) = \text{scaling temperature}$$

$$C^*_{va} = - \left(\frac{1}{ku^*}\right) \left(\frac{E}{\rho}\right) = \text{scaling water vapor mixing ratio.}$$

By definition, then, within the surface boundary layer, the exchange coefficients for momentum, heat and diffusivity can be shown to be:

$$K_m = \frac{u^* kz}{\phi_m\left(\frac{z}{L_s}\right)} \qquad \text{(A-7)}$$

$$K_h = \frac{u^* kz}{\phi_h(\frac{z}{L_s})} \qquad (A-8)$$

$$K_d = \frac{u^* kz}{\phi_d(\frac{z}{L_s})} \qquad (A-9)$$

In the advection fog model, these turbulent exchange coefficients are multiplied by the factor $\exp\left[-8fz/u^*\right]$, obtained by Shir (1973) in a numerical study of a neutral boundary layer, to provide a reasonable behavior of the turbulent exchange coefficients above the constant flux layer in the model.

In this model, the relations of non-dimensional wind shear $\phi_m(\frac{z}{L_s})$; temperature gradient, $\phi_h(\frac{z}{L_s})$; and water vapor flux gradient, $\phi_d(\frac{z}{L_s})$; are used. These parameters are based upon atmospheric measurement within the surface boundary layer under relatively steady-state and horizontally homogeneous conditions (Panofsky, 1974).

Under stable conditions $L_s > 0$, the relations (Webb, 1970)

$$\phi_m = \phi_h = \phi_d = 1 + 5\frac{z}{L_s} \qquad (A-10)$$

are used. Under unstable conditions or $L_s < 0$, the relations (Dyer, 1974)

$$\phi_m = (1 - 16\frac{z}{L_s})^{-\frac{1}{4}} \qquad (A-11)$$

$$\phi_h = \phi_d = \phi_m^2 = (1 - 16\frac{z}{L_s})^{-\frac{1}{2}} \qquad (A-12)$$

are used. Under neutral conditions or H = 0. both the stable and

unstable relations reduce to (Dyer, 1974; Huang, 1979)

$$\phi_h = \phi_d = \phi_m = 1 \qquad \text{(A-13)}$$

The turbulent exchange coefficients K_m, K_h and K_d can then be computed for every grid point in the model from Equations (A-1) to (A-12), using the friction velocity u* and the scaling length L_s determined for the column.

(ii) Infrared Radiation Flux Divergence

The model for the infrared radiative flux divergence produced by fog adopted the model proposed by Goody (1964)

$$\frac{\partial R_f(z)}{\partial z} = 0.4\ \sigma_s\ T^4 K_w(z)\ \rho C_{wa}(z) \cdot \exp\left[-1.6 \int_z^{z_T} K_w(z')\ \rho C_{wa}(z')\ dz'\right] \qquad \text{(A-14)}$$

where σ_s is the Stefan-Boltzmann constant; K_w, spectrally-averaged mass absorption coefficient of fog for infrared radiation (cm^2/g); and z_T, the height of the fog top. The absorption coefficient K_w is the model proposed by Zdurkowski and Nielsen (1969)

$$1.6\ K_w\ \rho C_{wa} = 1.6\ (\pi N)^{1/3}\ \left(\frac{3}{4\pi\rho_v}\right)^{2/3}\ (\ \rho C_{wa}\ )^{2/3} \qquad \text{(A-15)}$$

for the absorption per unit path length in the fog.

(iii Terminal Velocity of Fog Drops

The sedimentation of the fog drops can be simulated through the mean terminal velocity U_t which follows Stokes relationship (Fletcher, 1966)

$$U_t = 1.2 \times 10^6 \quad r^2 \qquad \text{(cm/sec)} \qquad \text{(A-16)}$$

where r is the radius of the fog drops.

APPENDIX B

PROGRAM DOCUMENTATION

B.1. Introduction

The program documentation provided in this Appendix is separated into several parts. (1) Within the introduction the essential features of the program are described together with a discussion of some model capabilities. (2) A brief discussion of the control which can be exercised over the program in order to study particular features of advection fog. (3) A description of input cards. (4) A listing and definition of variables and controls used in the program. (5) Three pages of sample output. This presentation is designated to allow others to make the program accomplish their desired aims with a minimum expenditure of learning time.

The program described here provides a tool for studying both the formation and dissipation of advection fogs in the vertical (X-Z) plane. In the discussion which follows, quantities which occur in the computer program are capitalized; those that are input quantities are underlined.

The model can describe the evolution of the fields of U, V, Y, PT, R and W from a variety of initial conditions, subject to the imposed upper and lower boundary conditions. The initial conditions are put into the program by sets of input cards which are based on the field observations. The lower boundary conditions represent the earth's surface, either land or ocean, at which PT is constrained to be equal

to the surface temperature. The surface temperature can take on many desired configurations along the X-axis. At the upward boundary, the dependent variables are maintained equal to their initial values. At the downwind boundary, however, the dependent variables are continually adjusted to equal their computed value in the adjacent upwind grid column.

Wihtin each time step (DT), the U, V, Y, PT, W and R fields are changed by the simulated processes, in accordance with the boundary conditions, by an implicit integration scheme. The temperature (T) field is then diagnosed from the potential temperature (PT) field. The occurrence of any condensation or evaporation (FC) is accounted for by the local conditions and is calculated by the microphysics equation subroutine RKF. From these final fields, the diagnostic variables, turbulent exchange coefficient (KA and KM), total water below a height (Z) in a column (INT), specific heat of saturated air (CPT), radius of droplet (RAD) and visibility (VISITY) are computed and stored for use in taking the next time step.

Output is controlled by output time (OT) and ending time (ET), which occurs when the total time elapsed (TIME) at the end of a set of time steps equals the print time (PRT). Printout of the fields of wind velocity (U, V and Y), vertical eddy heat flux (HC), T, R, liquid water content, turbulent exchanges coefficient, radiative flux, radiative cooling rate, water vapor flux, radius of droplet and visibility, in that order, is provided. Integration then continues, with output occurring at PRT equal to integer multiples of output time (OT), until program termination at the ending time (ET).

B.2. Control of Program

Flexibility of the program to investigate various aspects of advection fog formation and dissipation rests with the way the configuration of the program can be changed through specification of input data and control indices. These quantities fall into the following categories:

a. time parameters

b. grid spacing and configuration in the vertical and horizontal

c. input parameters controlling which physical processes operate and their magnitude, and the initial values of the dependent variables

d. boundary conditions on temperature and water vapor at the earth's surface boundary

e. options for printout

a. Time

The basic time varibale is the length of the time step DT, which can be changed to insure computational stability, and control running time on the computer. Additional time variables are OT, for multiples of which the program prints out and ET, which is the total meteorological time the program is to run.

b. Grid Spacing

The vertical grid is composed of (KE) levels (up to a maxium of 50) with the space between adjacent levels expanding based on the height of the first level (ZAL) above the earth's surface and an expansion factor (ZAK).

The horizontal grid is composed of (IE) columns (up to a maximum

of 40). IE can be specified as any number greater than two and ≤ 40, except that printout is conveniently grouped in units of ten columns per page. The horizontal grid is basically specified by (DELX) which is the uniform spacing between columns in that portion of the grid located between (IL) and (IR), the (I)-values of the left and right boundaries of the region of uniform grid spacing. Outside these limits, the grid spacing expands to the upwind and downwind grid limits with the size of spacing controlled by the expansion factor (XAI) and DELX. In the output, negative X's indicate columns located upwind of the uniformly spaced grid and positive values label the uniform portion and columns in the downward expanding portion.

c. Initial Values

If ISED = 1 and IRAD = 1, sedimentation and radiational cooling, respectively, are included in the model; if ISED and IRAD ≠ 1, then the processes are excluded.

PT, W and R can be initialized to be uniform everywhere having values (PTI), (ZERO), and (RI), when the corresponding control indices (IPT, IW and IRR) = o. If IPT = -1, then the temperature profile is isothermal with a value of (TP) and the corresponding initial PT is computed from the hydrostatic relationship. If IPT, IRR, IW and IU all = 1, the corresponding varibales are uniform in X, and T, R, W, U and V are read from a card listing for K = 1, ..., KE; the prognostic variables PT then be computed. If IU = 0, then U and V is an adiabatic profile at all columns, using friction velocity (UF) and roughness length (ZO).

of 40). IE can be specified as any number greater than two and < 40, except that printout is conveniently grouped in units of ten columns per page. The horizontal grid is basically specified by (DELX) which is the uniform spacing between columns in that portion of the grid located between (IL) and (IR), the (I)-values of the left and right boundaries of the region of uniform grid spacing. Outside these limits, the grid spacing expands to the upwind and downwind grid limits with the size of spacing controlled by the expansion factor (XAI) and DELX. In the output, negative X's indicate columns located upwind of the uniformly spaced grid and positive values label the uniform portion and columns in the downward expanding portion.

c. Initial Values

If ISED = 1 and IRAD = 1, sedimentation and radiational cooling, respectively, are included in the model; if ISED and IRAD ≠ 1, then the processes are excluded.

PT, W and R can be initialized to be uniform everywhere having values (PTI), (ZERO), and (RI), when the corresponding control indices (IPT, IW and IRR) = 0. If IPT = -1, then the temperature profile is isothermal with a value of (TP) and the corresponding initial PT is computed from the hydrostatic relationship. If IPT, IRR, IW and IU all = 1, the corresponding varibales are uniform in X, and T, R, W, U and V are read from a card listing for K = 1, ..., KE; the prognostic variables PT then be computed. If IU = 0, then U and V is an adiabatic profile at all columns, using friction velocity (UF) and roughness length (ZO).

d. Boundary Values

The boundary condition of potential temperature on the surface is controlled by the index (IDTEM). If IDTEM = 0, then DTFM(I), the surface temperature change being investigated (negative for advection fog formation, positive for fog dissipation) equal to zero. If IDTEM = 1, then DTEM(I) is uniformly equal to DTEMI between ITEMI, and ITEMR, the left and rigrt I- boundaries of this warmer or colder region. If IDTEM = -1, then DTEM(I) is read from a card list for all I's except I = 1 and IE. In all these cases, DTEM(I) is introduced gradually to avoid pulsing the integration. The length of time over which DTEM(I) is introduced is equal to (TIM).

If (IRSFC) = 0, then a boundary condition of no vertical flux is imposed on R at the surface. If (IRSFC) = 1, then the boundary condition of R is set as saturation mixing ratio at surface temperature and pressure equal to 1000 mb. If (IRSFC) = 2, then the boundary condition of R at surface is kept the same as the initial.

Conditions at the upstream boundary remain unchanged throughout the integration, while conditions at the downstream boundary are set equal to those at the adjacent column at the end of each time step.

e. Output

Output from the program is controlled by the main program and performed by a print subroutine (PRNT). For variables in storage, a call of PRNT, with proper arguments, accomplishes the output. For variables not in storage, the values are computed in the main program and stored in a dummy storage location called HC, and output occurs by calling PRNT with HC as an argument.

The print subroutine prints [illegible] data columns per page for each output quantity, along with documentary vertical and horizontal distance information. Each column covers the entire vertical extent of the grid. Logic in the program provides for printing only 11 columns of data when IE is less than 40 and an integer multiple of 10. In addition, the first page identifies the output variable, output time, and other selected information which identifies the simulation.

f. Units

Internally, the program operates in cgs units, except that DELX is in meters and when heat is an explicit unit it is expressed in calories.

g. Computational Requirements

The program has been written in Fortran and run on a Univac 1108 digital computer. Approximately 20 K words of core storage were required for execution of the program. CPU time requirements for execution of the program depend upon the ratio ET/DT, the total number of grid points (IE) x (KE), and the amount of output specified. In addition, more computations per time step are required in fog than in non-fog regions.

The primary limitation on the maximum time step (DT) that should be employed is the computational stability criterion,

$$\frac{U \cdot DT}{DELX} \leq 1, \qquad (1)$$

for the integration of the horizontal advection terms. It is advisable, however, to restrict DT≤60 seconds, even when condition (1) can be satisfied by a larger DT, in order to avoid serious truncation errors and/or computational instabilities in the vertical integrations.

B.3. Sample Set of Input Cards

a. Time Variable Constants, Temperarure and Wind Input

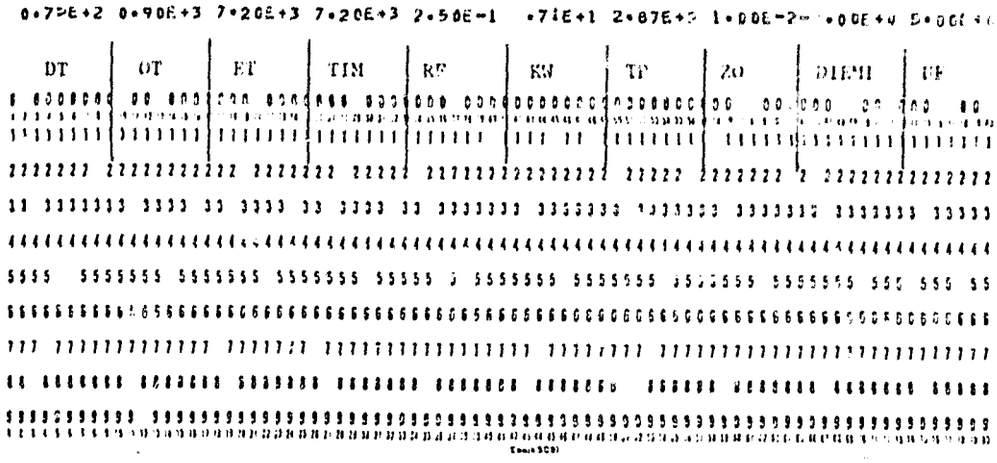

DT time step (seconds)

OT time interval at which output occurs (seconds)

ET length of simulation (seconds)

TIM time interval from t = 0 at which the colder or warmer surface temperature reaches its desired value (seconds)

RF fraction of surface black body radiation used as net upward infrared flux through upper boundary

KW a constant multiplied times liquid water content raised to the two-thirds power

TP temperature in degrees Kelvin used to initialize the temperature profile to isothermal

ZO roughness length (cm)

DTEMI change from surface potential temperature in column 1 needed to obtain a uniform surface temperature among the other columns when a uniform discontinuity in surface temperature is desired

UF friction velocity which enters into the quasi-adiabatic velocity profiles when they are used to initialize the velocity field (cm/sec)

b. Control Index Card

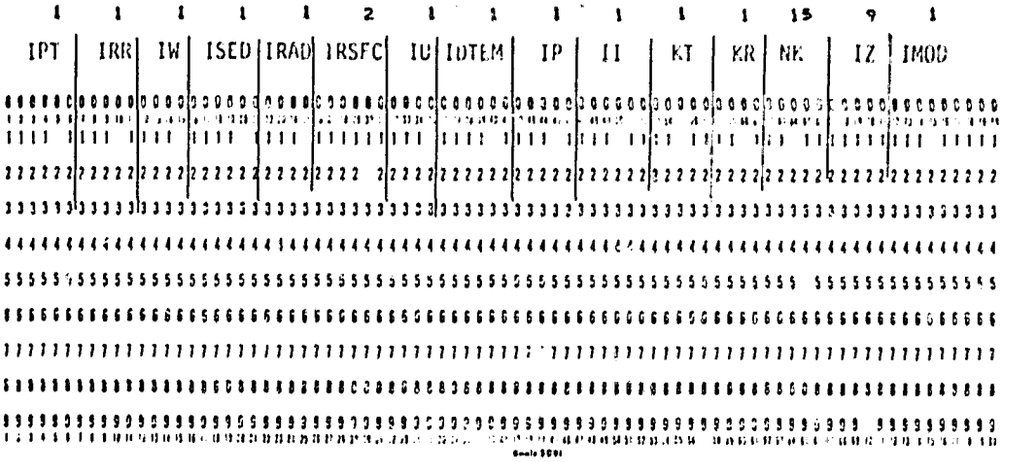

IPT = -1 $PT(I,K) = TP(\frac{1000}{P})^{.286}$, isothermal

= 0 PT(I,K) = PTI, adiabatic

= 1 PT(I,K) = input data, based on field observation

IRR = 0 R(I,K) = RI

= 1 R(I,K) = input data, based on field observation

IW = 0 W(I,K) = 0

= 1 W(I,K) = input data, based on field observation

ISED = 1 with sedimentation

≠ 1 without sedimentation

IRAD = 1 with radiational cooling

≠ 1 without radiational cooling

IRSFC = 0 R(I,1) = R(I,2)

= 1 R(I,1) = saturation mixing ratio at surface temperature and 1000 mb

IU = 0 Quasi-adiabatic U and V profiles

= 1 U and V = input data, based on field observation

IDTEM = 0 DTEM(I) = 0.0

= 1 DTEM(I) = DTEMI between ITEML and ITEMR, and equals zero elsewhere

= -1 DTEM(I) = input data, desired ground temperature distribution

HR = net radiative flux, cal-cm^{-2}-min^{-1} (positive upward)

COOL = rate of radiative cooling, ^{o}c-hr^{-1}

IP = 0 no HR and COOL output provided

≠ 0 HR and COOL output provided

II = 1 turbulent exchange coefficient does not depend on local condition

= 2 turbulent exchange coefficient depends on local conditions

KT = 1 two-dimensional simulation is initialized from list generated by one-dimensional simulation

≠ 1 vertical grid level to which first potential temperature in list is to be assigned

KR = perform the same function for mixing ratio and liquid water content that KT does for the potential temperature

IZ = specifies the number of the column for which wind, potential temperature, mixing ratio and liquid water will be punched out

NK = vertical grid level to which hygroscopic material is to be spread

IMOD = 0 modification by heating

= 1 modification by spraying hygroscopic material

c. Grid Specification Card

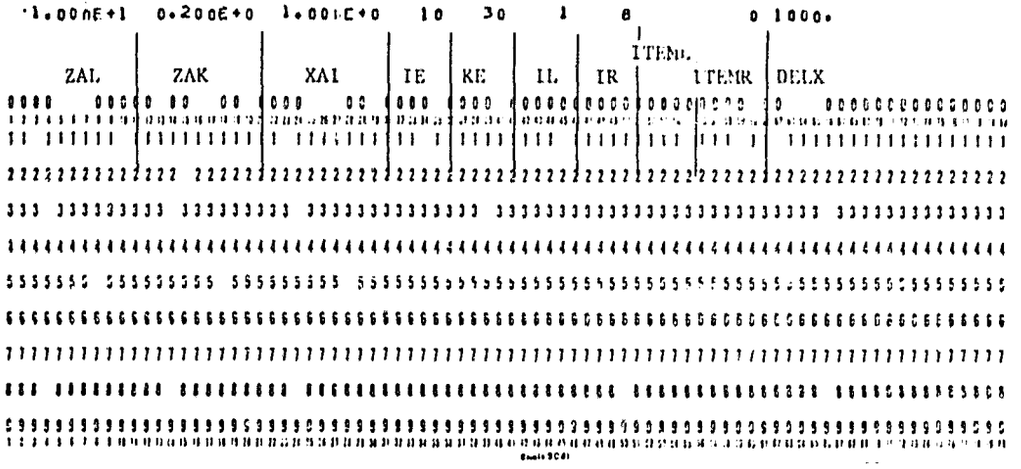

ZAL = height of lowest vertical grid point in the atmosphere (cm)

ZAK = expansion factor in the vertical

XAI = expansion factor in the horizontal

IE = number of horizontal columns

KE = number of vertical levels

IL = leftmost grid point of unexpanded grid

IR = rightmost grid point of unexpanded grid

ITEML = left I-limit on non-zero, uniform DTEM(I)

ITEMR = right I-limit on non-zero, uniform DTEM(I)

DELX = uniform X-spacing (meters)

d. Output Formats

The printed output for the various quantities is in convenient standard units as shown in the format heading statements 3000-3800 in the program listing in Appendix C.

FMTH = Format for hieght and variable informations, including wind velocity, R, liquid water content, RAD and visibility.

FMTT = Format for height and temperature information.

e. Microphysics Parameters Control Card

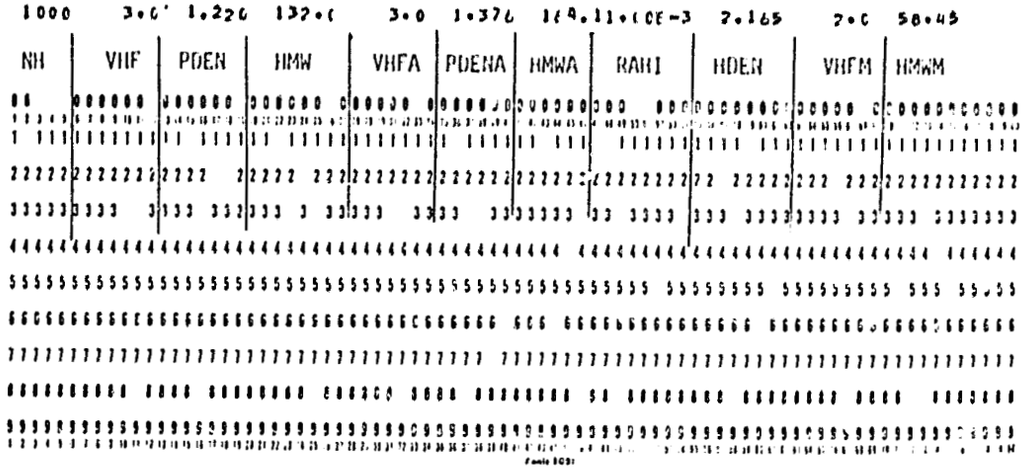

NH = number density of hygroscopic material for modification

VHF = Van't Hoff factor

PDEN = density of pollutant

HMW = molecular weight of pollutant

VHFA = Van't Hoff factor of the other pollutant A

PDENA = density of the other pollutant A

HMWA = molecular weight of the other pollutant A

RAHI = initial radius size of hygroscopic material

HDEN = density of hygroscopic material

VHFM = Van't Hoff factor of hygroscopic material for modification

HMWM = molecular weight of hygroscopic material for modification

f. Aerosol Particle Control Cards

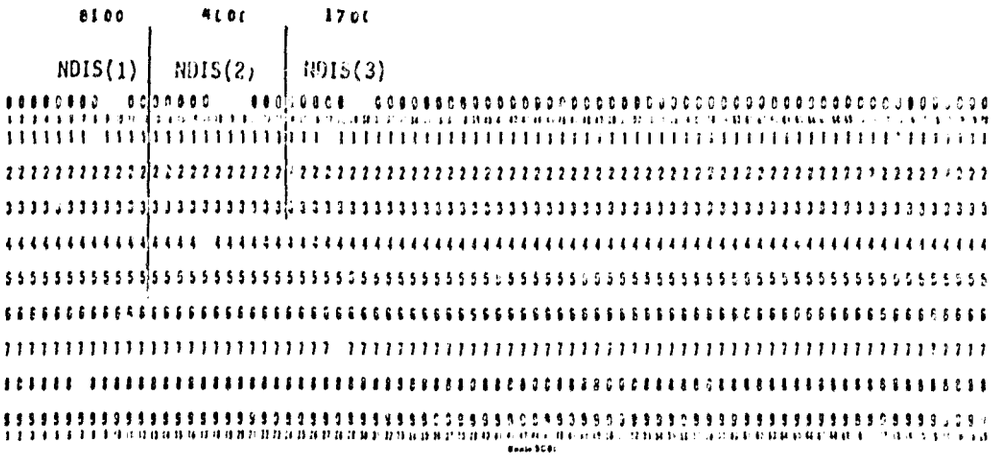

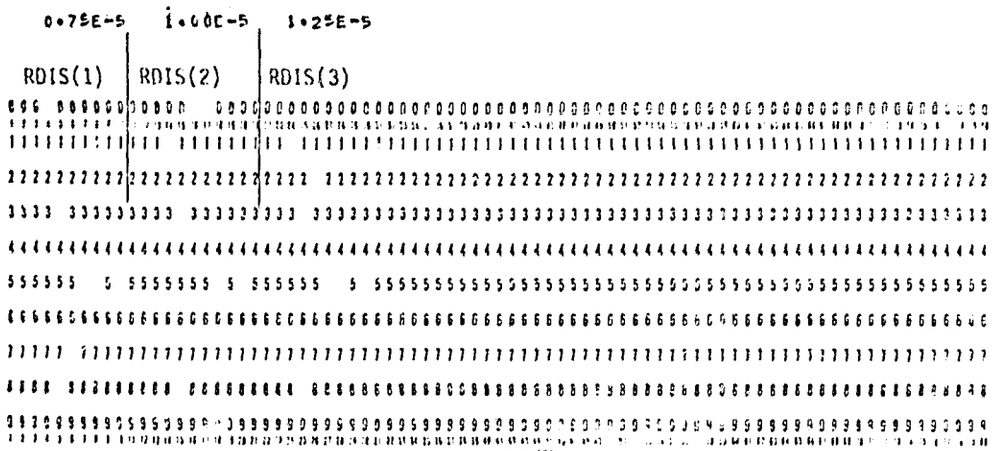

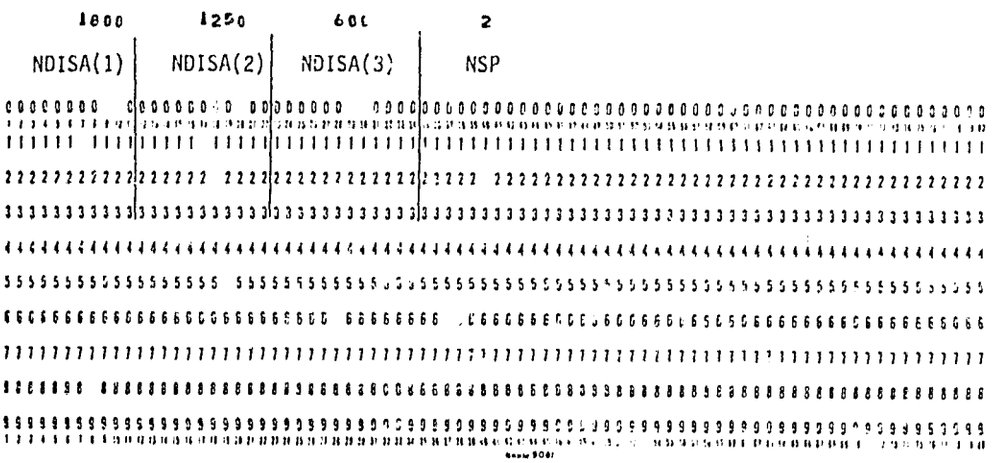

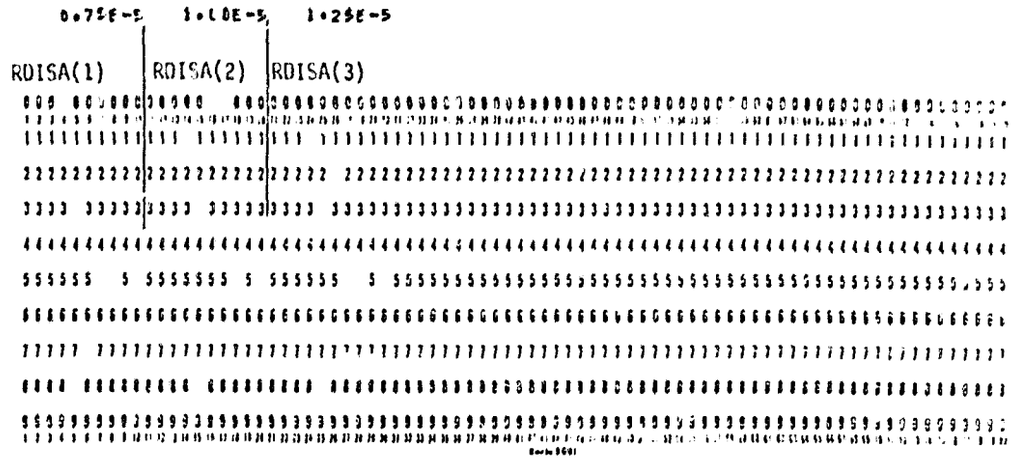

NDIS(J) = number density distribution of pollutant

RDIS(J) = radius size distribution of pollutant

NDISA(J) = number density distribution of pollutant A

NSP = number of species

RDISA(J) = radius size distribution of pollutant A

g. Other Input Parameters

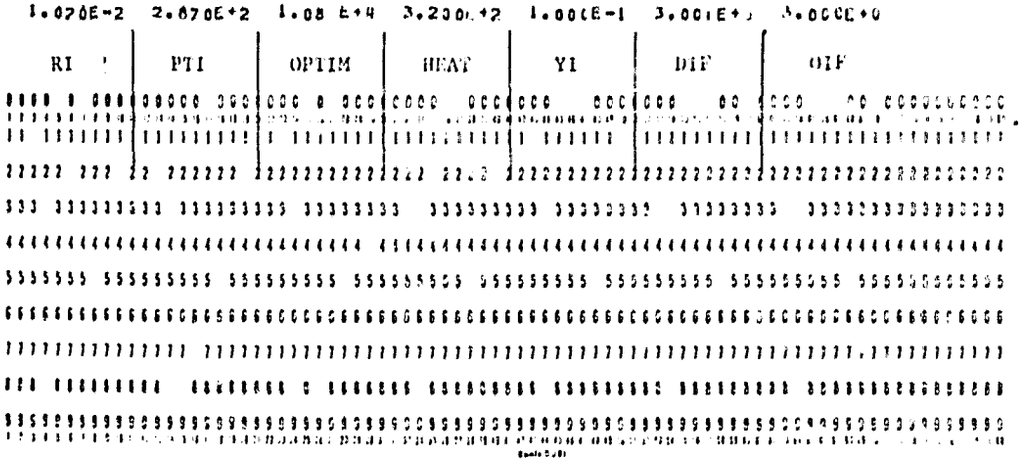

RI = initial value of water vapor mixing ratio, if set IRR = 0

PTI = initial value of potential temperature , if set IPT = 0

OPTIM = start time of modification

HEAT = source temperature, if set IMOD = 0

YI = initial vertical wind velocity

DTF = time step factor

OTF = output time factor

b. Variable Input, Non-uniform with Height

1. Horizontal Wind Velocity (X-Direction)

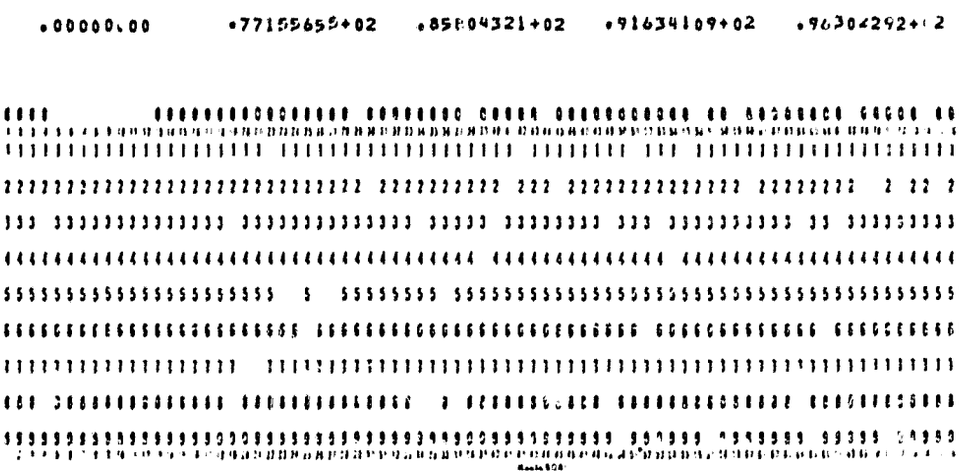

2. Horizontal Wind Velocity (Y-Direction)

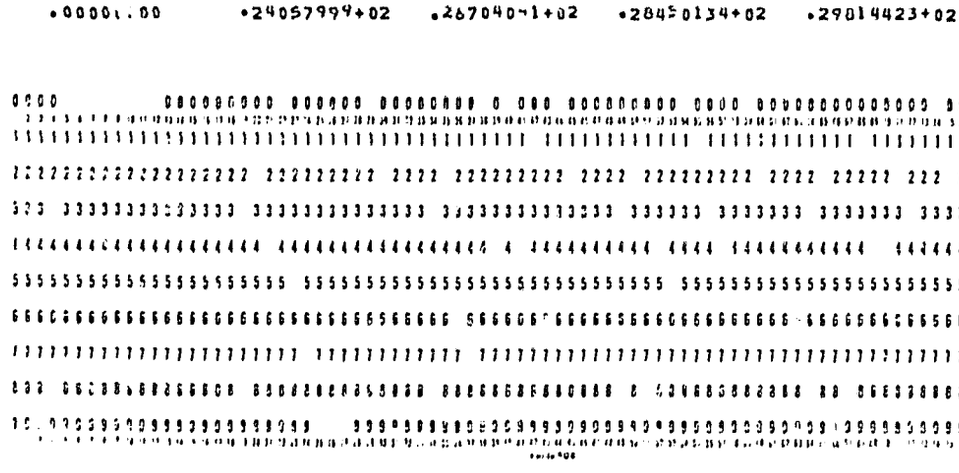

3. Temperature

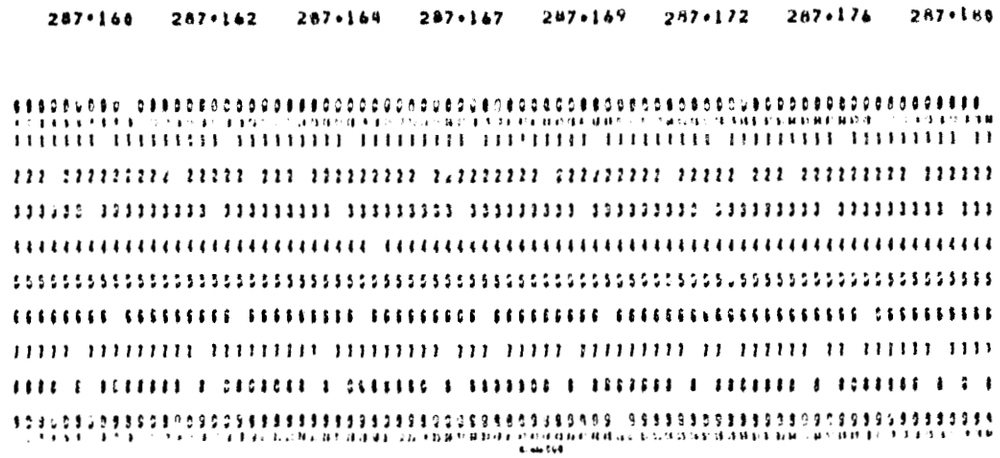

4. Water Vapor Mixing Ratio

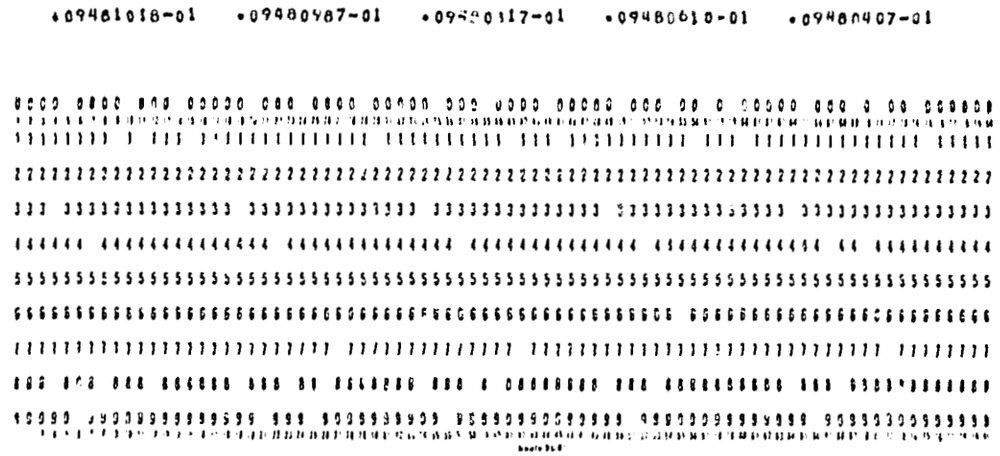

5. Liquid Water Mixing Ratio

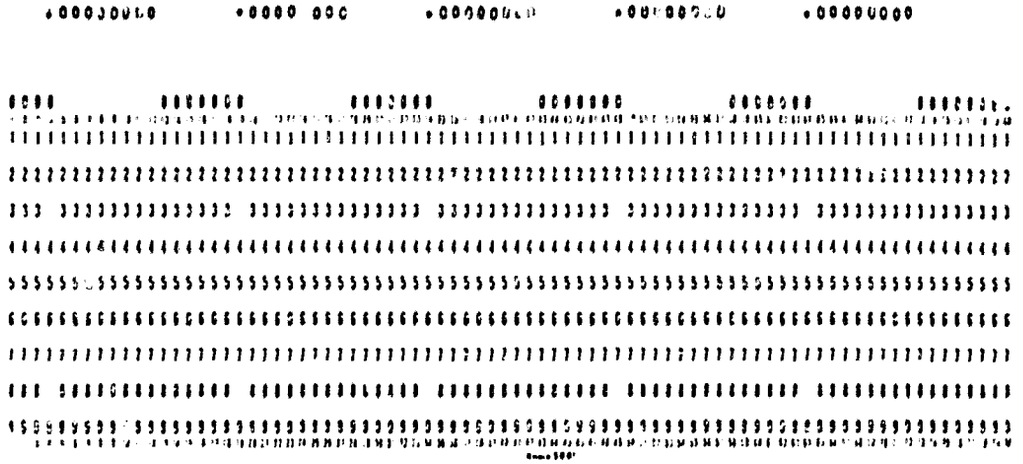

B.4. List of Computer Variables

The following list of variables is not arranged in alphabetical order, but rather variables of a common type of variables which are concerned with a given program operation are listed together.

a. Grid Specification

1. Vertical Grid

K = index for vertical grid

KE = number of vertical levels

KN = KE - 1

ZA(K) = vertical coordinate at level K

DZA(K) = grid spacing between level K and K - 1

ZAL = height of lowest vertical grid point in the atmosphere

ZAK = expansion factor in the vertical

2. Horizontal Grid

I = index for horizontal grid

IE = number of horizontal columns

IN = IE - 1

X(I) = Horizontal coordinate at column I

DX(I) = grid spacing between columns I and I - 1

DELX = uniform X-spacing

IL = leftmost grid point of unexpanded grid

IR = rightmost grid point of unexpanded grid

XAI = expansion factor in the horizontal

b. Variables

1. Prognostic

PT(I,K) = potential temperature

RW = gas constant for water vapor

SIGMA = Stefan-Boltzmann constant

2. Variable

KW = mean mass absorption coefficient of fog for infrared radiation ($cm^2 g^{-1}$)

RF = fraction of surface black body radiation used as net upward infrared flux through upper boundary

UF = friction velocity used for computing KA

ZO = roughness length

CV = sedimentation constant

B.5. Samples of Output

1. Temerature

2. Relative Humidity

3. Visibility

Three samples of each paramerer are illustrated in the next three pages.

TEMPERATURE IN DEG K

TIME= 300.00 SEC DTEMI= -1.0 K ITEML= 1 ITEMRE=10

X(KM)= Z(CM)	.00	1.00	2.00	3.00	4.00	5.00	6.00	7.00	8.00	9.00
9.84+03	287.206	286.209	286.201	286.201	286.201	286.201	286.200	286.199	286.199	286.198
8.19+03	287.205	286.619	286.615	286.616	286.616	286.616	286.616	286.616	286.616	286.616
6.82+03	287.202	286.857	286.856	286.856	286.856	286.856	286.856	286.856	286.856	286.856
5.67+03	287.200	287.004	287.003	287.003	287.003	287.004	287.004	287.003	287.003	287.003
4.72+03	287.198	287.096	287.095	287.095	287.095	287.095	287.095	287.095	287.095	287.095
3.92+03	287.197	287.155	287.154	287.154	287.154	287.154	287.154	287.154	287.154	287.153
3.25+03	287.196	287.191	287.190	287.190	287.190	287.193	287.190	287.190	287.190	287.190
2.71+03	287.195	287.212	287.211	287.211	287.211	287.211	287.211	287.211	287.211	287.211
2.25+03	287.194	287.223	287.222	287.222	287.222	287.222	287.222	287.222	287.222	287.223
1.87+03	287.193	287.226	287.227	287.227	287.227	287.227	287.227	287.227	287.227	287.228
1.55+03	287.192	287.229	287.228	287.227	287.227	287.227	287.227	287.227	287.228	287.229
1.28+03	287.190	287.226	287.225	287.224	287.221	287.224	287.224	287.225	287.226	287.226
1.06+03	287.186	287.223	287.221	287.220	287.220	287.220	287.220	287.220	287.222	287.225
8.74+02	287.184	287.215	287.216	287.215	287.214	287.214	287.214	287.215	287.217	287.221
7.20+02	287.180	287.213	287.211	287.209	287.209	287.209	287.210	287.213	287.215	287.219
5.92+02	287.178	287.206	287.206	287.204	287.204	287.204	287.206	287.208	287.212	287.216
4.85+02	287.176	287.204	287.202	287.200	287.200	287.200	287.200	287.201	287.204	287.208
3.95+02	287.174	287.203	287.198	287.196	287.195	287.195	287.195	287.197	287.200	287.205
3.22+02	287.172	287.197	287.195	287.192	287.192	287.192	287.192	287.194	287.197	287.201
2.63+02	287.170	287.194	287.191	287.189	287.188	287.188	287.188	287.191	287.194	287.199
2.03+02	287.169	287.191	287.188	287.185	287.185	287.185	287.185	287.188	287.191	287.196
1.65+02	287.168	287.189	287.185	287.182	287.181	287.181	287.181	287.185	287.189	287.194
1.35+02	287.167	287.186	287.183	287.178	287.178	287.178	287.178	287.182	287.186	287.192
1.10+02	287.166	287.184	287.180	287.175	287.175	287.174	287.174	287.179	287.184	287.190
9.00+01	287.165	287.181	287.177	287.171	287.171	287.171	287.171	287.176	287.182	287.188
7.37+01	287.164	287.178	287.173	287.166	287.166	287.166	287.166	287.172	287.178	287.185
6.04+01	287.163	287.175	287.168	287.160	287.160	287.160	287.160	287.167	287.175	287.183
4.93+01	287.162	287.171	287.163	287.153	287.153	287.153	287.153	287.162	287.171	287.180
4.04+01	287.161	287.165	287.155	287.143	287.143	287.142	287.142	287.154	287.166	287.177
3.00	287.160	287.132	287.104	287.077	287.077	287.077	287.077	287.104	287.132	287.160

RELATIVE HUMIDITY

TIME= 300.00 SEC DTEMIZ= -1.0 K ITEMLE= 1 ITEMR=10

X(KM)= Z(M)	.00	1.00	2.00	3.00	4.00	5.00	6.00	7.00	8.00	9.00
9.64+03	9.52677-01	8.98935-01	9.01948-01	9.01391-01	9.00925-01	9.00738-01	9.00579-01	9.00565-01	9.00729-01	9.00934-01
8.19+03	9.01497-01	9.29745-01	9.30431-01	9.30358-01	9.30279-01	9.30241-01	9.30226-01	9.30179-01	9.30070-01	9.29962-01
6.82+03	9.14546-01	9.31576-01	9.31843-01	9.31831-01	9.31761-01	9.31744-01	9.31735-01	9.31742-01	9.31760-01	9.31747-01
5.67+03	9.23643-01	9.33590-01	9.33832-01	9.33793-01	9.33769-01	9.33760-01	9.33757-01	9.33758-01	9.33850-01	9.33771-01
4.72+03	9.32836-01	9.37955-01	9.35041-01	9.35069-01	9.35070-01	9.35069-01	9.35269-01	9.35057-01	9.35033-01	9.37967-01
3.92+03	9.37[illegible]-01	9.40203-01	9.40145-01	9.40149-01	9.40148-01	9.40148-01	9.40148-01	9.40163-01	9.40183-01	9.40150-01
3.26+03	9.41[illegible]4-01	9.42210-01	9.42267-01	9.42310-01	9.42318-01	9.42319-01	9.42319-01	9.42299-01	9.42258-01	9.42147-01
2.71+03	9.44069-01	9.43455-01	9.43512-01	9.43531-01	9.43535-01	9.43536-01	9.43536-01	9.43539-01	9.43528-01	9.43438-01
2.25+03	9.46192-01	9.44652-01	9.44717-01	9.44765-01	9.44773-01	9.44775-01	9.44775-01	9.44750-01	9.44694-01	9.44544-01
1.87+03	9.47264-01	9.45532-01	9.45615-01	9.45664-01	9.45672-01	9.45674-01	9.45674-01	9.45647-01	9.45582-01	9.45426-01
1.55+03	9.48310-01	9.46278-01	9.46369-01	9.46429-01	9.46439-01	9.46439-01	9.46440-01	9.46430-01	9.46317-01	9.46117-01
1.29+03	9.48768-01	9.46890-01	9.46995-01	9.47059-01	9.47066-01	9.47070-01	9.47070-01	9.47027-01	9.46935-01	9.46742-01
1.06+03	9.49188-01	9.47444-01	9.47563-01	9.47636-01	9.47647-01	9.47649-01	9.47650-01	9.47597-01	9.47469-01	9.47263-01
8.74+02	9.49669-01	9.47960-01	9.48085-01	9.48175-01	9.48188-01	9.48190-01	9.48190-01	9.48121-01	9.47994-01	9.47752-01
7.23+02	9.50108-01	9.48424-01	9.48555-01	9.48661-01	9.48675-01	9.48678-01	9.48678-01	9.48593-01	9.48446-01	9.48191-01
5.92+02	9.50363-01	9.48834-01	9.48968-01	9.49090-01	9.49106-01	9.49109-01	9.49109-01	9.49009-01	9.48846-01	9.48562-01
4.45+02	9.50656-01	9.49195-01	9.49333-01	9.49468-01	9.49487-01	9.49490-01	9.49491-01	9.49375-01	9.49198-01	9.48927-01
3.95+02	9.50861-01	9.49511-01	9.49652-01	9.49803-01	9.49823-01	9.49827-01	9.49828-01	9.49697-01	9.49506-01	9.49232-01
3.22+02	9.51134-01	9.49790-01	9.49935-01	9.50103-01	9.50125-01	9.50128-01	9.50129-01	9.49982-01	9.49779-01	9.49498-01
2.67+02	9.51342-01	9.50034-01	9.50187-01	9.50374-01	9.50397-01	9.50401-01	9.50402-01	9.50237-01	9.50017-01	9.49730-01
2.03+02	9.51487-01	9.50251-01	9.50417-01	9.50625-01	9.50650-01	9.50654-01	9.50655-01	9.50469-01	9.50230-01	9.49934-01
1.65+02	9.51595-01	9.50445-01	9.50632-01	9.50865-01	9.50891-01	9.50896-01	9.50897-01	9.50686-01	9.50425-01	9.50114-01
1.29+02	9.51690-01	9.50626-01	9.50838-01	9.51102-01	9.51132-01	9.51134-01	9.51136-01	9.50894-01	9.50605-01	9.50274-01
9.93+01	9.51815-01	9.50796-01	9.51041-01	9.51344-01	9.51372-01	9.51377-01	9.51378-01	9.51100-01	9.50778-01	9.50418-01
7.44+01	9.51954-01	9.50964-01	9.51252-01	9.51599-01	9.51629-01	9.51633-01	9.51634-01	9.51311-01	9.50946-01	9.50551-01
5.37+01	9.52056-01	9.51177-01	9.51513-01	9.51922-01	9.51952-01	9.51956-01	9.51957-01	9.51579-01	9.51162-01	9.50719-01
3.64+01	9.52117-01	9.514[illegible]0-01	9.51812-01	9.52289-01	9.52319-01	9.52321-01	9.52323-01	9.51872-01	9.51767-01	9.50931-01
2.29+01	9.52253-01	9.51655-01	9.52155-01	9.52739-01	9.52767-01	9.52771-01	9.52772-01	9.52224-01	9.51644-01	9.51050-01
1.03+01	9.52335-01	9.52003-01	9.52669-01	9.53395-01	9.53421-01	9.53424-01	9.53425-01	9.52720-01	9.51994-01	9.51258-01
.00	0.00000	0.00000	0.00000	0.00000	0.00000	0.00000	0.00000	0.00000	0.00000	0.00000

ORIGINAL PAGE IS
OF POOR QUALITY

VISIBILITY (METER)

TIME= 300.00 SEC DTEMI= -1.0 K ITEML= 1 ITEMR=10

X(KM)= Z(M)	.00	1.00	2.00	3.00	4.00	5.00	6.00	7.00	8.00	9.00
9.84+03	3.60247+03	2.55794+03	2.62950+03	2.64150+03	2.64737+03	2.65329+03	2.66160+03	2.65907+03	2.65793+03	2.65926+03
8.19+03	2.32951+03	1.99233+03	1.99929+03	2.00156+03	2.00355+03	2.00133+03	2.00160+03	2.00213+03	2.00344+03	2.00535+03
6.82+03	2.61908+03	1.96043+03	1.95644+03	1.95721+03	1.95335+03	1.95886+03	1.96113+03	1.95156+03	1.95135+03	1.96073+03
5.67+03	2.45563+03	1.91350+03	1.91523+03	1.90967+03	1.91594+03	1.91578+03	1.91577+03	1.91532+03	1.91444+03	1.91262+03
4.72+03	2.30338+03	1.79945+03	1.79880+03	1.79952+03	1.79852+03	1.79835+03	1.79833+03	1.79842+03	1.79864+03	1.79934+03
3.92+03	2.20433+03	1.73560+03	1.73932+03	1.74092+03	1.74015+03	1.74005+03	1.74004+03	1.73970+03	1.73920+03	1.73865+03
3.26+03	2.12717+03	1.58718+03	1.68624+03	1.68762+03	1.68691+03	1.68661+03	1.68581+03	1.68702+03	1.65750+03	1.68867+03
2.71+03	2.09514+03	1.65469+03	1.64291+03	1.65082+03	1.65025+03	1.65018+03	1.65016+03	1.64996+03	1.64978+03	1.65033+03
2.25+03	2.05113+03	1.61340+03	1.60809+03	1.61490+03	1.61410+03	1.61398+03	1.61397+03	1.61392+03	1.61416+03	1.61573+03
1.87+03	2.03494+03	1.58870+03	1.58923+03	1.58421+03	1.58437+03	1.58446+03	1.58449+03	1.58462+03	1.58571+03	1.58843+03
1.55+03	2.01923+03	1.56470+03	1.56865+03	1.56372+03	1.55757+03	1.55797+03	1.55800+03	1.55866+03	1.57163+03	1.57537+03
1.29+03	2.00027+03	1.55023+03	1.54166+03	1.54469+03	1.54521+03	1.54534+03	1.54535+03	1.54596+03	1.54734+03	1.55973+03
1.06+03	1.99368+03	1.53885+03	1.53003+03	1.53347+03	1.53342+03	1.53343+03	1.53342+03	1.53399+03	1.53544+03	1.53923+03
8.74+02	1.98656+03	1.52258+03	1.52127+03	1.51042+03	1.51012+03	1.51009+03	1.51007+03	1.51102+03	1.52422+03	1.52556+03
7.20+02	1.97991+03	1.50421+03	1.49812+03	1.50507+03	1.50461+03	1.50455+03	1.50454+03	1.50507+03	1.50569+03	1.50795+03
5.92+02	1.97605+03	1.49240+03	1.49432+03	1.48950+03	1.48896+03	1.48839+03	1.48869+03	1.49076+03	1.49375+03	1.50695+03
4.85+02	1.97163+03	1.48159+03	1.47622+03	1.47479+03	1.47422+03	1.47415+03	1.47413+03	1.48348+03	1.48605+03	1.48691+03
3.96+02	1.96853+03	1.47388+03	1.46557+03	1.47105+03	1.47046+03	1.47038+03	1.47036+03	1.47256+03	1.47279+03	1.47965+03
3.22+02	1.96441+03	1.47149+03	1.46223+03	1.45667+03	1.45609+03	1.45600+03	1.45599+03	1.45896+03	1.45974+03	1.46995+03
2.60+02	1.96128+03	1.45860+03	1.45135+03	1.44565+03	1.44565+03	1.44565+03	1.44565+03	1.44829+03	1.45931+03	1.45705+03
2.08+02	1.95910+03	1.44979+03	1.45142+03	1.43758+03	1.43759+03	1.43760+03	1.43759+03	1.44258+03	1.45773+03	1.46051+03
1.65+02	1.95744+03	1.44399+03	1.43783+03	1.43506+03	1.43305+03	1.43805+03	1.43804+03	1.44417+03	1.44540+03	1.45551+03
1.29+02	1.95605+03	1.44053+03	1.44061+03	1.42694+03	1.42693+03	1.42693+03	1.42691+03	1.43800+03	1.43751+03	1.45157+03
9.97+01	1.94232+03	1.44061+03	1.43127+03	1.42172+03	1.42158+03	1.42157+03	1.42155+03	1.42870+03	1.44150+03	1.45103+03
7.44+01	1.94021+03	1.43575+03	1.42340+03	1.40981+03	1.40957+03	1.40955+03	1.40954+03	1.42421+03	1.43219+03	1.44016+03
5.37+01	1.93862+03	1.43751+03	1.42025+03	1.40694+03	1.40655+03	1.40651+03	1.40649+03	1.41751+03	1.42177+03	1.43757+03
3.64+01	1.93772+03	1.41716+03	1.40235+03	1.38817+03	1.38760+03	1.38755+03	1.38752+03	1.40009+03	1.41546+03	1.42959+03
2.20+01	1.93566+03	1.40796+03	1.39738+03	1.37985+03	1.37933+03	1.37929+03	1.37925+03	1.39532+03	1.41577+03	1.43126+03
1.00+01	1.93442+03	1.40291+03	1.38477+03	1.36005+03	1.35963+03	1.35959+03	1.35957+03	1.38304+03	1.39704+03	1.42222+03
.00	0.00000	0.00000	0.00000	0.00000	0.00000	0.00000	0.00000	0.00000	0.00000	0.00000

APPENDEX C

FORTRAN LISTING OF COMPUTER PROGRAM

```
C
C
C
C     TWO-DIMENSIONAL MODEL OF CONDENSATION NUCLEI ASSOCIATED WITH
C     A POLLUTED ATMOSPHERE AND THE ADVECTION FOG FORMATION AND
C     DISSIPATION
C
C
C
      PARAMETER JX=10,JZ=31,JY=1
      REAL*4 KA,INT,KW,L,KM
      COMMON/BL0/ KA(JX,JZ),KM(JX,JZ),INT(JX,JZ),CRT(JX,JZ),RC(JX,JZ)
     *            ,RH(JX,JZ),VISITY(JX,JZ),NDIS(JY),RDIS(JY),NDISA(JY)
     *            ,RDISA(JY),NSP,IMOD
      COMMON/BL1/  U(JX,JZ), EU(JZ), FU(JZ)
      COMMON/BL2/  V(JX,JZ), EV(JZ), FV(JZ)
      COMMON/BL3/  Y(JX,JZ), EY(JZ), FY(JZ)
      COMMON/BL4/  R(JX,JZ), ER(JZ), FR(JZ)
      COMMON/BL5/  W(JX,JZ), EW(JZ), FW(JZ)
      COMMON/BL6/ PT(JX,JZ),EPT(JZ),FPT(JZ),T(JX,JZ)
      COMMON/BL7/ P(JX,JZ),PR(JZ),ITEM(JX),DX(JX),Z(JZ),DZ(JZ),DZA(JZ)
      COMMON/BL8/ ZA(JZ),X(JX),IE,KE,TIME,ITEMI,ITEML,ITEMR,DTF,DTE
      COMMON/BL9/ L,CP,G,DT,TIM,CV,ZAF,CC,CM,CI,CO,F,IN,IN,ISED,IRAD,
     *            IPSFC,II,OPTIM,HEAT,ZO,CR,DEN,PRT
      COMMON/BL10/ RC(JX,JZ),RAD(JX,JZ),RANI,NH,NH,HEIGHT,VHF,RDEN,HRW,
     *              VHFA,RDENA,HRWA,HDEN,VHFF,HMW
      COMMON/BL11/ RAE(JX,JZ,JY),RAE(JX,JZ,JY),PW(JZ)
      DIMENSION FMTH(11),FMTT(11)
C
C     PHYSICAL CONSTANTS
C
      L=592.
      DPW=1.27E-5
      CP=.240
      G=980.6
      RA=.0685
      RW=.1102
      SIGMA=1.355E-12
      CV=-405.
      F=1.0E-4
C
C     DATA INPUT
C
   10 READ(5,1000,END=400) DT,OT,ET,TIM,HF,KW,TP,ZO,ITEMI,UF
      READ(5,1100) IPT,IKK,IW,ISED,IRAD,IPSFC,IN,ISTEP,IP,II,KT,KR,KW,IZ
     *             ,IMOD
      READ(5,1200) ZAL,ZAF,XAI,IE,KE,IL,IR,ITEML,ITEMR,DELX
      READ(5,1205) FMTH,FMTT
      READ(5,1210) NH,VHF,RDEN,HRW,VHFA,RDENA,HRWA,RANI,HDEN,VHFF,HMW
      READ (5,1211) (NDIS(J),J=1,JY)
      READ (5,1212) (RDIS(J),J=1,JY)
      READ (5,1211) (NDISA(J),J=1,JY),NSP
      READ (5,1212) (RDISA(J),J=1,JY)
C
C     DATA LISTING
```

```
C
      WRITE(6,2200) DT,GT,ET,TIM,RF,KW,TP,SG,GIEMI,UF
      WRITE(6,2100) IPT,IRK,IW,ISED,IPAD,IRSEC,IU,IDTE,IP,IA,KT,KK,GY,I
     *              Z,JYOT
      WRITE(6,2200) ZAL,ZAK,ZAI,IE,KE,IL,IR,ITEML,ITEMK,DELX
      WRITE(6,2210)RH,VHF,PDEN,HMW,VHFA,PDENA,HMWA,RAPI,HOLA,VHFN,HMWN
      WRITE(6,2211) (U0IS(J),J=1,JY)
      WRITE(6,2211) (R0IS(J),J=1,JY)
      WRITE(6,2211) (U0ISA(J),J=1,JY),NSP
      WRITE(6,2212) (R0ISA(J),J=1,JY)
C
C     WORKING CONSTANT DEFINITION
C
      CC=.622*(L**2)/(GP*PA)
      CM=K_REF*SIGMA/(GP*DEN**.333)
      CI=KW*(DEN**.667)/G.
      CH=(L**2)/KH
      CK=.4*GP
      CS=P/4.1_6E+7
      IN=IE-1
      KN=KE-1
C
C     VERTICAL GRID SPECIFICATION
C
      ZA(1)=0.0
      ZA(2)=ZAL
      DZA(2)=ZAL
      DO 20 K=3,KE
      DZA(K)=(1.+ZAK)*DZA(K-1)
   20 ZA(K)=ZA(K-1)+DZA(K)
      DO 25 K=2,KE
      Z(K)=(ZA(K)+ZA(K-1))/2.
   25 CONTINUE
      HEIGHT=ZA(KE)
C
C     HORIZONTAL GRID SPECIFICATION
C
      DO 30 I=IL,IR
   30 X(I)=(I-IL)*DELX
      I1=IR+1
      DO 31 I=I1,IE
   31 X(I)=X(I-1)+XAI*(X(I-1)-X(I-2))
      IF(IL .EQ. 1) GO TO 33
      I1=IL-1
      DO 32 I2=1,I1
      I=I1-I2+1
   32 X(I)=X(I+1)-XAI*(X(I+2)-X(I+1))
   33 DO 35 I=2,IE
      DX(I)=X(I)-X(I-1)
   35 CONTINUE
C
C
C     VARIABLE INITIALIZATION
C
C
      READ (5,1300) RI,PTI,OPTIM,HEAT,YI,DIF,OTF
      WRITE(6,2300) RI,PTI,OPTIM,HEAT,YI,DIF,OTF
```

```
      TP=TP+.10
      PTI=PTI+.10
      W(1,1)=0.0
C
C     UNIFORM WITH HEIGHT
C
      DO 40 I=1,IR
      DO 40 K=1,KE
      WAH(I,K)=0.0
      RC(I,K)=0.
      Y(I,K)=YI
      IF(I.LT.IT.OR. ... I. T.ITEMP ) Y(I,K)=-YI
      W(I,K)=0.0
      DO 41 J=1,JT
      RAL(I,K,J)=FLIQ(J)
      RAL(I,K,J)=FLIQA(J)
41    CONTINUE
      R(I,K)=RI
      PT(I,K)=PTI
      P(I,K)=1000.*EXP(-G*ZA(K)/(R*(TP+Z*...*TP)))
      IF(IPT.EQ.-1) PT(I,K)=TP*((1000./P(I,K))**.286)
      IF(IU.EQ.0) U(I,K)=2.5*UF*ALOG((ZA(K)+Z0)/Z0)*COS(.174..)
      IF(IU.EQ.0) V(I,K)=2.5*UF*ALOG((ZA(K)+Z0)/Z0)*SIN(.1754)*(1-
     *                  ZA(K)/ZA(KE))
   40 CONTINUE
C
C     INITIALIZE ... SIMULATION
C     UPWIND BOUNDARY
C
      IF(IU .EQ. 1) READ(5,4000) (U(1,K),K=1,KE)
      IF(IU .EQ. 1) READ(5,4000) (V(1,K),K=1,KE)
C
C     NON-UNIFORM INITIALIZATION OF SIMULATION FROM KT AND KR LEVELS
C     TO TOP OF THE MODEL
C
      IF(IPT .EQ. 1) READ(5,5000) (PT(1,K),K=KT,KE)
      IF(IRR .EQ. 1) READ(5,4000) (R(1,K),K=KR,KE)
      IF(IW .EQ. 1) READ(5,4000) (W(1,K),K=KW,KE)
      IF(IU .EQ. 1) WRITE(6,2500) (U(1,K),K=1,KE)
      IF(IU .EQ. 1) WRITE(6,2500) (V(1,K),K=1,KE)
      IF(IPT .EQ. 1) WRITE(6,2400) (PT(1,K),K=1,KE)
      IF(IRR .EQ. 1) WRITE(6,2500) (R(1,K),K=KR,KE)
      IF(IW .EQ. 1) WRITE(6,2500) (W(1,K),K=1,KE)
C
C     INITIALIZATION ALL COLUMNS
C
      DO 50 I=2,IR
      DO 50 K=1,KE
      U(I,K)=U(1,K)
      V(I,K)=V(1,K)
      PT(I,K)=PT(1,K)
      R(I,K)=R(1,K)
   50 W(I,K)=W(1,K)
C
C     INITIALIZATION,EXCHANGE COEFFICIENT, INTEGRATED LIQUID WATER,AND
C     SPECIFIC HEAT OF MOIST AIR
C
```

```
      CE=14.*(A.1*/PI(1,1)
      INT(1,1)=0.0
      T(1,1)=PT(1,1)
      DO 50 K=2,KE
      PR(K)=(1.0/P(1,K))**.286
      DZ(K)=(1.+ZA(K))*(DZA(K)**2)
      T(1,K)=PI(1,K)/PI(K)
      DWZ=SQRT((U(1,K)-U(1,K-1))**2+(V(1,K)-V(1,K-1))**2+(Y(1,K)-Y(1,K-1
     *    ))**2)/DZA(K)
      IF(W(1,K) .LT. 0.0) GO TO 65
      CPT(1,K)=CP
C
C     INITIALIZATION OF EXCHANGE COEFFICIENTS COVERING NEUTRAL,STABLE AND
C     UNSTABLE CONDITIONS BETWEEN K=2 AND THE SURFACE.
C
      S=(PT(1,K)-PT(1,K-1))/DZA(K)
      GO TO 70
65    CPT(1,K)=CP+CB*RSF(T(1,K),P(1,K))/(T(1,K)**2)
      S=(T(1,K)-T(1,K-1))/DZA(K)+CS/CPT(1,K)
70    CONTINUE
      KM(1,K)=.1*SQRT(U(1,K)**2+V(1,K)**2+Y(1,K)**2)*DZA(K)/(ALOG(ZA(K)
     */Z0)**2)
      KA(1,K)=KM(1,K)
      UF1=SQRT(KM(1,K)*0.7)
      IF(S .EQ. 0.) GO TO 75
      TL=(UF1**2)*PT(1,K)/(.4*G*KA(1,K)*S)
      IF(S .GT. 0.) GO TO75
      IF(S .LT. 0.) GO TO 77
      PHI=DSQRT(DSQRT(1.00-15.00*Z(K)/TL))
      KM(1,K)= .4*Z(K)*UF1*PHI
      KA(1,K)=KM(1,K)*PHI
      GO TO 79
   75 KM(1,K)=(.4*Z(K)*UF1)/(1.+5.*(Z(K)/TL))
      GO TO 7
   77 KM(1,K)=.4*Z(K)*UF1
   78 KA(1,K)=KM(1,K)
      GO TO 79
C
C     SHIR-TYPE EXPONENTIAL DECREASE
C
79    DEC=EXP(-0.*F*Z(K)/UF1)
      KM(1,K)=KM(1,K)*DEC
      KA(1,K)=KA(1,K)*DEC
   80 INT(1,K)=INT(1,K-1)+CI*(W(1,K)**.667+W(1,K-1)**.667)*DZA(K)
      CPT(1,1)=CPT(1,2)
      KA(1,1)=KA(1,2)
C
C     INITIALIZATION ALL COLUMNS
C
      DO 81 I=2,IE
      DO 81 K=1,KE
      IF(K .EQ. 1) W(I,K)=0.0
      T(I,K)=T(1,K)
      CPT(I,K)=CPT(1,K)
      KM(I,K)=KM(1,K)
      KA(I,K)=KA(1,K)
   81 INT(I,K)=INT(1,K)
```

```
C
C     INITIALIZATION OF SURFACE TEMPERATURE DIFFERENCE
C
      IF(ISTEM.EQ.-1) GO TO 96
      DO 85 I=1,IN
      IF(ISTEM.EQ.0) DTEM(I)=0.
      IF(ISTEM .EQ. 1) DTEM(I)=TEMI
      ML=ITEML+(ITEMH-ITEML)/3
      MU=ITEML+(ITEMH-ITEML)*2/3
      IF((ISTEM.EQ.1).AND.(I.LT.ML)) DTEM(I)=TEMI*(I-ITEML)*3/(ITEMH-
     *ITEML)
      IF((ISTEM.EQ.1).AND.(I.GT.MU)) DTEM(I)=TEMI*(ITEMH-I)*3/(ITEMH-
     *ITEML)
      IF((ISTEM .EQ. 1) .AND. (I .LT. ITEML)) DTEM(I)=0.0
      IF((ISTEM .EQ. 1) .AND. (I .GT. ITEMH)) DTEM(I)=0.0
   85 CONTINUE
      GO TO 97
96    READ(5,1400) (DTEM(I), I=2,IN)
      WRITE(6,1400)(DTEM(I), I=2,IN)
      DTEM(1)=0.
      DTEM(IE)=0.
C
C     UPPER BOUNDARY CONDITION FOR IMPLICIT INTEGRATION
C
   97 EU(KE)=0.
      EV(KE)=0.
      EPT(KE)=0.0
      EP(KE)=0.0
      EW(KE)=0.0
      EY(KE)=0.0
      FY(KE)=Y(1,KE)
      FU(KE)=U(1,KE)
      FV(KE)=V(1,KE)
      FPT(KE)=PT(1,KE)
      FP(KE)=P(1,KE)
      FW(KE)=W(1,KE)
C
C     OUTPUT TIME, END TIME, AND TIME STEP CONTROL
C
      TIME=0.0
      PRT=DT
   90 IF(TIME .LT. PRT) GO TO 95
      PRT=TIME+DT
      GO TO 200
   95 IF(TIME .GE. ET) GO TO 10
      TIME=TIME+DT
      CALL STEP
      IF(TIME.EQ.DFTIM) DT=DT/DTF
      IF(TIME .EQ.DFTIM) DT=DT/DTF
      IF(TIME.EQ.DFTIM) PRT=DPTIM
      GO TO 90
  200 CONTINUE
C
C
C     OUTPUT OF VARIABLES
C
C
```

```
C     EDDY HEAT FLUX OUTPUT
C
  300 WRITE(6,3000)
      DO 311 I=1,IL
      DO 310 K=3,KN
      IF(CPT(I,K) .LE. CP) HC(I,K)=-DEN*CP*((KA(I,K+1)*(PT(I,K+1)-PT(I,K
     1))/(ZA(K+1)-ZA(K)))+(KA(I,K)*(PT(I,K)-PT(I,K-1))/(ZA(K)-ZA(K-1))))/
     2*2.1
  310 IF(CPT(I,K) .GT. CP) HC(I,K)=-DEN*CPT(I,K)*(((KA(I,K)+KA(I,K+1))/2
     1.)*((T(I,K+1)-T(I,K-1))/(ZA(K+1)-ZA(K-1))+G/CPT(I,K)))*4.2
      WINDVL=SQRT(U(I,2)**2+V(I,2)**2)*.07
      IF(CPT(I,2) .LE. CP) HC(I,2)=-DEN*CP*60.*.16*WINDVL*(PT(I,2)-PT(I,
     11))/(ALOG(ZA(2)/Z0)**2)
      IF(CPT(I,2) .GT. CP) HC(I,2)=-DEN*CPT(I,2)*60.*.16*WINDVL*(T(I,2)-
     1T(I,1)+G*ZA(2)/CPT(I,2)))/(ALOG(ZA(2)/Z0)**2)
      HC(I,1)=HC(I,2)
      HC(I,KE)=HC(I,KN)
  311 CONTINUE
      CALL PRNT(HC,FMTH)
C
C     WIND OUTPUT
C
      WRITE(6,2009)
      CALL PRNT(U,FMTH)

      WRITE(6,2010)
      CALL PRNT(V,FMTH)
C
      WRITE(6,2011)
      CALL PRNT(Y,FMTH)
C
C     TEMPERATURE OUTPUT
C
      WRITE(6,2100)
      CALL PRNT(T,FMTT)
C
C     MIXING RATIO OUTPUT
C
      WRITE(6,2200)
      CALL PRNT(R,FMTH)
C
C     LIQUID WATER CONTENT OUTPUT
C
      WRITE(6,3200)
      DO 315 I=1,IL
      DO 315 K=1,KE
  315 HC(I,K)=DEN*W(I,K)*1.0E+6
      CALL PRNT(HC,FMTH)
C
C     TURBULENT EXCHANGE COEFFICIENT OUTPUT
C
      WRITE(6,3500)
      DO 331 I=1,IL
      DO 330 K=3,KN
      EX=(KA(I,K)+KA(I,K+1))/2.
  330 HC(I,K)=EX
      HC(I,2)=.16*SQRT(U(I,2)**2+V(I,2)**2)*ZA(2)/ALOG(ZA(2)/Z0)
```

```
      HC(I,1) [illegible]
  331 HC(I,K) [illegible]
      CALL PRNT(HC,FMTH)
C
      IF(IS [illegible] T [illegible]
C
C     RADIATIVE FLUX OUTPUT
C
      WRITE(6, [illegible])
      DO 340 I=1,I[illegible]
      DO 340 K=1,K[illegible]
      HR [illegible] *(T(I,1)**4)*EXP(-INT(I,K [illegible] +INT(I,K))*[illegible]
  340 HC(I,K) [illegible]
      CALL PRNT(HC,FMTH)
C
C     RADIATIVE [illegible] RATE OUTPUT
C
      WRITE(6, [illegible])
      DO 350 I=1,I[illegible]
      DO 350 K=1,K[illegible]
      [illegible] *(W(I,K)**.667)*[illegible]*(T(I,1)**4.)*EXP(-INT(I,K)+INT(I,K
     1)*[illegible] INT(I,K)
  350 HC(I,K) [illegible]
      CALL PRNT(HC,FMTH)
C
C     WATER VAPOR FLUX OUTPUT
C
      WRITE(6,[illegible])
      DO 360 I=1,I[illegible]
      DO 360 K=1,K[illegible]
      HC(I,K)=[illegible]*((ZA(I,K+1)*(Q(I,K+1)-Q(I,K))/(ZA(K+1)-ZA(K)))+[illegible]
     1(I,K)*(Q(I,K)-Q(I,K-1))/(ZA(K)-ZA(K-1))))
  360 CONTINUE
      WIND [illegible](I,1)**2+V(I,1)**2)
      HC(I,1)=[illegible]*WINDV*(Q(I,1)-Q(I,1))/(AL[illegible](ZA(1)/Z[illegible]
      HC(I,1)=[illegible](I,1)
      HC(I,K)=[illegible](I,K)
  361 CONTINUE
      CALL PRNT(HC,FMTH)
C
C     RELATIVE HUMIDITY
C
      WRITE(6,[illegible])
      CALL PRNT(RH,FMTH)
C
C     VISIBILITY OF FOG
C
      WRITE(6,[illegible])
      CALL PRNT(VISITY,FMTH)
C
      GO TO [illegible]
  400 STOP
C
  100 FORMAT([illegible])
 1000 FORMAT([illegible])
 1100 FORMAT([illegible])
 1200 FORMAT([illegible])
```

```
 1 0  FORMAT(11A4/15)
1010  FORMAT(I5,1 E7.3)
1700  FORMAT(2 I5,3)
 1    FORMAT( I5 ,3)
 000  FORMAT(1H1,////,30X,10HINPUT DATA,//,1H0,1P10E10.2)
 100  FORMAT(1H0,1015)
 200  FORMAT(1H ,1P7E10.2,  6I5,-2PF6.0)
  10  FORMAT(1H ,I5,1 E10.3)
 700  FO MAT(1H0,7E10.3)
 200  FORMAT(1H0,7F10.3)
   0  FORMAT(1H ,7F10.2)
1011  FORMAT(7,10)
1012  FORMAT(7E1.3)
 011  FORMAT(1H ,7I10)
 012  FORMAT(1H0,7E10.3)
 000  FORMAT('UHIFUEY HEAT FLUX IN WATTS/CM**2///)
 100  FORMAT( HIFHILTAUN VELOCITY IN CM/SEC///)
 000  FORMAT('1 U COMPONENT OF WIND VELOCITY (CM/SEC.) ',///)
 010  FORMAT('1 V COMPONENT OF WIND VELOCITY (CM/SEC.)'///)
2011  FORMAT('1 VERTICAL WIND VELOCITY (CM/SEC.)',///)
 100  FORMAT('1H1TEMPERATURE IN DEG K///)
 200  FORMAT( UHIXING RATIO IN G/G///)
 200  FORMAT(1H1,'  RELATIVE HUMIDITY ',///)
 200  FORMAT('1H1LIQUID WATER CONTENT IN G/M**3///)
 200  FORMAT( 1H1DROPLET RADIUS IN CM ///)
 200  FORMAT( 1H1  FURFh SIMULATION OF HAR  FOG FORMATION  /)
 200  FORMAT('1 DROPLET RADIUS OF HYGROSCOPIC MATERIAL ')
 770  FORMAT(  TIME=,F7.0,4H SEC,6X,  DTE  =,F5.1,   ,6X,  TEMP=,
     1X,  IT    ,I ,/ X,'HEIGHT'/2X,'( M )')
 1    FORMAT(1H , F . ,1X,1A1, 20A4     )
 103  FORMAT(1H , X,1 A1)
 120  FORMAT(1H0,10X,2 (-5PF4,0 )//  X,'ADVECTION DISTANCE  (KM)')
 400  FORMAT('1H1 EW POINT DEPRESSION IN DEG C///)
 500  FORMAT(  1TURBULENT EXCHANGE COEFFICIENT IN CM**2/SEC///)
 600  FORMAT('1H1RADIATIVE FLUX IN CAL/CM**2MIN///)
 700  FORMAT('1H1RADIATIVE COOLING IN DEG C/HR///)
 800  FORMAT(  1 DEY MOISTURE FLUX IN G/CM**2 S C///)
 000  FORMAT(1H1,'   VISIBILITY  ( METER ) ',///)
4000  FORMAT(5E10.3)
5000  FORMAT(F 10.5)
      END
```

```
C
C
C     INTEGRATION SUBROUTINE
C
C     INTEGRATION ONE TIME STEP AND COMPUTE NEW PROGNOSTICS & DIAGNOSTIC
C     VARIABLES
C
      SUBROUTINE STEP
C
C
      PARAMETER JX=10,JZ=71,JY=1
      REAL*8 KA,INT,L,KM
      DIMENSION TFA(JZ),FCC(JX,JZ)
      DIMENSION TFC(JX,JZ,JY), TFCA(JX,JZ,JY)
      COMMON/BL0/ KA(JX,JZ),KM(JX,JZ),INT(JX,JZ),CNT(JX,JZ),HC(JX,JZ)
     *            ,RH(JX,JZ),VISITY(JX,JZ),NDIS(JY),RDIS(JY),NDISA(JY)
     *            ,RDISA(JY),NSP,IMOD
      COMMON/BL1/  U(JX,JZ), EU(JZ), FU(JZ)
      COMMON/BL2/  V(JX,JZ), EV(JZ), FV(JZ)
      COMMON/BL3/  Y(JX,JZ), EY(JZ), FY(JZ)
      COMMON/BL4/  R(JX,JZ), ER(JZ), FR(JZ)
      COMMON/BL5/  W(JX,JZ), EW(JZ), FW(JZ)
      COMMON/BL6/ PT(JX,JZ),EPT(JZ),FPT(JZ),T(JX,JZ)
      COMMON/BL7/ P(JX,JZ),PR(JZ),BTEM(JX),DX(JX),Z(JZ),DZ(JZ),DZA(JZ)
      COMMON/BL8/ ZA(JZ),X(JX),IL,KF,TIME,ITEMI,ITEML,ITEMR,DTF,UTF
      COMMON/BL9/ L,CP,G,DT,TIM,CV,ZAM,CC,CH,CI,CS,F,FN,IN,ISED,IRAD,
     *            INSFC,II,OPTIM,HEAT,ZO,CN,DEN,PCT
      COMMON/ L10/ FC(JX,JZ),RAH(JX,JZ),RAHI,NK,NH,HEIGHT,VHF,RDEN,HMW,
     *              VHFA,RDENA,HMWA,HDEN,VHFM,HMWM
      COMMON/BL11/ RAL(JX,JZ,JY),RAE(JX,JZ,JY),PP(JZ)
      IF(TIME.EQ.DT) DLT=DT
      IF(TIME.EQ.DT) AOPTIM=OPTIM+DT
      IF(TIME.LT.OPTIM) GO TO 130
      IF(NK.LT.1) GO TO 130
      NDT=0
      INDT=0
      IF(IMOD.EQ.0) GO TO 133
      DO 120 I=6,6
      DO 120 K=NK,2,-1
      IF(TIME.EQ.AOPTIM) RAH(I,NK)=RAHI
      IF(K.NE.NK) GO TO 30
      IF(K.LE.1) GO TO 30
      FCC(I,K+1)=0.
      RAH(I,K+1)=0.
      FCC(I,K)=0.
      RRAH=RAH(I,K)
      HNM=4*3.1416*RAHI**3*HDEN/3.
      CALL RKF(RAH(I,K),T(I,K),P(I,K),R(I,K),VHFM,HNM,HMWM,NH)
      TRAH=RAH(I,K)
      TV=1.20E+6*RAH(I,K)**2
      DIST=ZA(NK)-ZA(NK-1)
      FCC(I,K)=4*3.1416*(RAH(I,K)**3-RRAH**3)*NH/(3*DEN*DT)
      RAH(I,K-1)=TRAH
 30   CONTINUE
 120  CONTINUE
```

```
      DT=DIST/IV
      PDT=TIME*DT-DDT
      IF(DT.LE.DDT) GO TO 130
      NDT=DT/DDT
      DT=DDT
      FCC(I,K)=FCC(I,K)/NDT
130   CONTINUE
C
C     UPWIND DO LOOP OVER HORIZONTAL GRID SYSTEM
C
      DO 50 I=2,IM
      DDX=DT/DX(I)
C
C     DOWNWARD DO LOOP OVER VERTICAL GRID SYSTEM TO SET UP IMPLICIT
C     INTEGRATION
C
      DO 20 N=2,KM
      K=KM+2-N
C
C     COMPUTE WORKING VARIABLES
C
      IF(TIME.LE.DT) TPR(K)=PR(K)
      DD=DT/DZ(K)
      DDZ=DD*DZA(K)
      A=DD*KA(I,K+1)/(1.+ZAK)
      AW=A
      AU=DD*KM(I,K+1)/(1.+ZAK)
      AUU=II*AU
      AT=A
      C=DD*KA(I,K)
      CW=C
      CU=DD*KM(I,K)
      CUU=II*CU
      CT=C
      IF(ISED .NE.1) GO TO 10
C
C     DROP SEDIMENTATION
C
      AW=AW+DDZ*EV*(W(I,K+1)**.667)/2.
      CW=CW-DDZ*EV*(W(I,K-1)**.667)/2.
C
   10 B=1.+A+C
      BUU=1.+AUU+CUU
      BT=1.+AT+CT
      DPT=PT(I,K)-U(I,K)*(PT(I,K)-PT(I-1,K))*DDX+(100./P(I,K))**.286*
     1  EE* FCC(I,K)*DT/CP-V(I,K)*(PT(I,K)-PT(I,K-1))*DT/DZA(K)
      IF((IMOD.EQ.1).AND.(TIME.GT.OPTIM).AND.(K.LE.MX)) DPT=DPT+(1000./
     *   P(I,K))**0.286*EE*FCC(I,K)*DT/CP
C
C     RADIATIONAL COOLING
C
      IF((ISAD .EQ. 1) .AND. (W(I,K) .GT. 0.0)) DPT=DPT-CP*W(I,K)*(PT(I,
     11)**4.)*EXP(-INT(I,KE)+INT(I,K))*PR(K)*DT/(W(I,K)**.233)
C
      DU=U(I,K)-U(I,K)*(U(I,K)-U(I-1,K))*DDX-(P(I,K)-P(I-1,K))*DDX/DEN+
     1F*V(I,K)*DT-V(I,K)*(U(I,K)-U(I,K-1))*DT/DZA(K)
      DV=V(I,K)-U(I,K)*(V(I   ,K)-V(I-1,K))*DDX+F*(U(I,KE)-U(I,K))*DT
```

```
     1    -Y(I,K)*(V(I,K)-V(I,K-1))*DT/DZA(K)
          DW=RK(I,K)-D(I,K)*(W(I,K)-W(I-1,K))*DDX+FC(I,K)*DT
     1    -Y(I,K)*(W(I,K)-W(I,K-1))*DT/DZA(K)
          DR=RK(I,K)-D(I,K)*(R(I,K)-R(I-1,K))* DDX-FC(I,K)*DT
     1    -Y(I,K)*(R(I,K)-R(I,K-1))*DT/DZA(K)
          IF((IMOD.EQ.1).AND.(TIME.GT.OPTIM).AND.(K.LE.KK))DR=DR-FCC(I,K)*DT
          EW(K)=CW/(1.-AW*EW(K+1))
          FW(K)=(BW+AW*FW(K+1))*EW(K)/CW
          EU(K)=CUU/(1.DU-AUU*EU(K+1.)
          EV(K)=CVV/(1.VV-AVV*EV(K+1))
          EPT(K)=CT/(1.T-AT*EPT(K+1))
          ER(K)=C/(1.-A*ER(K+1))
          FU(K)=(BU+AUU*FU(K+1))*EU(K)/CUU
          FV(K)=(BV+AVV*FV(K+1))*EV(K)/CUU
          FPT(K)=(BT+AT*FPT(K+1))*EPT(K)/CT
          FR(K)=(BR+A*FR(K+1))*ER(K)/C
          PP(K)=AM(I,K+1)*(Y(I,K+1)-Y(I,K))
          TT=T(1,1)/TFR(K)
          P(I,K)=P(I,K-1)-(U(I,K)*(Y(I,K)-Y(I-1,K))/DX(I)+Y(I,K)*(Y(I,K)-
     1         Y(I,K-1))/DZA(K)-PP(K)/(DZ(K)*(1+ZA*K)
     2         )+AM(I,K)*(Y(I,K)-Y(I,K-1))/DZ(K)+G*( T(I,K)/ TT     -1.))*
     3         DEN*DZA(K)
   20 CONTINUE
C
C      UPDATE SURFACE BOUNDARY CONDITION
C
       IF(TIME.LE.TIM) PT(I,1)=PT(1,1)+DTEM(I)*TIME/TIM
       IF((IMOD.EQ.0).AND.(TIME.GT.OPTIM).AND.(I.GE.4).AND.(I.LE.5))
      *   PT(I,1)=PLAT
       T(I,1)=PT(I,1)
       IF(IRSFC .EQ. 0) R(I,1)=FR(2)/(1.-ER(2))
C
C
C      SATURATION SURFACE BOUNDARY CONDITION ON P
C
       IF(IRSFC  .EQ. 1) R(I,1)=RSF(T(I,1),1000.)
C
C      UPWARD DO LOOP OVER VERTICAL GRID SYSTEM TO COMPUTE NEW PROGNOSTIC
C      AND DIAGNOSTIC VARIABLES
C
       INT(I,1)=0.0
       DO 70 K=2,KE
       U(I,K)=EU(K)*U(I,K-1)+FU(K)
       V(I,K)=EV(K)*V(I,K-1)+FV(K)
       Y(I,K)=Y(I,K-1)-(U(I,K)-U(I-1,K))*DZA(K)/DX(I)
       PT(I,K)=EPT(K)*PT(I,K-1)+FPT(K)
       R(I,K)=ER(K)*R(I,K-1)+FR(K)
       PR(K)=(1000./P(I,K))**0.286
       T(I,K)=PT(I,K)/PR(K)
       TW=W(I,K)
       W(I,K)=EW(K)*W(I,K-1)+FW(K)
C
C      COMPUTE RADIUS OF WATER DROPLET BY LIQUID WATER CONTENT
C
       IF(W(I,K) .LT. 0.0) W(I,K)=0.0
       DMASS=(W(I,K)-TW)/ABS(FC(I,K)*DT)
       DO 22 J=1,JY
```

```
      AMASS=DMASS*TFC(I,K,J)
      IF(NSP.NE.1)  GO TO 23
      AMASA=DMASS*TFC(I,K,J)
      TESTA=AMASA*3/(4*3.1416*NDISA(J))+RAD(I,K,J)**3
      TRDISA=RAD(I,K,J)**3
      IF(TESTA.LT.TRDISA) TESTA=TRDISA
      RAD(I,K,J)=TESTA**(1./3.)
23    CONTINUE
      TEST=AMASS*3/(4*3.1416*NDIS(J))+RAD(I,K,J)**3
      TRDIS=RAD(I,K,J)**3
      IF(TEST.LT.TRDIS) TEST=TRDIS
22    RAD(I,K,J)=TEST**(1./3.)
C
C     COMPUTE NEW VALUES OF INT, CPT, AND KA
C
      INT(I,K)=INT(I,K-1)+CI*(W(I,K)**.667+W(I,K-1)**.667)*DZA(K)
      DWZ=SQRT((U(I,K)-U(I,K-1))**2+(V(I,K)-V(I,K-1))**2+(Y(I,K)-Y(I,K-1
     *))**2)/DZA(K)
      IF(W(I,K) .GT. 0.0) GO TO 50
      CPT(I,K)=CP
C
C     DIAGNOSIS OF EXCHANGE COEFFICIENTS COVERING NEUTRAL,STABLE AND
C     UNSTABLE CONDITIONS BETWEEN K=2 AND THE SURFACE
C
      S=(PT(I,K)-PT(I,K-1))/DZA(K)
      IF(K.EQ. 2) SS=S
      GO TO 60
50    CPT(I,K)=CP+CH*RSF(T(I,K),P(I,K))/(T(I,K)**2)
      S=(T(I,K)-T(I,K-1))/DZA(K)+CS/CPT(I,K)
      IF(K .EQ. 2) SS=S
60    IF(K .EQ. 2) GO TO 71
      IF(SS .GT. 0.) GO TO 75
      IF(SS .EQ. 0.) GO TO 77
      PHI=DSQRT(DSQRT(1.D0-15.D0*Z(K)/TL))
      KM(I,K)= .4*Z(K)*UF1*PHI
      KA(I,K)=KM(I,K)*PHI
      GO TO 79
75    KM(I,K)=(.4*Z(K)*UF1)/(1.+5.*(Z(K)/TL))
      GO TO 78
77    KM(I,K)=.4*Z(K)*UF1
78    KA(I,K)=KM(I,K)
      GO TO 79
71    KM(I,2)=.16*SQRT(U(I,2)**2+V(I,2)**2+Y(I,2)**2)*DZA(2)/(ALOG(ZA(2)
     */Z0)**2)
      KA(I,2)=KM(I,2)
      UF1=SQRT(KM(I,2)*DWZ)
      IF(S .EQ. 0.0) GO TO 70
      TL=(UF1**3)*PT(I,2)/(.4*G*KA(I,2)*S)
      GO TO 70
C
C     SHIR-TYPE EXPONENTIAL DECREASE
C
79    DFC=EXP(-3.*F*Z(K)/UF1)
      KM(I,K)=KM(I,K)*DFC
      KA(I,K)=KA(I,K)*DFC
C
70    CONTINUE
```

```
C
C     UPDATE SURFACE BOUNDARY CONDITION ON R AFTER SATURATION ADJUSTMENT
C     IF NO FLUX CONDITION USED
C
      IF(IRSFC .LE. 0) R(I,1)=R(I,2)
C
   80 CONTINUE
C
C     COMPUTE GROWTH OF WATER DROPLET BY MICROPHYSICS EQUATION
C
      DO 35 I=1,IX
      DO 35 K=KL,KF
      RS=RSF(T(I,K),P(I,K))
      RH(I,K)=R(I,K)/RS
      TVIS=0.
      FC(I,K)=0.
      DO 34 J=1,JY
      RRAD=RAD(I,K,J)
      DISM=4*3.1416*RDIS(J)**3*PDMN/3.
      CALL RKF(RWE(I,K,J),T(I,K),P(I,K),R(I,K),VHF ,DISM,HRW, NDIS(J))
      TFC(I,K,J)=4*3.1416*(RAD(I,K,J)**3-RRAD**3)*NDIS(J)/3.
      FC(I,K)=FC(I,K)+TFC(I,K,J)/(DEN*DT)
      TVIS=TVIS+NDIS(J)*(RAD(I,K,J)**2)
      IF(NSP.EQ.1) GO TO 33
      RRAF=RAC(I,K,J)
      DISM=4*3.1416*RDISA(J)**3*PDMA/3.
      CALL RKF(RWE(I,K,J),T(I,K),P(I,K),R(I,K),VHFA,DISM,HRWA,NDISA(J))
      TFCA(I,K,J)=4*3.1416*(RAE(I,K,J)**3-RRAF**3)*NDISA(J)/3.
      FC(I,K)=FC(I,K)+TFCA(I,K,J)/(DEN*DT)
      TVIS=TVIS+NDISA(J)*(RAE(I,K,J)**2)
33    CONTINUE
34    CONTINUE
      TVIS=TVIS*PI*(RHO(I,K)**2)
      VISITY(I,K)=3.912/(2*3.1416*TVIS*100.)
35    CONTINUE
      INDT=INDT+1
      IF(INDT.LE.NDT) TIME=TIME+DT
      IF(INDT.LE.NDT) GO TO 130
      IF(NK.EQ.1) DT=EDT
      IF(TIME.GT.OPTIM) NK=NK-1
      RETURN
      END
```

```
C
C
C     PRINT SUBROUTINE
C
      SUBROUTINE PRNT(O,FORM)
C
      PARAMETER JX=10,JZ=21,JY=1
      COMMON/FLP/ ZA(JZ),X(JX),IL,KE,TIME,DTEMI,ITEML,ITEMR
      DIMENSION O(JX,JZ),FORM(11)
C
C     OUTPUT DOCUMENTATION
C
      KE=KE-1
      WRITE(6,4000) TIME,DTEMI,ITEML,ITEMR
C
C     PAGE 1 COLUMNS 1-10
C
      WRITE(6,4100) (X(I),I=1,10)
      DO 450 J=1,KE
      K=KE-J+1
  450 WRITE(6,FORM) ZA(K),(O(I,K),I=1,10)
C
      IF(IL .LT. 11) GO TO 490
C
C     PAGE 2 COLUMNS 11-20
C
      WRITE(6,4105) (X(I),I=11,20)
      DO 460 J=1,KE
      K=KE-J+1
  460 WRITE(6,FORM) ZA(K),(O(I,K),I=11,20)
C
      IF(IL .LT. 21) GO TO 490
C
C     PAGE 3 COLUMNS 21-30
C
      WRITE(6,4105) (X(I),I=21,30)
      DO 470 J=1,KE
      K=KE-J+1
  470 WRITE(6,FORM) ZA(K),(O(I,K),I=21,30)
C
      IF(IL .LT. 31) GO TO 490
C
C     PAGE 4 COLUMNS 31-IL
C
      WRITE(6,4105) (X(I),I=31,IL)
      DO 480 J=1,KE
      K=KE-J+1
  480 WRITE(6,FORM) ZA(K),(O(I,K),I=31,IL)
C
  490 CONTINUE
      KE=KE+1
 4105 FORMAT(1H1,6HX(XX)=,3X,10(-5PF12.2) / 1H ,3X,5HZ(CM))
 4000 FORMAT(/8HTIME=,F9.2,4H SEC,6X,6HDTEMI=,F5.1,3H K,6X,6HITEML=,I2,2
     1X,6HITEMR=,I2)
 4100 FORMAT(1H0,6HX(XX)=,   10(-5PF12.2) / 1H ,3X,5HZ(CM))
      RETURN
      END
```

ORIGINAL PAGE IS
OF POOR QUALITY

```
C
C
C     MICROPHYSICS SUBROUTINE
C
C     SOLVE GROWTH RATE EQUATION
C           R*DR/DT=G*(S-A/R+B/R**3)
C
      SUBROUTINE RAF(RAD,T,P,R,VHF,HNW,HRW,N)
C
C
C     PHYSICAL CONSTANTS
C
      TR=R
      DEN=1.0E-3
      ALPHA=0.03
      BETA=0.036
      GAMA=1.4
      RV=0.1102
      RA=0.0[illegible]
C
C     COMPUTE WORKING CONSTANTS
C
      RS=RSF(T,P)
      D=11.711*T**1.75/P
      TL=777.44-0.55*T
      CK=0.127E-6*(T-273.15)+2.5725E-4
      SIGMA=75.7-0.146*(T-273.16)
      DPES=6.1078E-3*(273.16/T)**5.7723104*EXP(6716.735*(1./273.16-1./T))
      DE=DPES*(6716.235/T-5.7723104)/T
      DEFF=1./D+DE*TL/CK
      GC=DEN/DEFF
      AL=(1-ALPHA/2.)*CK/(ALPHA*P)*(GAMA-1.)*(2*3.1416*T/RA)**.5/(GAMA+
     $ 1.)
      BL=(1-BETA/2)*(D/BETA)*(2*3.1416/(RV*T))**0.5
      CL=(BL/D+AL*DE*TL/CK)*DEFF
      CA=2*SIGMA/(RV*T*4.184E7)
      CB=4.3*VHF*HNW/HRW
C
C     INTEGRATION
C
      I=0
      DT=0.01
      TIME=0.
20    CONTINUE
      RH=R/RS
      SUPS=RH-1.
      I=I+1
      TRAD=RAD
      TIME=TIME+DT
      DR=GC*(SUPS-CA/RAD+CB/(RAD**3))/(RAD+CL)
      RAD=RAD+DT*DR/RAD
      DR=4*3.1416*(RAD**3-TRAD**3)*N/(3*DEN)
      R=R-DR
      DRAD=ABS(RAD-TRAD)
      IF(I.GT.2000) GO TO 30
      IF(DRAD.GT.1.0E-7) GO TO 20
30    CONTINUE
      R=TR
      RETURN
      END
```

```
C
C
C     SATURATION MIXING RATIO AS A FUNCTION OF TEMPERATURE A AND
C     PRESSURE P
C
      FUNCTION ESF(A, P)
C
      C=10.**(-7.90298*(373.16/A-1.)+5.02808*ALOG10(373.16/A)-1.3816E-7
     1*(10.**(11.344*(1.-A/373.16))-1.)+8.1328E-3*(10.**(-3.49149*(373.1
     96/A-1.))-1.))+ALOG10(1013.246)
      ESF=C*10./(P*29.9)
      RETURN
      END
```